



University of
Massachusetts
Amherst

Characterizing Colorectal Cancer Cells and Their Interactions with Polymethoxyflavones by Raman Microscopy

Item Type	Dissertation (Open Access)
Authors	Zhang, Hua
DOI	10.7275/9044267.0
Download date	2026-05-19 21:42:45
Link to Item	https://hdl.handle.net/20.500.14394/20015

**CHARACTERIZING COLORECTAL CANCER CELLS AND
THEIR INTERACTIONS WITH POLYMETHOXYFLAVONES
BY RAMAN MICROSCOPY**

A Dissertation Presented

By

HUA ZHANG

Submitted to the Graduate School of the
University of Massachusetts Amherst in partial fulfillment
of the requirements for the degree of

DOCTOR OF PHILOSOPHY

SEPTEMBER 2016

Food Science

©Copyright by Hua Zhang 2016

All Rights Reserved

**CHARACTERIZING COLORECTAL CANCER CELLS
AND THEIR INTERACTIONS WITH
POLYMETHOXYFLAVONES BY RAMAN MICROSCOPY**

A Dissertation Presented
by
HUA ZHANG

Approved as to style and content by:

Hang Xiao, Co-Chair

Lili He, Co-Chair

Zhenhua Liu, Member

Eric A. Decker, Department Head
Department of Food Science

DEDICATION

To my father and mother,

All of my families and friends,

Without whom, none of my success would be possible

ACKNOWLEDGMENTS

I would like to express my gratitude to my advisors, Dr. Hang Xiao, and Dr. Lili He, whose expertise, understanding, and patience, added considerably to my Ph.D. experience and also support me with their kind guidance, intelligence and strong experiences in my research. I would like to thank Dr. Zhenhua Liu for being members of my committee. I appreciated for all of their donating valuable times. Also, I gratefully acknowledge the government scholarship by Chinese Scholarship Council (CSC) for my graduate study.

Many thanks to all previous and present Xiao's group members, Tom, Mon, Mingyue, Xian, Jinkai, Christina, Jason, Jingjing, Minqi, Fuki, Dr.Fang, Ziyuan, Zili, Xiaokun, CiCi, Olivia, Nok, Dr. Suyao, Fang, Zhengze, Yue, Dr. Sun, Dr. Qi, Xiaoqiong, Min, Will, Panche, Yanhui and Jiazhi. Also all previous and present He's group members, Shintaro, Mike, Kevin, Dr. Li, Wisiani, Dr. Lang, Dr. Hou, Dr. Wang, Panxue, Kirsten, Siyue, Chen Tan, Bin Zhao, Brook and Tianxi. Thanks for their continuing and unconditional friendship and their fully supports over the years; I could not finish my project without their help. I also would like to thank all of my undergraduate students that I have supervised. I also would like to thank all faculties, staffs and Food Sciences graduate students with my special thanks to Fran, Jean, and Deby. Also, I would like to thank all my Chinese friends in UMass Amherst for their friendship. I have never missed my hometown since I was here.

ABSTRACT

**CHARACTERIZING COLORECTAL CANCER CELLS AND
THEIR INTERACTIONS WITH POLYMETHOXYFLAVONES
BY RAMAN MICROSCOPY**

SEPTEMBER 2016

HUA ZHANG

B.E., NORTHWEST A&F UNIVERSITY, SHAANXI, CHINA

Ph.D., UNIVERSITY OF MASSACHUSETTS AMHERST

Directed by: Professor Hang Xiao and Lili He

Polymethoxyflavones (PMFs), especially Nobiletin (NBT) and 5-demethylnobiletin (5DN), have been widely studied and proved to have anti-cancer effects. However, their exact modes of action against cancer cells are not fully understood. Raman spectroscopy is a molecular vibrational spectroscopy can be used to measure overall biochemical function of single cells noninvasively and without adding any chemical labels. Herein, we characterized the cellular responses of human colorectal cancer HT29 and HCT116 cells, that grow on the gold coated slides, to the treatments of NBT and 5DN using Raman microscopy. Raman microscopic images obtained indicated the different modes of action of these two PMFs against colorectal cancer cells. NBT induced more changes in the nucleic acid peaks and protein peaks, while 5DN induced more changes in the localized lipid peaks.

We further analyzed both attached and floating cells in response to NBT and 5DN treatments using Raman microscopy and principal component analysis. Result showed

large spectral heterogeneity of floating cells compared to attached cells, particular in the range for protein spectral profiles. In response to the treatments, the difference between the floating cells and attached cells became smaller over time. This indicates the different sensitivity and behavior of individual cells to the treatment.

Identification of individual cancer stem cells (CSC) from normal cancer cells is challenging. We applied Raman microscopy to identify and characterize CSC. CSC were enriched in non-attachable petri-dish to form cell spheres. The spheres containing both CSC and normal cancer cells and could be separated based on the density. It is interesting that 70% of CSC enriched density layer produced a distinct Raman peak at around 1049 cm^{-1} , while almost no normal cells contained this peak. This finding demonstrates the 1049 cm^{-1} peak might be used as indicator peak for CSC. Further validation is needed. Overall, our research demonstrates the feasibility of Raman microscopy to characterize individual cells and to investigate the heterogeneous response of the cell population to treatment. Moreover, there is a great potential of using Raman microscopy for identify individual CSC from normal cancer cells and investigate their heterogeneous response to the treatment.

TABLE OF CONTENTS

	Page
ACKNOWLEDGMENTS	v
ABSTRACT	vi
LIST OF TABLES	xi
LIST OF FIGURES	xii
CHAPTER	
1. INTRODUCTION	1
2. LITERATURE REVIEW	6
2.1 Polymethoxyflavones	6
2.1.1 Introduction to polymethoxyflavones	6
2.1.2 Anti-cancer effect of polymethoxyflavones	10
2.1.3 Biotransformation of polymethoxyflavones	11
2.2 Colorectal cancer	13
2.2.1 Introduction to colorectal cancer	13
2.2.2 Biological studies of colorectal cancer	14
2.2.2.1 MTT study	15
2.2.2.2 Cell Cycle Study	15
2.2.2.3 Cell Apoptosis Analysis	16
2.2.2.4 Western Blot Study	17
2.2.2.5 ELISA	17
2.2.3 Heterogeneity of colorectal cancer	20
2.3 Colorectal Cancer Stem Cells	24
2.3.1 Introduction to Colorectal Cancer Stem Cells	24
2.3.2 Biological Studies of Colorectal Stem Cells	26
2.4 Raman Microscopy	29

2.4.1	Introduction of Raman Scattering	29
2.4.2	Introduction of Raman Spectroscopy	30
2.4.3	Introduction of Raman Microscopy	31
2.4.4	Statistical Analysis for Raman Spectral and Images	33

3. LABEL-FREE IMAGING AND CHARACTERIZATION OF CANCER CELL

RESPONSES TO POLYMETHOXYFLAVONES USING RAMAN MICROSCOPY.. 37

3.1	Introduction	37
3.2	Materials and Methods	39
3.2.1	PMFs and cell lines	39
3.2.2	Cell Treatment for Raman measurement.....	40
3.2.3	DXR Raman Microscope	40
3.2.4	Data analysis	42
3.2.5	Cell Cycle Analysis.....	42
3.3	Results and discussion.....	43
3.3.1	Single cell imaging of HT 29 Cells and HCT116 Cells in responses to the treatment with NBT and 5DN.....	43
3.3.2	Cell population analysis of HT29 Cells in responses to the treatment with NBT and 5DN.....	49
3.3.3	Cell cycle study of HT29 Cells in responses to the treatment with NBT and 5DN	49
3.3.4	Raman and cell cycle study of HCT116 cells treated by NBT and 5DN	52
3.3.5	PCA analysis of the cellular responses of HT29 and HCT116 cells	53
3.4	Conclusions	56

4. CHARACTERIZING HETEROGENEOUS CELLULAR RESPONSES TO

POLYMETHOXYFLAVONES USING RAMAN MICROSCOPY 57

4.1	Introduction	57
4.2	Materials and Methods	59
4.2.1	PMFs and cell lines	59
4.2.2	Cell Treatment for Raman measurement.....	60
4.2.3	DXR Raman Microscope	60

4.2.4	Data analysis	61
4.3	Results and Discussion	62
4.3.1	Characterization of the heterogeneity of attached and floating cells.....	62
4.3.2	The effect of treatment time on cell heterogeneity.....	65
4.3.3	The effect of PMF types on cell heterogeneity	67
4.4	Conclusion.....	69
5.	CHARACTERIZATION COLORECTAL CANCER STEM CELLS USING RAMAN MICROSCOPY.....	71
5.1	Introduction	71
5.2	Material and Methods.....	73
5.2.1	Cell Culture	73
5.2.2	Cell Sorting in Continuous Gradient Solution.....	73
5.2.3	Raman Microscopy	75
5.2.4	ELDA analysis	75
5.2.5	Data analysis	76
5.3	Results and Discussion	76
5.3.1	Raman Microscopic Characterization of Attached and Sphere Cells.....	76
5.3.2	Characterize Cells from Different Density Layers	78
5.3.3	ELDA Study of Cells from Different Layers	81
5.4	Discussion	82
6.	OVERALL CONCLUSION AND FUTURE WORK.....	84
6.1	Conclusions	84
6.2	Future Study	85
	BIBLIOGRAPHY.....	86

LIST OF TABLES

Table	Page
1 . Effects of different drugs on activities of SOD, MDA, GSH-Px in H ₂ O ₂ -treated PC12 cells.....	9
2 Spectral regions with nonoverlapping standard deviations for M1 and MR1 nuclei	36

LIST OF FIGURES

Figure	Page
2.1 Chemical structures of major PMFs, namely nobiletin (NBT), 3'-hydroxynobiletin, 4'-hydroxynobiletin, 3', 4'-dihydroxynobiletin, 5-hydroxynobiletin (5DN), 5, 3'-dihydroxynobiletin, 5, 4'-dihydroxynobiletin, and 5, 3', 4'-trihydroxynobiletin....	6
2.2 Suppression by nobiletin of TPA-induced skin morphological changes observed by H&E staining. Ac: Acetone. TPA: TPA induced. NOB, nobiletin.....	8
2.3 Histological characterization of colonic mucosa and tumors of AOM/DSS-treated mice. (i) H&E staining of colonic tissues of the control (A) and NBT-treated (B) groups (magnification: 100×); (ii) PCNA staining of colonic mucosa of the control (C) and NBT-treated (D) groups (magnification: 400×); (iii) cleaved caspase-3 staining of colonic tumors of the control (E) and NBT-treated (F) groups (magnification:400×); (iv) quantification of PCNA-positive and caspase-3-positive cells in colonic mucosa and tumors (G);*statistical significance with $p < 0.01$, $n = 6$.	12
2.4 Ten Leading Cancer Types for the Estimated New Cancer Cases and Deaths by Sex, United States, 2016.....	13
2.5 Western blot demonstrated that combined treatments with atorvastatin/celecoxib for 48 hr activated caspase cascade. b-Actin served as an equal loading control. The results were representative of 3 experiments.....	18

2.6 Western blot analysis to check EMT-related gene expression. Densitometry shows data from three experiments; the values from each experimental set were normalized with control as related percentage (* <i>P</i> < 0.05, ** <i>P</i> < 0.01, or *** <i>P</i> < 0.001 compared to TGF-β1 treatment alone).	19
2.7 Inter- and Intraline Variation (A) Fate profiles of DLD-1, HCT116, and RKO cells following exposure to 0.1 mM taxol. (B) Fate profiles for A549 cells exposed to 30 ng/ml nocodazole, 0.3 mM taxol, and 1 mM AZ138.	21
2.8 Impact of the treatment with siRNAs on HCT 116, HCT 116 p53 ^{-/-} , and HT-1080 cancer cell lines. A, 72 h after transfection, cells were harvested and processed to determine the impact of RNAi on A1 and A2 expression. Western blot analysis was performed with the polyclonal anti-A1/A2 antibody. B, effect of the siRNA treatments on cell growth as measured by population doublings. The gray area indicates that cells displayed an altered morphology reminiscent of apoptotic cells. C, phase contrast microscopy (magnification, ×200) of cells treated with siRNAs. D, the DNA content profile of HCT 116 p53 ^{-/-} cells treated with siRNAs is shown.....	23
2.9 The construction of cancer and the therapy results assumptions. Normal cancer treatment could only decrease the number of normal cancer cells. The cells would grow back after certain amount of time. CSC targeted therapy could decrease the number of CSC, decrease the cancer in the long run.....	25
2.10 Sphere-forming prostate cells generated and passaged in vitro. (A) Spheres in suspension generated from single cells of PC3, imaged on indicated day of culture. (B) PC3 spheres could be serially passage in vitro.....	26

2.11 The relationship between infrared, Rayleigh scattering and Raman scattering.....	29
2.12 A grade 1R (mild rejection) endomyocardial biopsy sample is examined by Raman spectroscopy (A), optical microscope (B), and histopathology (C). Raman spectra are collected at locations marked in , B. Rejected Raman spectra ($I_{758} > I_{718}$) and their corresponding locations are marked in red, and the normal spectra ($I_{758} < I_{718}$) in blue.	31
2.13 Raman spectra of doxorubicin-treated leukemic T cells (Jurkat T cell line), where the cells have been treated with two different concentrations of doxorubicin as indicated in the figure. a) Spectra for cells treated for 24 h are indicative of chromatin condensation. b) Spectra for cells treated for 36 h are indicative of membrane blebbing. c) Spectra for cells treated for 72 h are indicative of apoptotic body formation.....	32
2.14 (A) High-resolution Raman imaging of a 1:1:1 diyne-SM/DOPC/chol ternary monolayer taken with slit-scanning Raman microscopy. The image was reconstructed using the diyne peak intensity at $2,262\text{ cm}^{-1}$. The images consist of 412×400 pixels. (Scale bar: $10\text{ }\mu\text{m}$.) (B) Raman and fluorescence images of a 1:1:1 diyne-SM/DOPC/chol ternary monolayer containing 0.2 mol% Bodipy-PC. Raman and fluorescence images were obtained in the same imaging area of the same sample. Fluorescence background during Raman imaging was suppressed by photobleaching of Bodipy-PC under 532-nm laser exposure. (C) Line profiles of lipid rafts calculated along the dotted lines of the Raman and fluorescence images in B (red and gray, respectively). The line profile from the Raman image was smoothed using the moving average.....	34

3.1 A: PMF formula, Nobiletin (NBT) and its metabolize 5-demethylnobiletin (5DN). The 5DN is the hydroxyl-PMF counter part of NBT.	39
3.2 Corresponding cellular optical images of the HT29 and HCT116 chosen for the Raman images of control or after treated with NBT (100 μ M) and 5DN (20 μ M for HT29 and 8 μ M for HCT116) for 48H.....	44
3.3 Raman images of the HT29 cells obtained by integrating over the CH2 twist (lipid) at peak 1301 cm-1, over Sym. Ring br Phe (protein) at peak 1005 cm-1, and O–P–O stretching of the DNA backbone at peak 1095 cm-1.....	45
3.4 Raman images of the HCT116 cells obtained by integrating over the CH2 twist (lipid) at peak 1301 cm-1, over Sym. Ring br Phe (protein) at peak 1005 cm-1 and O–P–O stretching of the DNA backbone at peak 1095 cm-1. The red spots in the HCT 116 images were likely from the impurity on the gold slide.	46
3.5 Cellular optical images and corresponding Raman images of the HT29 and HCT116 chosen for the Raman images of control (A: HT29 cells, D: HCT116 cells) or after treated with NBT (B: 100 μ M for HT29 cells, E: 100 μ M for HCT116 cells) and 5DN (C: 20 μ M for HT29 ,F: 8 μ M for HCT116) for 48H. Raman images cells obtained by integrating over the CH2 twist (lipid) at peak 1301 cm-1, over Sym. Ring br Phe (protein) at peak 1005 cm-1 and O–P–O stretching of the DNA backbone at peak 1095 cm-1. The red spots in the images were likely from the impurity on the gold slide.....	47

3.6 Raman intensity analysis of the Raman shift at 1301 cm^{-1} (lipid), 1005 cm^{-1} (protein), 1095 cm^{-1} (nucleic acids) of a population of control HT29 cells, and cells after treatment with NBT and 5DN. A: Statistical analysis was conducted among control and treated cells, and different notations in the bar charts indicate statistical significance. All data represented mean \pm SD (n = 75). Different characters represented a significant difference (p < 0.05) within the same category. B: Raman spectra of the control and treated cells, and different vertical dash lines marked different Raman shift.	48
3.7 Cell population analysis of the HT29 cell cycle after treatments with NBT and 5DN by flow cytometry. Statistical analysis was conducted among control and treated groups in G0/G1, S, and G2/M phases separately, and different notations in the bar charts indicate statistical significance. All data represented mean \pm SD (n = 3). Different characters represented a significant difference (p < 0.05) within the same category.....	50
3.8 Raman intensity analysis of the Raman shift at 1301 cm^{-1} (lipid), 1005 cm^{-1} (protein), 1095 cm^{-1} (nucleic acids) of a population of control HCT 116 cells, and cells after treated with NBT and 5DN. A: Statistical analysis was conducted among control and treated cells, and different notations in the bar charts indicate statistical significance. All data represented mean \pm SD (n = 75). Different characters represented a significant difference (p < 0.05) within the same category. B: Raman spectra of the control and treated cells, and different vertical dash lines marked different Raman shift.	51

3.9 Cell population analysis of the HCT116 cell cycle after treatments with NBT and 5DN by flow cytometry. Statistical analysis was conducted among control and treated groups in G0/G1, S, and G2/M phases separately, and different notations in the bar charts indicate statistical significance. All data represented mean \pm SD (n = 3). Different characters represented a significant difference ($p < 0.05$) within the same category.	53
3.10 The 3D PCA plot of the control HT29 and HCT116 cells and treated with NBT 100 μ M for 48h and the ANOSIM result based on the PCA plot. PC 1 explained 71.64% of the total data variance and the PC 2 explained 8.83% of the total data variance and the p-value < 0.01%	54
3.11 The 3D PCA plot of the control HT29 and HCT116 cells and treated with NBT 100 μ M for 48h. PC 1 explained 71.64% of the total data variance and the PC 3 explained 2.56% of the total data variance.	55
4.1A: A: Spectra and B: PCA score 3D display of both floating and attached cells treated with NBT (100 μ M) under 72H treatment. C: Spectra and D: PCA score 3D display of the attached cells treated with NBT (100 μ M) under 72H treatment. The floating cells are not as overlapped as attached cells, indicate more heterogeneous than the attached cells. The heterogeneity of the floating cells came from Raman peak shift between 1050-1150 cm^{-1} and 1250-1350 cm^{-1}	62
4.2 PCA scores of the difference between attached and floating cells of the two treatments NBT (100 μ M) and 5DN(20 μ M) from different time spot, 24H, 48H and 72H.	64

4.3 Raman Spectra and PCA scores of the variances along with the time of the 2 treatments of NBT (100 μ M) and 5DN (20 μ M) from different time spot, 24H, 48H and 72H.....	66
4.4 Raman spectra of the attached and floating HT29 cells at 72H under NBT(100 μ M), 5DN(20 μ M) and control.....	68
5.1 Methods Process for Continuous Gradient	74
5.2 Raman spectra of PBS control, cell media control, stem cell media control, normal cell and CSC. The Raman spectra of CSC showed a distinct peak at 1049 cm^{-1} with a high intensity around 2000 but the others do not contain that peak.	77
5.3 Special spectra count in 50 cells from different layers of the cells spheres after gradient centrifugation. The cell number from the layer 1 doesn't reach 50 and the layer 4 and layer 5 doesn't contain any cells.....	78
5.4 A: The optical images of the cells sorted by Percoll continuous solution. The CSC formed the cell layer at an upper layer while the normal cancer cell formed the layer at the lower layer. The tube containing both CSC and normal cancer cell formed an extended cell layer.	79
5.5 Statistical analysis of the peak 1049 cm^{-1} intensity. The intensity from stem cells was much higher than the same peak from the normal cancer cells. The average intensity showed significant difference between normal cancer cell and cell sphere. The A one way Student's t-test was used to assess the statistical significance and p-value of<0.05 was considered statistically significant.	80

5.6 ELDA of the cells from different layers. Bulk cells contained least stem cells and followed by cells from spheres which considered to be stem cells. Stem Layer 2 represents the second layer of cells from cell spheres gradient centrifugation. After second centrifugation of Stem Layer 2, cells from layer 3, 4 and 5 labeled Stem Layer 2-3, 2-4 and 2-5. Stem Layer 2-5 contained most stem cells. 81

CHAPTER 1.

INTRODUCTION

Cancer burden is still increasing worldwide. It now affects 24 million people around the world resulting in 6 million death annually. The increased aging populations as well as adopted cancer-causing habits leads to more cancer incidents in developing countries¹. In the United States, cancer continues to be a major public health problem. Among the population ages between 45-64 years old, cancer is number one leading cause of death and the second to heart disease in the older populations (National Center for Health Statistics, CDC). Within one's lifetime, individual have approximately 40% chance to be diagnosed with any type of cancer. Cancer, especially colorectal cancer, is normally considered to be a severe disease that has been the leading death cause in the US for successive years. Colon cancer affects million people annually and the overall survival rates for patients is just about 65%². The serious situation attracts great attention from the scientists.

A major reason about how the recovery rate of cancer patients after scientific proved therapy is below expectation is probably due to the cancer cell heterogeneity³. Cancer is a combination of differentiated malignant cells. Though studies discovered increasing number of great findings to eliminate one kind of cancer cells every year, there is still almost no sign of stopping cancer from growing more serious. In a tumor or even in the same cancer cell line, the existence of subpopulations of cells always interfere with the interaction between treatments and cancer cells reactions. The heterogeneity of cells requires the treatment to

display a broad spectrum anti-cancer ability to eliminate the entire cancer cell population to prevent them growing back. Due to this situation, studies of cancer cell heterogeneity is of great importance. Firstly, It could help determine the heterogeneity of the cancer cells. A better understanding of the heterogeneity of cancer cells would help determine the effectiveness of treatments. Secondly, it would provide the information about how the treatment interacts with the entire cancer population. The heterogeneity change of the cells could reveal the mechanism of interaction. In summary, it could monitor the cell transformation due to the time or stimuli change to keep tracking the key factors.

Within the existing causes of the heterogeneity including genotypes and phenotypes, the cancer stem cells are highly believed to be the main reason⁴. Cancer stem cells are a kind of cells existing among cancer cells that possess the ability of self-renewal, generating daughter cell and differentiation. Besides, cancer stem cells are always considered with higher resistance to therapy⁵. Therefore, the elimination of cancer stem cells might inhibit the cancer proliferation and be the key of defeating cancer. Current identification method of cancer stem cells is by their cell-surface-marker expression. However, the cell-surface-marker is not a universal method to identify cancer stem cell yet, therefore the isolation of cancer stem cells continues to be a big challenge. In a word, an effective and reliable method of isolating and identifying cancer stem cells is in need. With the isolated and purified cancer stem cells, more specific studies could be conducted which would benefit the studies of cancer stem cell treatments.

Flavonoids, which are rich in fruits and vegetables, have long been believed to display biological health-beneficial effects. Among all these flavonoids, scientist found several specific types possessed the great anti-cancer property, and one of these types is polymethoxyflavones (PMFs). PMFs, which exclusively exist in the citrus genus,

especially abundant in sweet orange (*Citrus sinensis* (L.) Osbeck) and mandarin (*Citrus reticulata* Blanco).⁶ This specific type of flavones has attracted great attention due to their broad spectrum of biological activities, including anti-inflammatory^{7,8}, anti-carcinogenic^{9,10} and anti-oxidant^{11,12}. In this study, we mainly focused on the anti-carcinogenic property of the PMFs. The hydroxyl-PMFs could also be extracted from the citrus genus and showed anti-carcinogenic properties¹³ as well. Many studies proved that hydroxyl-PMFs showed greater bioactivity than their counterpart PMFs⁶. In this study, we picked two representative PMF and hydroxyl-PMF namely nobiletin(NBT) and 5-demethylnobiletin (5DN) to study the mechanisms of the inhibition effect of these PMFs to the cancer cells.

Raman spectroscopy is a vibrational technique has been widely applied for molecule identification and structural characterization. It provides molecular ‘fingerprint’ about structural information of analyte molecules. Raman spectroscopy is non-destructive and rapid. Raman microscopy combined Raman spectroscopy with microscopic technique. The application of Raman microscopy on the cells enabled people to image the distribution of biochemical composition in a single cell and study its chemical profile changes due to the stimuli. The advantages of non-label and non-destruction of the technique simplified the sample preparation and protected the integrity of the cell.

The overall objective of this project is to characterize colon cancer cells and their interactions with PMFs by Raman microscopy. Our central hypothesis is Raman microscopy can be used for study the modes of action of PMF against colon cancer cells based on single cell imaging. The Raman spectra collected from a population of cells can be used for analyzing the heterogeneity in the population and their response to treatment. Moreover,

Raman microscopy could also identify the difference between normal cancer cell and cancer stem cell.

Take all these into consideration and to test our hypothesis and achieve our objectives, we conducted the research by following **specific aims:**

1. Label-free Imaging and Characterization of Cancer Cells Responses to Polymethoxyflavones Using Raman Microscopy

In this study, we characterized the responses of cancer cells to NBT and 5DN using Raman microscopy. Flow cytometry analysis of the cell cycle was also performed to determine the effects of PMFs on cell availability. Cells were grown on gold coated slides and measured using Raman microscopy. Combined with the cell cycle result and the Raman cell image, the mechanism of the interaction between cancer cells and PMFs could be revealed.

2. Characterizing Heterogeneous cellular responses to Polymethoxyflavones Using Raman Microscopy.

In this study, we studied cell heterogeneity of both floating cells and attached cells in response to NBT and 5DN over time. With the Raman spectra and principal component analysis score provided by Raman microscopy, we could analyze the heterogeneity of the cells before, during and after treatment. It would help to analyze the cell heterogeneity.

3. Isolation and Characterization colorectal cancer stem cells using Raman microscopy

In this study, we developed a more efficient way to isolate colorectal cancer stem cells from normal cancer bulk cells by cell density and characterized the cancer stem cells using Raman microscopy. The stemness of the cells were determined by Extreme Limiting Dilution Analysis (ELDA). Combined with the Raman spectra and ELDA, the goal of isolation and identification of cancer stem cells had been achieved.

CHAPTER 2.

LITERATURE REVIEW

2.1 Polymethoxyflavones

2.1.1 Introduction to polymethoxyflavones

Increasing number of studies suggesting the beneficial effects of diet abundant in fruits and vegetable. Among all the beneficial effects, anti-carcinogenic^{14,15}, anti-inflammatory^{16,17} and antioxidant^{18,19} are the most presented in these bioactive foods. Most of the beneficial effects are believed to link to the existence of flavonoids, also various kinds of flavonoids showed distinct bioactive abilities. Flavonoids is a molecular that structures arranged in a C6–C3–C6 configuration. More than 4000 unique flavonoids have been identified in plants. The flavonoids could be subdivided into 12 subclasses,

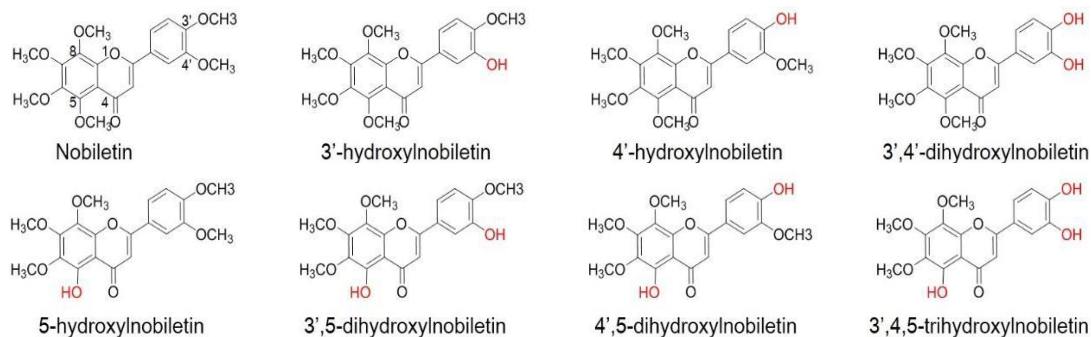


Figure 2.1 Chemical structures of major PMFs, namely nobiletin (NBT), 3'-hydroxynobiletin, 4'-hydroxynobiletin, 3', 4'-dihydroxynobiletin, 5-hydroxynobiletin (5DN), 5, 3'-dihydroxynobiletin, 5, 4'-dihydroxynobiletin, and 5, 3', 4'-trihydroxynobiletin.

including flavonols, flavones, flavanones, flavanols, isoflavones, flavanonols, chalcone, and anthocyanidins.

Citrus including oranges, lemons tangerines,, limes and grapefruits, are widely consumed and have become an important part of daily diet. In 2013-2014, current annual citrus production in the United States was 17,800,000 boxes , according to the National Agricultural Statistics Service. The leading state is Florida constituting 65% as, followed by California, Texas and Arizona. About 30% of the citrus was used for juice production to generate 4-5 billion lbs. The by-products citrus peels are processed to obtain the volatile and nonvolatile fractions in many areas including food, pharmaceutical and cosmetic industry. In China, aged citrus peels have been utilized as traditional medicine since ancient times to treat various diseases. Its outstanding effect on diseases including abdominal fullness and distention, cough, and hypertension made it popular for daily consumption. In addition to the effects on the diseases, citrus fruits contain considerable amount of vitamins and flavonoids, carotenoids, and limonoids. The PMFs is a unique class of flavonoids bearing two or more methoxyl groups on their basic heterocyclic C6–C3–C6 skeleton with a carbonyl group at the position 4(Figure 2.1).

Polymethoxyflavones (PMFs), which is a unique class of bioactive flavonoids (Chemical structure showed in Figure 2.1), have been received particular interest during recent years. They are almost exclusively found in the citrus genus and more than 20 polymethoxylated flavonoids being isolated and identified. Recent studies showed it possessed a broad spectrum of biological activities including anti-inflammatory^{7,20}, antioxidant¹², anti-atherogenic, antimicrobial and anti-carcinogenic^{21,22}.

Anti-inflammation studies suggested that PMFs obtain promising anti-inflammation ability. In a study focused on the anti-inflammation ability of nobiletin, TPA, which could induce O₂⁻ production and skin edema formation in mice, was used to

cause mouse skin inflammation. The result suggested that nobiletin treatments 30mins before each TPA application(twice in total) showed the highest inhibition of H₂O₂ production and most effective of edema suppression(Figure 2.2)⁸ than the other TPA applications. The nobiletin mechanism was believed to be the inhibition of the release of both LPS-induced and IFN- γ -induced TNF- α and IL-1 β . It suggested that PMFs is an effective anti-inflammation flavonoid.

Anti-oxidant studies suggested PMF could provide the great protective ability to cells from oxidative damage. A previous study used H₂O₂⁻ treated PC12 cells as oxidative

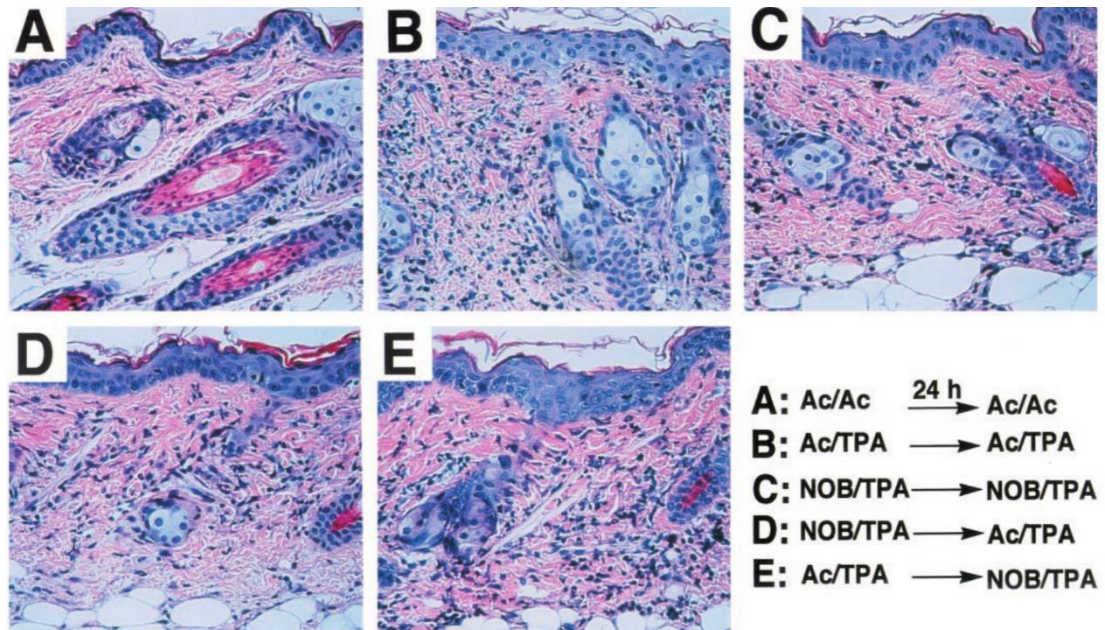


Figure 2.2 Suppression by nobiletin of TPA-induced skin morphological changes observed by H&E staining. Ac: Acetone. TPA: TPA induced. NOB, nobiletin.

damage cells to determine the anti-oxidation ability of PMFs. The malondialdehyde(MDA) level could measure the effectiveness, which indicates the free radical activity, and the antioxidant enzyme activities including SOD and GSH-Px. The results showed that certain PMFs could decrease the MDA levels and also improved the activities of SOD and GSH-Px²³, suggesting the antioxidant effectiveness of PMFs.

Antimicrobial is another major bioactive ability of PMFs that attracted attentions from researchers. In a study, the ability of PMFs against *Pseudomonas* was studied. The study used nobiletin and tangeretin and the SEM and TEM images showed their abilities to destroy the permeability of the cell membrane. Furthermore, nobiletin and tangeretin also could inhibit the protein synthesis. The inhibition of protein synthesis would cause metabolic dysfunction, and eventually to cell death.²⁴ The result suggested the antimicrobial potential of PMFs.

Table 1 . Effects of different drugs on activities of SOD, MDA, GSH-Px in H₂O₂-treated PC12 cells.

Treatment	MDA (nmol mg ⁻¹ prot)	SOD (U mg ⁻¹ protein)	GSH-Px (U mg ⁻¹ prot)
Control group	7.03 ± 1.26	105.53 ± 6.85	295.14 ± 12.46
H ₂ O ₂ -injured group	22.59 ± 1.89*	80.35 ± 3.62*	241.16 ± 11.63*
ECRP	12.26 ± 1.47**	91.07 ± 5.93**	265.12 ± 16.9**
Hesperidin	21.18 ± 1.12 [▲]	87.54 ± 7.63 [▲]	252.61 ± 13.55 [▲]
Nobiletin	13.84 ± 1.53**	93.68 ± 6.17**	270.38 ± 11.14**
Tangeretin	12.98 ± 1.22**	90.3 ± 2.88**	263.56 ± 18.32**
PMF 3	21.71 ± 1.37 ^{▲▲}	84.38 ± 5.45 ^{▲▲}	244.17 ± 12.96 ^{▲▲}
PMF 4	21.03 ± 1.97 ^{▲▲}	83.24 ± 4.12 ^{▲▲}	243.58 ± 16.55 ^{▲▲}
PMF 5	7.91 ± 1.14**	96.28 ± 3.77**	280.96 ± 14.16**
PMF 6	7.86 ± 0.96**	96.41 ± 2.87**	281.02 ± 15.93**

There are also many studies focused on other areas, as PMFs are such a type of flavonoids that possessed many effective bioactivities. In a word, it is necessary and important to study the PMFs. Furthermore, all the anti-inflammation, anti-oxidant and antimicrobial and other bioactivities are always linked to the property of anti-carcinogenic.

2.1.2 Anti-cancer effect of polymethoxyflavones

Take the anti-carcinogenic property particularly; there are many types of research related in vivo or in vitro. Studies showed that PMFs could induce cell apoptosis, cell cycle arrest, and cell anti-proliferation in cancer cell population. Xiao et al. reported that⁹ the interaction between lung cancer cells and two major PMFs plus two major monodemethylated PMFs. The study showed that monodemethylated PMFs could induce better growth inhibition of lung. Cell cycle analysis and apoptosis analysis revealed that different PMFs showed different inhibition mechanism when treated H1299 cells. Qiu et al.²⁵ focused her study on the three major PMFs and their 5-hydroxy counterpart on human colon cancer HCT116 and HT29 cells. Cell cycle analysis and apoptosis results suggested that 5-Hydroxy PMFs showed much stronger inhibitory effects on the growth of colon cancer. The mechanism of action was revealed to be apoptosis and cell-cycle arrest induced by p53-, Bax- and p21-dependent.²⁶ Besides, related animal study²⁷ was conducted. The result suggested that dietary consumption of hydroxylated PMFs could induce significant inhibition of AOM- induced ACF formation in mice.

Oral consumption of NBT could also effectively inhibit colitis-associated colon carcinogenesis in mice.²⁸ The histopathological and immunohistochemical analysis showed that PMFs could maintain the histological characteristics of normal mucosa and decreased the number of PCNA positive colonocytes. PCNA is a cofactor of DNA polymerase (As showed in Figure 2.3).

In summary, PMFs could inhibit many types of cancers including lung cancer, breast cancer and colon cancer.

2.1.3 Biotransformation of polymethoxyflavones

Increasing number of evidences suggested that biotransformation played important roles in the biological activities of orally administered compounds^{29,30}. Studies proved that the metabolites generated in the body by the biotransformation showed more potent bioactivities compared to their parent compound. Also oral consumption of a parent compound may result in higher levels of metabolites. Therefore, the metabolites exhibit dominant effects under the aforementioned circumstance in those tissues³¹. In recent years, though considerable amount of studies about the biological properties of PMFs have been reported, knowledge of their biotransformation profile is still limited. Previous studies suggested that the primary sites of biotransformation of PMFs are 3' and 4' positions on the B-ring. The number and position of the hydroxyl and methoxyl groups on the B-ring would affect the metabolism and biological activities of PMFs significantly.

Nobiletin is a major PMFs compound. Many studies had reported its bioactivities (5,6,7,8,3',4'-hexamethoxyflavone, NBT). It has been found to exert various protective effects against various cancers in animal models. In particular, previous studies have showed that dietary administration of NBT effectively suppressed colon carcinogenesis in three different colon cancer animal models^{32,33}. The studies suggested that dietary consumption of NBT possess the inhibition effect on colon carcinogenesis induced by colon carcinogens *in vivo*.

Among different types of PMFs, 5-hydroxylated PMFs are a unique subclass. 5-demethylnobiletin (5DN) is an important 5-hydroxylated PMF, that has been demonstrated the anti-carcinogenic properties against lung and colon cancer²¹.

Although the abundance of 5-hydroxylated PMFs is relatively less compared to their permethoxylated counterparts. Some previous studies demonstrated that 5DN exhibited superior anticancer potential than their counterparts against multiple types of cancers. The result indicated higher inhibition potential to the cancer cells than the NBT. It also suggested that demethylation at 3' position may contribute to the enhancement of the growth inhibitory effects on colon cancer cells.

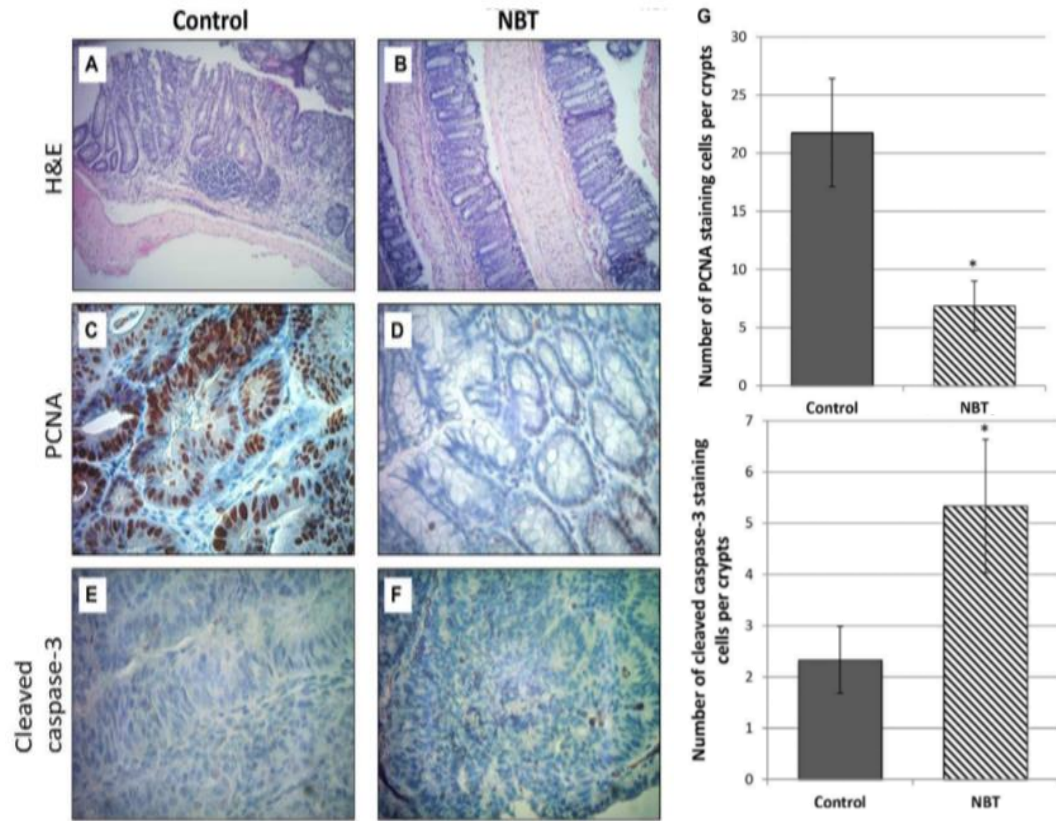


Figure 2.3 Histological characterization of colonic mucosa and tumors of AOM/DSS-treated mice. (i) H&E staining of colonic tissues of the control (A) and NBT-treated (B) groups (magnification: 100×); (ii) PCNA staining of colonic mucosa of the control (C) and NBT-treated (D) groups (magnification: 400×); (iii) cleaved caspase-3 staining of colonic tumors of the control (E) and NBT-treated (F) groups (magnification: 400×); (iv) quantification of PCNA-positive and caspase-3-positive cells in colonic mucosa and tumors (G); *statistical significance with $p < 0.01$, $n = 6$.

2.2 Colorectal cancer

2.2.1 Introduction to colorectal cancer

Colorectal cancer is always the second-leading cause of cancer death in the US. According to the data (Figure 2.4) collected by National Cancer Institute, the Centers for Disease Control and Prevention and the North American Association of Central Cancer Registries. Estimated new cases and estimated deaths of 2016 was 8%, as showed in Figure 2.4 ³⁴. It is about 134,490 estimated new cases and 49,190 estimated deaths. That

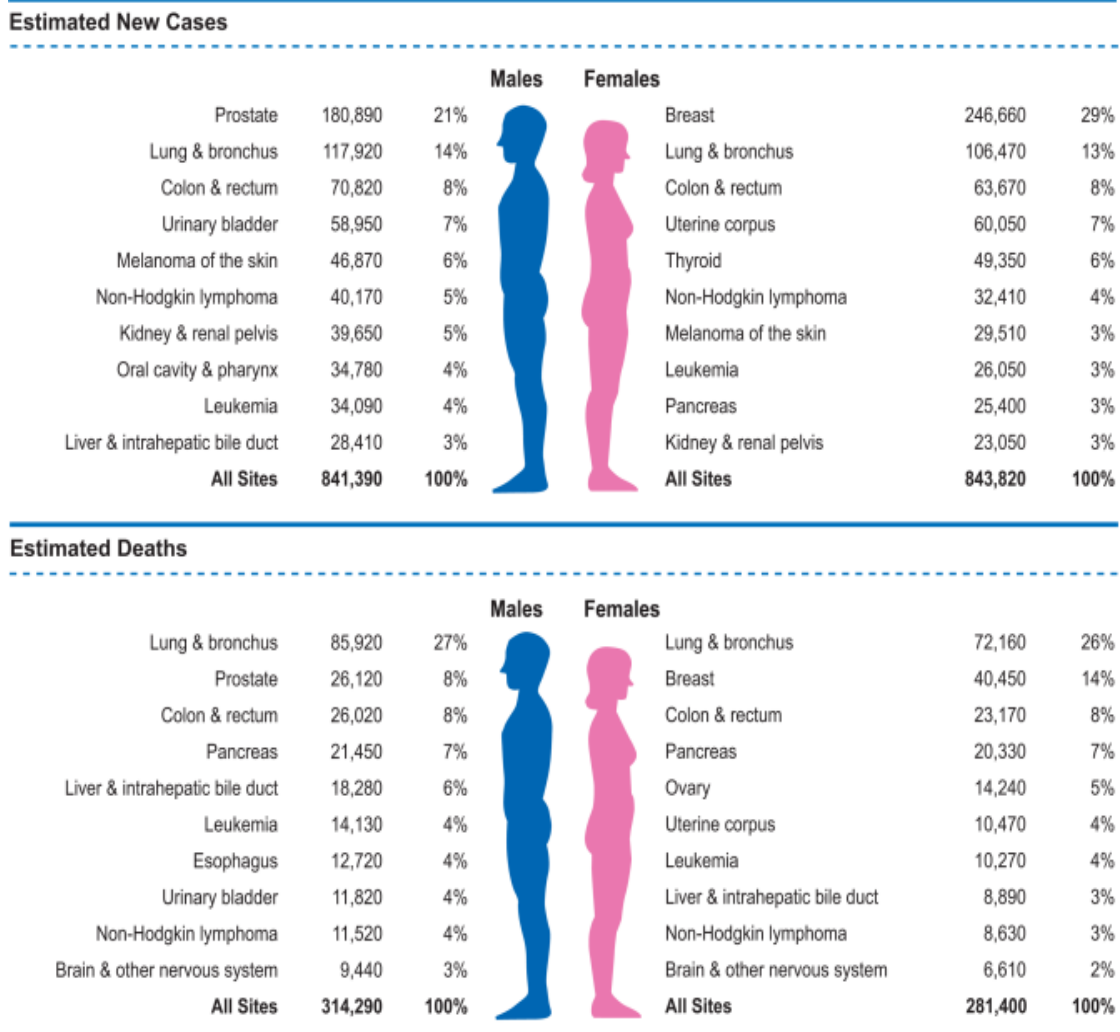


Figure 2.4 Ten Leading Cancer Types for the Estimated New Cancer Cases and Deaths by Sex, United States, 2016.

remained to be a large population compared to the increasing amount of research work regarding on characterization and prevention of colorectal cancer has been done. The importance of better understanding the cancer cells remained.

Colorectal cancer starts as polyps or adenomas on the surface of the upper layer and develops to grow into underneath layer. Later on, cancer cells invade the body furthermore. The different cancer development phases could be classified into four stages. Stage 1, cancer cells are in the inner layers of the colon; stage 2, cancer cells spread through the muscle wall of colon; stage 3, cancer cells spread to the lymph nodes and stage 4, cancer cells metastasized to other organs.³⁵ Epidemiological studies have proved that the occurrence of colorectal cancer is possibly related with inherited cancer predisposition syndromes, and some other risk factors, such as high fat diet, smoking, environmental procarcinogens, alcohol consumption, inadequate intake of vitamins and dietary fiber, and lack of physical exercise^{36,37}.

2.2.2 Biological studies of colorectal cancer

The modern idea of how cancer produced is when tumor progression initiated in one cell and experiences a series of random DNA mutations. After these random mutations, cells possessed the property to proliferate and survive and then became the malignant phenotype.³⁸ To study the process, numerous studies about cancer cells have been discovered and utilized in recent years.

2.2.2.1 MTT study

Most studies are focused on the interactions between treatments and cells to further understand the possibilities of eliminating cancer cells. The 3-(4,5-dimethylthiazol-2-yl)-2,5-diphenyl tetrazolium bromide (MTT) assay is a method that utilized in most widely used methods for drug analysis³⁹. The same cell amount would be cultured in the 96 well plate wells, and the MTT result relies on the cell survival percentage. Seed the cells in the 96 well plates and culture the cells to make the cells attach on the surface of the petri dish. When the cells attached to the surface of the Petri dish, the media containing the treatment would be added in the cell containing petri dish. After treated the cells with certain time and dose, the MTT dye would be added to the petri dish to replace the cell media. Discard the floating cells and the attached live cells would remain in the petri dish. In this way, the live cells would be dyed with MTT color and became dead. Replace the dye solution with a solvent to dissolve the dye from the cells. Color absorption could determine the cell live percentage. Based on the dose and treatment time, the drug effectiveness to the cells could be determined.

2.2.2.2 Cell Cycle Study

For further analysis of the interactions between cells and the drugs is the cell cycle study^{40,41}. In a cell cycle, the status of the cell would be divided into different stages: G0/G1 phase, S phase, G2 phase and M phase. Cell cycle analysis plays an essential role in drug development of most cancers. In the G0/G1 phase, the cell would be rest and prepare for the cell division. When a mitotic signal is triggered, cells leave G0

phase, a quiescent state, and enter into the G1 phase, an active state. In the S phase, cells start to replicate the DNA. In G2 phase, cells grow bigger and are ready for the division. At last at the M (mitosis) phase, cells divide into two cells, and the cells would enter another cycle.

When cells treated with certain treatments, the cells would stop at a certain cycle phase namely cell cycle arrest. The cell cycle arrest result will provide information about the reaction mechanism between drug treatments and cells. It would provide much help to study the drugs. The whole process needs the DNA of the cells to be labeled and scanned by flow cytometry. By determining the degree of the DNA content, the cell cycle status would be confirmed.

2.2.2.3 Cell Apoptosis Analysis

Another approach that could be applied to the interactions studies is apoptosis analysis^{42,43}. Apoptosis is a process of programmed cell death. There are many biochemical events could lead to cell morphology and death. Cell apoptosis is unstoppable once the procedure begun. Apoptosis can be initiated in two ways, including intrinsic pathway and extrinsic pathway. The intrinsic pathway was the cell dead when the cells sensed pressure. For extrinsic pathway, cells dead when the cells got the signal from other cells. Cell apoptosis study is a method to study the initial of apoptosis. By understanding the apoptosis pathway, we could study the reaction mechanism of the treatments. We could also associate the effects of treatments with their ability in modulating key signaling proteins related to cell proliferation and apoptosis, such as

p21Cip1/Waf1, cyclin-dependent kinase (CDK)-2, CDK-4, phosphor-Rb, Mcl-1, caspases 3 and 8, and PARP. By inducing the apoptosis in cancer cells, it would be an effective method to control cancer cell growth. The apoptosis analysis is still in need of labels with Annexin V and propidium iodide.

2.2.2.4 Western Blot Study

Western blot could study the protein change due to the interactions^{44,45}. The western blot is an analytical technique that had been widely applied to study specific proteins in the cell or tissue sample. To do the western blot analysis, the gel electrophoresis it needed to separate the protein by 3-D structure or denatured protein by the polypeptide length. Then, the target protein would be stained with specific antibodies. As showed in Figure 2.5, with the utilization of western blot, the cell apoptosis analysis could be confirmed, and compare the protein content.

2.2.2.5 ELISA

To further understand the mechanisms, usually conducted inflammation studies. The inflammation studies use the enzyme-linked immunosorbent assay (ELISA) to analyse the protein type and content. ELISA is a method to uses an enzyme immunoassay to detect and identify the presence of a substance^{46,47}. ELISA had high sensitivity and had been widely used in many areas. When performing an ELISA, antigens are attached to a surface then add the specific antibody over the surface to let it

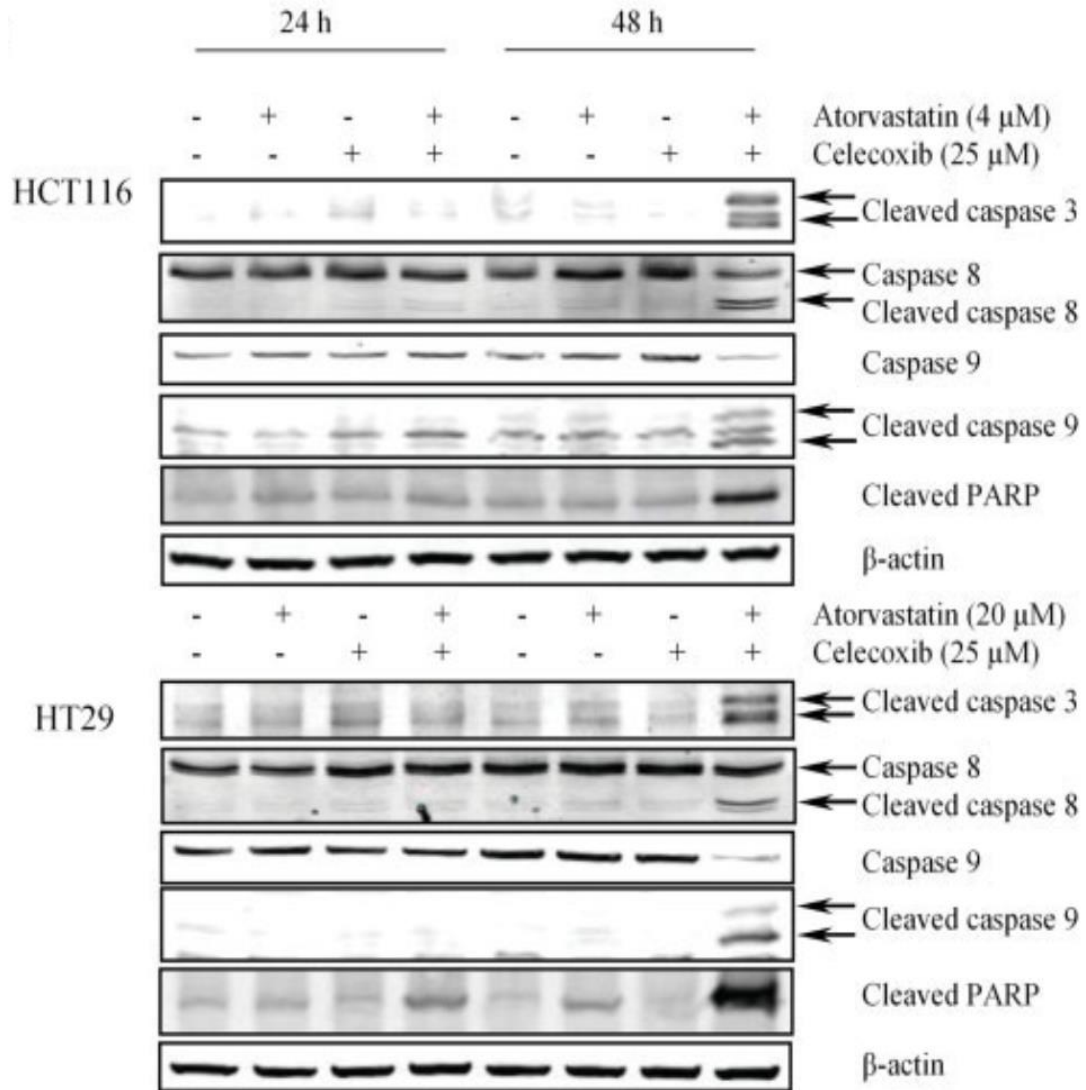


Figure 2.5 Western blot demonstrated that combined treatments with atorvastatin/celecoxib for 48 hr activated caspase cascade. b-Actin served as an equal loading control. The results were representative of 3 experiments.

bind to the antigen. At the other end of the antibody, an enzyme linked. With the enzyme's substrate containing substance added as a final step. In the end, the subsequent reaction would be determined by the substrate color change. Once the mechanism of the bulk cells had been studied and analyzed, usually conduct further researches like transwell study combined with Caco 2 cells.

Based on these biological approaches, there is a fact we found about previous studies was that they usually take cell population into consideration instead of the individual cells^{26,48,49}. The methods including cell viability analysis and synergy, apoptosis cell analyses, and immunoblotting analyses. The results of cell viability⁵⁰ could evaluate the interaction between cells and the treatments by survival percentage. Cell apoptosis⁵¹, which usually combine with Western blotting⁵², is based on the protein production⁵³ (as in Figure 2.6) to predicate the expression of the gene. With all these techniques and many others, we had a general information about how different treatments interacted with the cells as a whole. And after all these bulk cell studies, further studies would be conducted as in a tumor or animals.

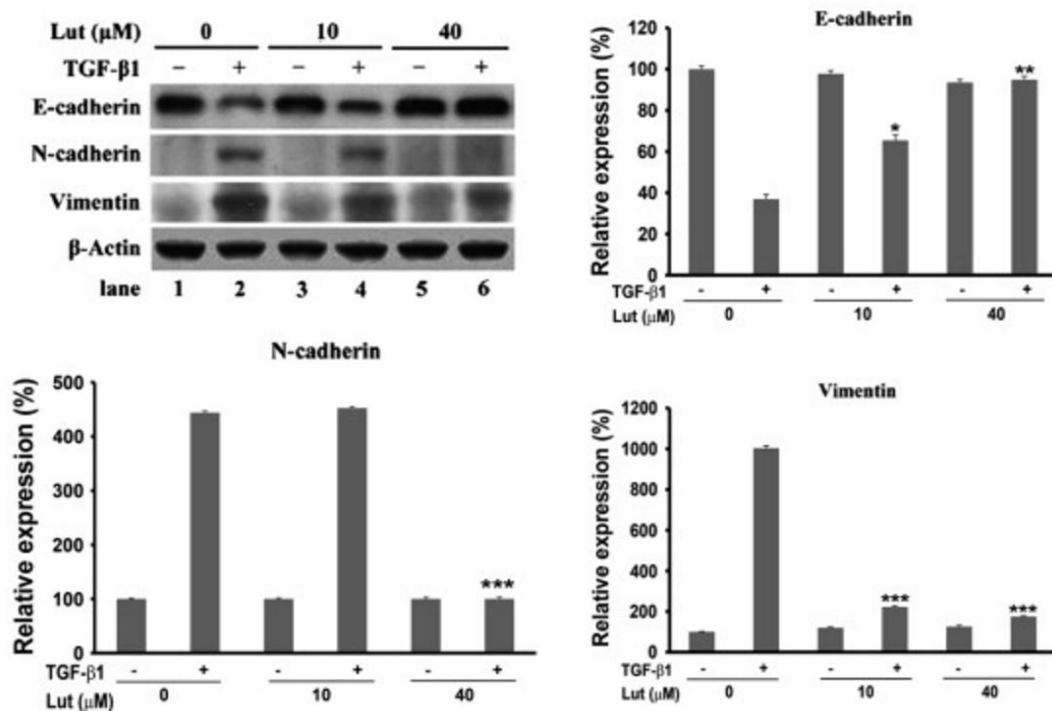


Figure 2.6 Western blot analysis to check EMT-related gene expression. Densitometry shows data from three experiments; the values from each experimental set were normalized with control as related percentage (* $P < 0.05$, ** $P < 0.01$, or *** $P < 0.001$ compared to TGF-β1 treatment alone).

However, instead of going to larger scale, not many researchers going to the smaller scale. The study of single cells seemed did not attract too many attentions. Single cell studies could provide us insight into how individual cells react to the treatment. It would help to study the real reaction mechanism and how the result agrees with the population study including cell chemical profile researches and further more.

2.2.3 Heterogeneity of colorectal cancer

Cancer is the leading death cause for successive years which attracted many scientists being doing research for decades. Though numerous cancer-related studies being published every year, there were no effective methods of inhibiting the new cancer cases and cancer death. One of the great obstacles of defeating cancer is the cell heterogeneity. The heterogeneity of cancer cells makes the cancer study remain to be a big challenge to understand fully cancer cells let alone get rid of them. It is even harder to eliminate all kinds of cancer cells with one kind of treatment. All these researches suggested the potential of dietary consumption of PMFs, especially hydroxylated PMFs, could against lung tumorigenesis and colonic tumorigenesis.

Cell heterogeneity had attracted great interests for a long time, though some of the researches focused on the mammalian sperm⁵⁴ or endothelial lining of blood vessels⁵⁵. The others mainly focused on the heterogeneity of cancer cells. No matter which area, the main challenge would be sorting or identifying the heterogeneous cells and purify the cells into a specific kind. It would be easier to study just one kind at a time than the whole heterogeneous cell population at the same time. Paulsson et al. analyzed some studies critically and came up with an equation that could unify and extend the

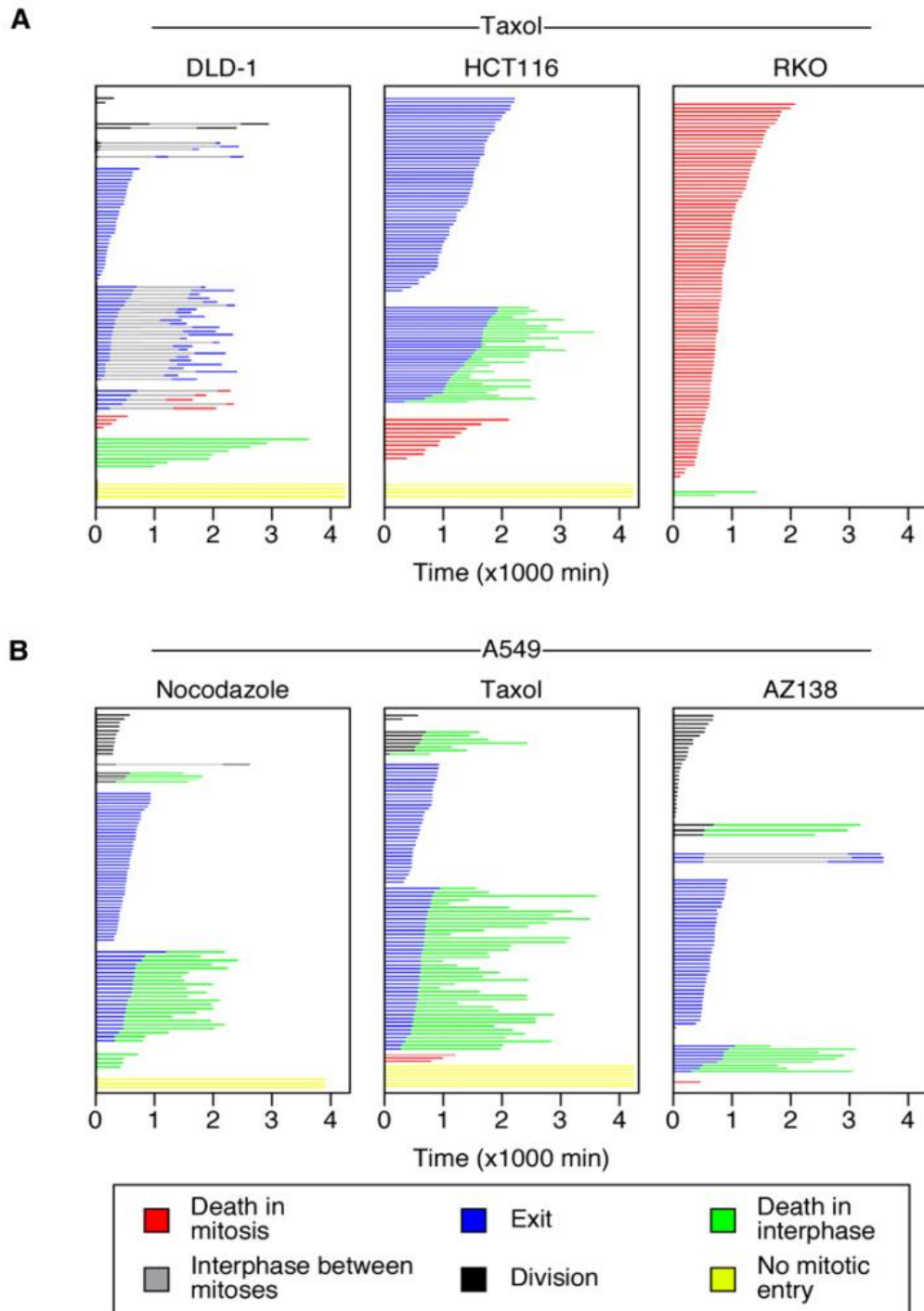


Figure 2.7 Inter- and Intraline Variation (A) Fate profiles of DLD-1, HCT116, and RKO cells following exposure to 0.1 mM taxol. (B) Fate profiles for A549 cells exposed to 30 ng/ml nocodazole, 0.3 mM taxol, and 1 mM AZ138.

perspectives in mathematics and biology.⁵⁶ It is a way to maintain the accuracy of the study result; it is a way to correct the problems caused by the heterogeneity. Colman-

Lerner et al. studied the mechanisms of cell-cell variability and population analysis of yeast⁵⁷. It indicated that better understanding of the cell-to-cell variation mechanisms might help narrow the heterogeneity of cellular responses to an anti-cancer study. He also indicated that variation was mainly from pathway and protein expression instead of expression. His study figured out two mechanisms that regulate cell-to-cell variation in pathway capacity.

Some cancer heterogeneity studies conducted based on the DNA sequencing, as gene transcription, in the tumor specimen. It is believed that better understanding of how genes heterogeneous function in cell population could modulate response to stimuli which might improve cancer healing rate⁵⁸. But the sensitivity of DNA sequencing was limited by the heterogeneity within cancer cell lines. A study conducted by Thomas et al. came up with a micro reactor-based pyrosequencing, with this method, with a specific DNA fragment from samples, he could detect rare cancer⁵⁹. It provided patient more targeted cancer therapies based on the accurate identification of the cell heterogeneous cancer.

Heterogeneity in cell populations came from not only intrinsic but also extrinsic factors. Slack et al. found out that cells heterogeneity was related to the drug's mechanism.⁶⁰ In all cases Snijder et al. analyzed and provided an explanation of the heterogeneous cellular activities.⁶¹ The fate of cancer cells could be studied and plotted in fate profile.⁶² The result indicated that stimuli could induce heterogeneity in intra- and interline (Figure 2.7).

There was still some studies base on the cell morphology^{53,63}, as showed in Figure 2.8, the lower expression of siA1+siA2 could relate most heterogeneity and cell morphology and western blot could help prove it. The direct observation of the cells could provide a clear image of how the cells would change the appearance due to the stimuli.

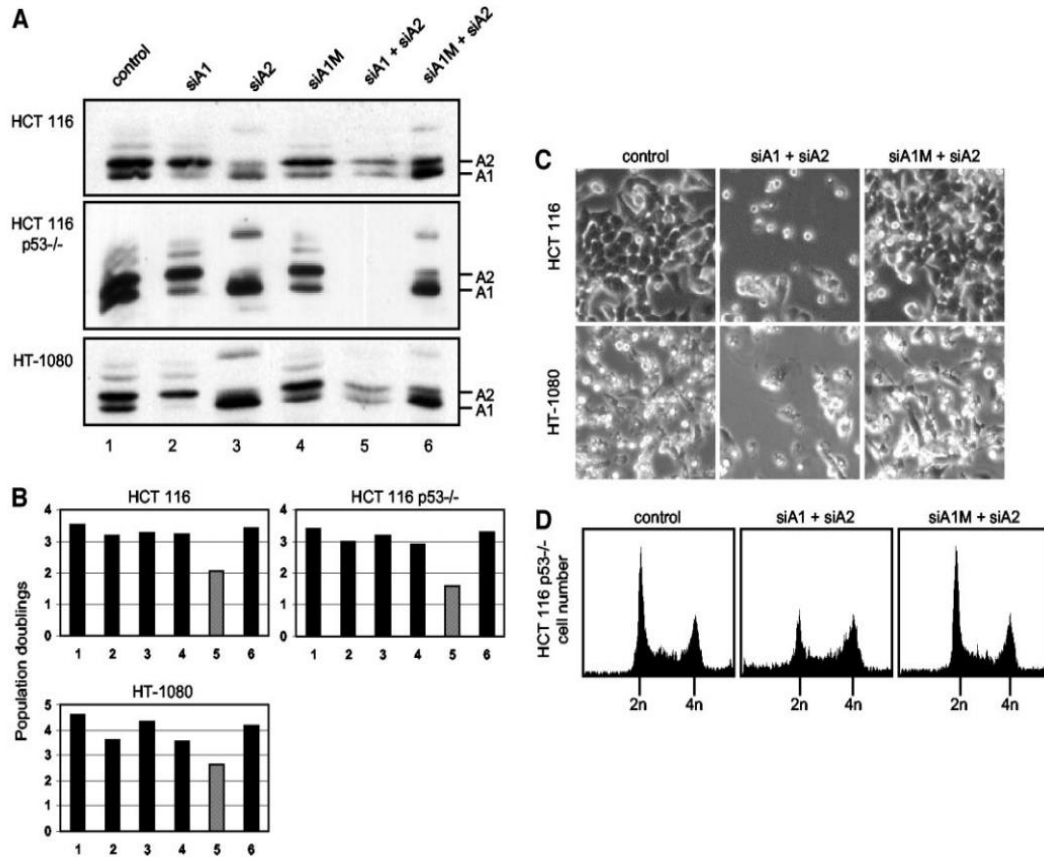


Figure 2.8 Impact of the treatment with siRNAs on HCT 116, HCT 116 p53^{-/-}, and HT-1080 cancer cell lines. **A**, 72 h after transfection, cells were harvested and processed to determine the impact of RNAi on A1 and A2 expression. Western blot analysis was performed with the polyclonal anti-A1/A2 antibody. **B**, effect of the siRNA treatments on cell growth as measured by population doublings. The gray area indicates that cells displayed an altered morphology reminiscent of apoptotic cells. **C**, phase contrast microscopy (magnification, $\times 200$) of cells treated with siRNAs. **D**, the DNA content profile of HCT 116 p53^{-/-} cells treated with siRNAs is shown.

2.3 Colorectal Cancer Stem Cells

2.3.1 Introduction to Colorectal Cancer Stem Cells

There are many reasons that cancer cells are heterogeneous. A possible reason was that the cancer cell clusters contain not only normal cancer cells but also cancer stem cells. Increasingly, scientists started to believe that, like life, cancer starts from a single stem cell. Stem cells are a kind of cells that are equipped with the ability to perpetuate through self-renewal as well as the ability to generate differentiated particular tissue cells. Therefore, cell population became heterogeneous after culture, passage and stimuli. The hierarchical, or cancer stem cell, model predicted that tumours comprised cells with diverse tumour growth potential and that not every cell within a tumour had equal tumour initiation potential and only cancer stem cells are the only cells that contain long-term self-renewal potential, a necessary prerequisite for clonal maintenance⁶⁴. The stem cells, which are not normal cancer bulk cells, required an alternative method to eliminate (Figure 2.9). Normal anti-cancer treatment may not be able to inhibit stem cells. Therefore, the specific study focused on stem cells is necessary and important.

The presence of leukaemia stem cells was widely discussed for years before technological advancements proved their existence. In order to demonstrate that a tumour is organized in a hierarchical manner, it is crucial to purify and assay the distinct cell types functionally. Researchers figured out that when cultured on special media and unattachable plates, cells could generate cell spheres. As shown in Figure 2.10A, the spheres could be generated and after a long time of culturing the cells, the size of the sphere would increase. And the fraction of the CSC would maintain and even increase. We considered it to be an enrichment and purification process⁶⁵. After culturing and passaging the

stem cells several passages, only the stem cell which fits the non-attachable environment the best could remain. Most of the normal cancer cells, though might attach on the stem cells at the first several passaging, would not be maintained in the environment and would be eliminated in the end⁶⁶. But even passaged for many passages, the cells could maintain the stemness (Figure 2.10B).

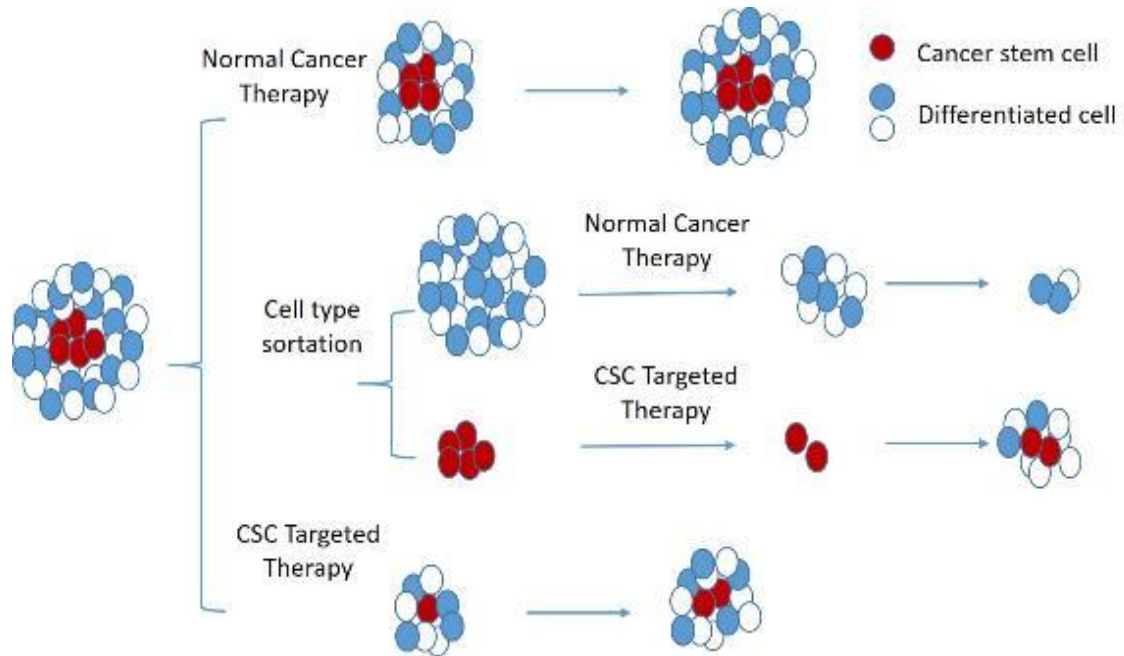


Figure 2.9 The construction of cancer and the therapy results assumptions. Normal cancer treatment could only decrease the number of normal cancer cells. The cells would grow back after certain amount of time. CSC targeted therapy could decrease the number of CSC, decrease the cancer in the long run.

There are still developing ideas about cancer stem cells, including more than one type of stem cells, which makes the study of the stem cells even harder.

2.3.2 Biological Studies of Colorectal Stem Cells

Stem cells though important, but rare in most tissues and cancer population as well. It is hard, though important, to identify and sort stem cells. The process of separating cells based on cell surface marker expression and testing the stemness function of separated cell fractions is considered as a test for the hierarchical model. There are many antibodies believed express differently between stem cells and normal cancer cells. Many kinds of methods are being used to identify and isolate CSC, especially the application of the markers (including phenotypic and functional markers). Studies always consider that the surface markers of the cancer stem cells are different from the normal cancer cells. To effectively sort the cancer stem cells out, unique biomarkers would be needed. Specific

markers could be found to identify and isolate CSC had been widely accepted (Figure 2.10). However, it was still hard to get a combination of markers efficient enough to purify the CSC fraction.⁶⁷ The first cell surface marker applied to isolate colon cancer stem

cell is CD133^{67,68}. Shipitsin et al. first studied the molecular definition of gene expression in the breast cancer

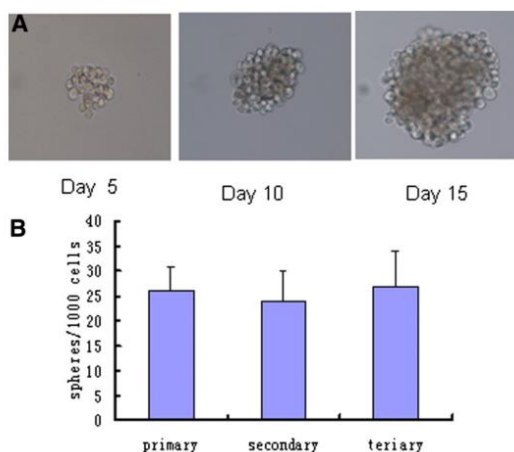


Figure 2.10 Sphere-forming prostate cells generated and passaged in vitro. (A) Spheres in suspension generated from single cells of PC3, imaged on indicated day of culture. (B) PC3 spheres could be serially passage in vitro.

However, take CD133, a five-transmembrane-domain glycoprotein, as an example. Previous studies showed controversial results. Some studies showed great evidence that CD133+ could be an important surface marker to isolate CSC^{71,74}, while many others believed CD133+ was irrelevant to tumor generating^{75,76}. While, CD44+, an adhesion molecule that binds hyaluronate⁷⁷, when combined with the epithelial cell adhesion molecule (EpCAM), also known as epithelial-specific antigen (ESA)⁷⁸, were seemed more robust as markers of CSC than the most reported marker CD133. The activity of aldehyde dehydrogenase isoform 1 (ALDH1) that can be assessed by the ALDE- FLUOR assay has also been identified as a common functional marker of CSC. In breast carcinomas, high ALDH activity identifies the tumorigenic cell fraction, capable of self-renewal and generating tumors that recapitulate the heterogeneity of the parental tumour⁷⁹. As believed that CD133+ cells are tumorigenic, magnetic separation was used in study⁷¹. Label the cells with CD133/1 microbeads, in this way, the magnetic could attract the labeled cells and complete the separation. These surface marker studies, along with other quantitative assays, was widely considered as first purification of cancer stem cells. However, results from the markers CD133 and the others showed the controversial result. Some studies proved the stem cells and the surface marker CD133 or CD44 are not related. Tumor-initiating cells could be found in both CD133+ and CD133- cell fractions⁸⁰.

Instead of trying to find the unique surface markers from the cancer stem cells, some other studies focused on physical properties of stem cell difference. Many researchers had been using density difference to isolate different kinds of cells including T cells⁸¹, animal samples⁸² and even stem cells⁸³. Michael Clarks' group made the first

identification of cancer stem cells in a solid tumour was achieved in human breast cancer⁸⁴. The cancer stem cell subset could be passaged serially. Also the parent tumour derived the histologically heterogeneous xenografts. In another study about separation of bone marrow cells, Rosca et al. applied Percoll discontinuous gradient to do the separation.⁸⁵ A small cell population segregated at density 1.070 g/ml could generate more colonies compared with total bone marrow. These cells were considered to be containing more stem cells. Percoll which is a solution of the silica-based colloidal medium has almost ideal property for density isolation. Percoll solution is non-toxic and ideal ionic strength and pH, which made it great for cell separation. The size of the silica colloidal made it impossible to penetrate into biological membranes could protect the cells from damage. The ability to form both self-generated gradients at moderate centrifugation force could minimize the damage to the fragile samples. After isolation and purification, the Percoll removal procedure is easy which guaranteed the reliability of the result.

The best application of determine the stemness of the cells is by carrying out in vivo limiting dilution assays. The assay enables one to calculate the cancer-initiating cell frequency in the unfractionated colon cancer cells.

Though a large number of researches had been done about cancer stem cells, the isolation and purification of them are still not effective enough. A more reliable method is still in need.

2.4 Raman Microscopy

2.4.1 Introduction of Raman Scattering

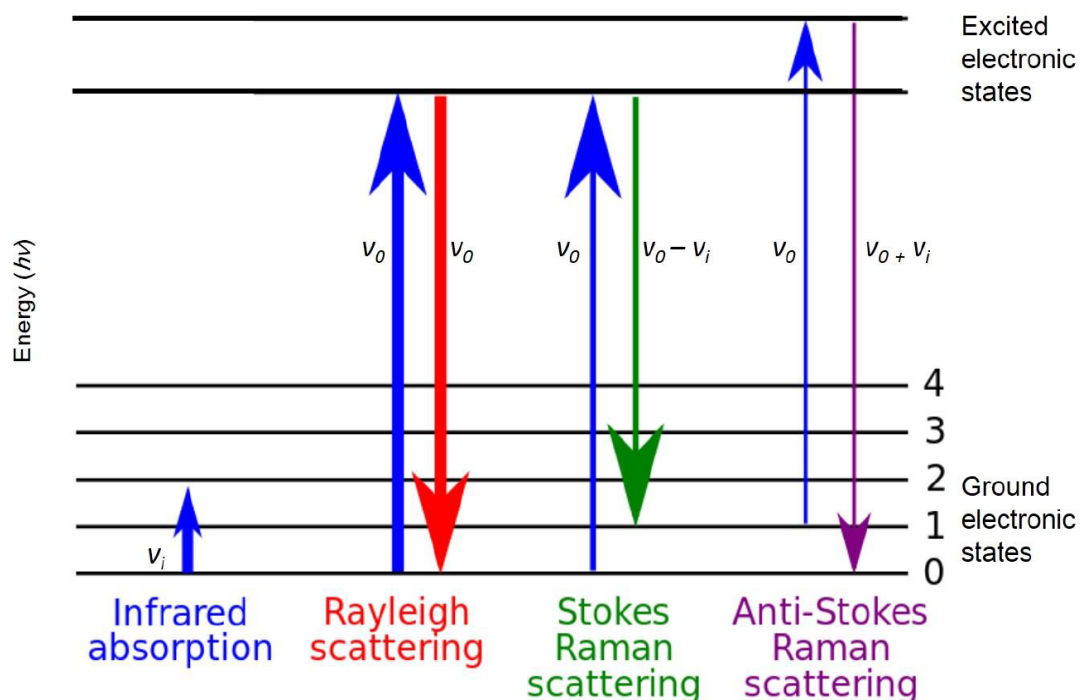


Figure 2.11 The relationship between infrared, Rayleigh scattering and Raman scattering.

The inelastic scattering of light was predicted by Adolf Smekal in 1923 and first observed in 1928. The inelastic scattering was named after one of the discoverers Sir C. V. Raman⁸⁶. The mechanism of Raman scattering is when the laser beam shoots a sample, two kinds of scattering, namely Rayleigh scattering and Raman scattering, would reflect back. The Rayleigh scattering is elastic scattering which means it does not change. However, the Raman scatter is a kind of inelastic scattering as the laser light interacts with molecular from sample and resulted in the shift of wavelength. The reflected Raman scattering carries information of different vibrational modes of a molecule. In this way, Raman spectroscopy offered a unique finger printing technique to characterize sample molecule.

2.4.2 Introduction of Raman Spectroscopy

Raman spectroscopy is based on Raman scattering that can be used for molecular characterization non-destructively and rapidly. Raman spectroscopy and Raman imaging has been shown to be a potential candidate for non-destructive and rapid identification of many compounds. It has been applied in many areas including archaeologically artefacts⁸⁷, drug abuse⁸⁸, crime scenes⁸⁹ and minerals from space mission⁹⁰ to determine the material.⁹¹ It could also be applied in food science including measure lipid oxidation⁹², evaluate microbial⁹³, identify and quantify of food contaminants⁹⁴ and so on. It is of great importance that the non-destructive analysis ability of Raman spectroscopy of biological samples⁹⁵. One of the applications of Raman spectroscopy is to diagnose many severe diseases⁹⁶. Allograft transplantation could be the rescue for patients with failed organs. The acute detection of allograft rejection after transplantation could be determined (Figure 2.12).

Raman spectroscopy could also be applied on a variety of biochemical samples including not only tissues but also single cells⁹⁷. The studies determined the application of human arteries and cancer was dominated by protein bands. And the application on kidney and biliary calculi could determine the stones existence. On hair and nails, Raman spectroscopy could measure metabolic disorders and drug poisoning. Also, Raman spectroscopy could also determine the tooth dentine by the fluorescence properties of demineralized dentine. When applying Raman spectroscopy on implants, prostheses and foreign inclusions, it could predict their long-term performance. Furthermore, Raman

spectroscopy could be applied in many other areas including eyes, single cells, DNA and stratum corneum for accurate and efficient detection.

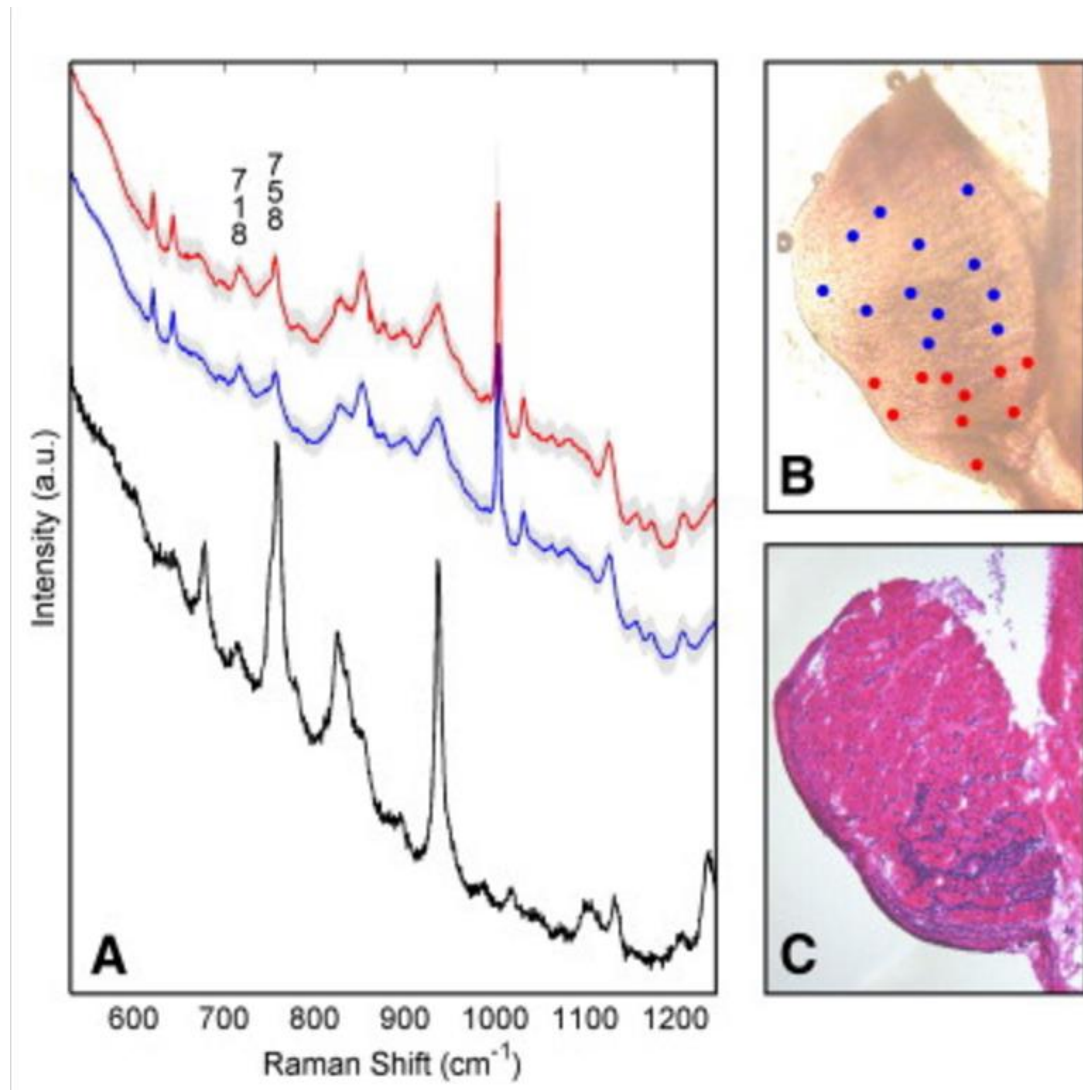


Figure 2.12 A grade 1R (mild rejection) endomyocardial biopsy sample is examined by Raman spectroscopy (A), optical microscope (B), and histopathology (C). Raman spectra are collected at locations marked in , B. Rejected Raman spectra ($I_{758} > I_{718}$) and their corresponding locations are marked in red, and the normal spectra ($I_{758} < I_{718}$) in blue.

2.4.3 Introduction of Raman Microscopy

Microscopy is a technique using microscopes to make naked eyes to view objects that are not within the resolution range of the normal eye. Raman microscopy is a

technique couples with microscopy and Raman spectroscopy and has been widely applied in the detection of the biological sample. It can provide rich biochemical information, such as proteins, peptides, nucleic acids, glucose, lipids and cells, and has been widely accepted as a routine analytical characterization methodology. Furthermore, Raman is also used in the detection of diseases, including various cancers, Alzheimer's disease, and Parkinson's disease.

Raman microscopy is a powerful tool, it could also help characterizing cell samples, tissue samples⁹⁸ and even live animal samples. Studies have applied Raman microscopy on brain or kidney tissues to create a database for future diagnosis⁹⁹. It could detect tumor existence¹⁰⁰ without sacrificing and dissection of the mice.

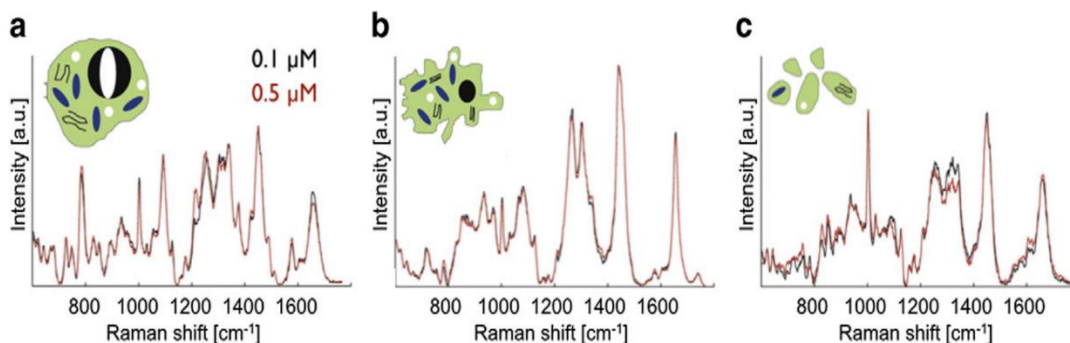


Figure 2.13 Raman spectra of doxorubicin-treated leukemic T cells (Jurkat T cell line), where the cells have been treated with two different concentrations of doxorubicin as indicated in the figure. a) Spectra for cells treated for 24 h are indicative of chromatin condensation. b) Spectra for cells treated for 36 h are indicative of membrane blebbing. c) Spectra for cells treated for 72 h are indicative of apoptotic body formation.

When coming to the cell sample analysis, Raman could characterize the sample individually¹⁰¹. Offered us a different and detailed way to study biology samples. By collecting the sample one spot by another, it could provide a detailed image of the cells¹⁰² with¹⁰³ or without chemical tags¹⁰⁴. Based on the peak assignment as Table 2, we could read information from the Raman spectra.¹⁰⁵ Combined with quartz chips, it could make the identification of cells¹⁰⁶, even by DNA¹⁰⁷.

While applying Raman microscopy on biology study, it could be used to study the interaction between cells, cell heterogeneity¹⁰⁸, and even cell identification¹⁰⁹. After detailed information gathered, we could predict what is going on in the individual cells¹¹⁰. The preparation procedure for Raman microscopy is quite simple. The cancer cells could just grow attached to the surface of gold slides and directly got characterized by Raman microscopy. Even if specific cells cannot grow adherent, they could also be centrifuged and got attached to the gold slides.

2.4.4 Statistical Analysis for Raman Spectral and Images

Multivariate methods have been applied to Raman to identify the relevant spectral features that distinguish sample classes, such as discrimination between peptide, bacterial and viral species, and certain cancer diagnose. Principal component analysis (PCA) is a common method used for building multivariate linear models of complex data sets using orthogonal basis vectors called principal components (PCs). The first PC describes the maximum amount of variance present in the spectral data set, whereas successive PCs describe features contributing progressively smaller variance. Therefore, PCA identifies and extracts major trends within a given spectral data set, which variables contribute most to this difference, and whether those variables contribute in the same way (i.e. are correlated) or independently (i.e. uncorrelated) from each other. To statistically determine the significance of the difference between treatments from the PCA, we introduced the one-way Analysis of Similarity (ANOSIM). ANOSIM is based on the PC score from the PCA to compare the similarity between the treatments. The difference between treatments could be expressed as R-value. The range of R-value is (-1, 1). An R-value >

0.75 indicates clearly difference, R-value > 0.5 indicates difference with some overlapping while an R-value < 0.25 indicates almost no differences, even p-value shows significant difference. R-values below 0 suggest more similarity between groups than within groups and therefore a problem in experiment design.

Raman microscopy could also do the Raman imaging of cells. The chemical images are obtained from a Raman spectral image by assigning each image spot from a set based on a pre-defined class. When collecting the sample from rows and columns of

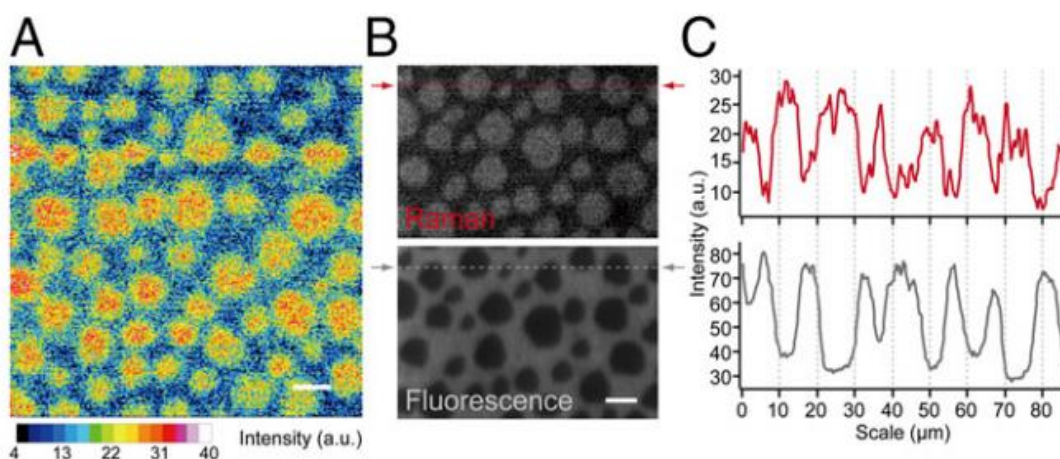


Figure 2.14 (A) High-resolution Raman imaging of a 1:1:1 diyne-SM/DOPC/chol ternary monolayer taken with slit-scanning Raman microscopy. The image was reconstructed using the diyne peak intensity at $2,262\text{ cm}^{-1}$. The images consist of 412×400 pixels. (Scale bar: $10\text{ }\mu\text{m}$.) (B) Raman and fluorescence images of a 1:1:1 diyne-SM/DOPC/chol ternary monolayer containing 0.2 mol% Bodipy-PC. Raman and fluorescence images were obtained in the same imaging area of the same sample. Fluorescence background during Raman imaging was suppressed by photobleaching of Bodipy-PC under 532-nm laser exposure. (C) Line profiles of lipid rafts calculated along the dotted lines of the Raman and fluorescence images in B (red and gray, respectively). The line profile from the Raman image was smoothed using the moving average.

the sample and analyzed with analytical software, a Raman image could be formed. With the image, the contribution and location of certain chemical structure of the sample could be determined and characterized. More detailed information could be revealed.

Raman imaging could be applied on many areas including determine the construction of carbon nanotube networks¹¹¹, crystallization of amorphous drug¹¹² and diagnose cancer¹¹³. High-resolution Raman imaging could be performed to visualize the distribution of diyne-sphingomyelin inside ternary monolayer of cell membrane (Figure 2.14)¹¹⁴. Raman microscopy used in this study was slit-scanning. In this study, the heterogeneous distribution of diyne-sphingomyelin in ordered domains. This study proved the feasibility of applying Raman imaging on cell membrane contribution.

Table 2 Spectral regions with nonoverlapping standard deviations for M1 and MR1 nuclei

Region (cm ⁻¹)	Assignment	Change*	<i>t</i> -test [†]
M1 Nuclei			
653–673	Guanine	Negative	99.0
763–779	Cytosine, uracil	Negative	97.5
789–861	Nucleic acids, protein	Positive	99.5
1000–1009	Phenylalanine	Positive	99.0
1049–1088	Lipid C-C stretch, nucleic acid O-P-O	Positive	99.0
1212–1266	Amide III, nucleic acid O-P-O	Negative	99.5
1278–1293, 1308–1338	CH ₂ twist and bend (protein, lipid), nucleic acids	Negative	95, 99.5
1565–1573	Guanine, adenine	Negative	99.5
MR1 Nuclei			
986–1006	Phenylalanine	Negative	99.0
1089–1111	Nucleic acid O-P-O	Negative	95.0
1229–1264	Amide III, nucleic acid O-P-O	Negative	95.0
1305–1342	CH ₂ twist and bend (protein, lipid), nucleic acids	Negative	99.5
1594–1617	Aromatic amino acids	Negative	95.0
1673–1681	Amide I	Negative	95.0

*The “change” is defined as M1/MR1 plateau minus M1/MR1 exponential nuclei.

[†]The Student’s *t*-test results give the percent of confidence that the means of the spectral regions are different.

CHAPTER 3.

**LABEL-FREE IMAGING AND CHARACTERIZATION OF
CANCER CELL RESPONSES TO
POLYMETHOXYFLAVONES USING RAMAN
MICROSCOPY**

3.1 Introduction

Cellular imaging techniques based on vibrational spectroscopy have become powerful tools in cell biology because the molecular composition of subcellular compartments can be visualized nondestructively and without a chemical label ¹¹⁵. These properties have been highlighted when compared to electron microscopy ¹¹⁶ and fluorescence microscopy that are invasive due to the necessity of fixation and the use of dyes or biomarkers ¹¹⁷. Raman spectroscopy is of particular interest for cellular imaging due to its capacity to monitor live cells in aqueous media ¹¹⁸. Raman imaging could provide the overall biochemical profile (distribution and abundance) of a single cell, including the lipids, proteins, and nucleic acids. Differences in the biochemical profiles are a good basis to distinguish different cells. In addition, the biochemical profile of a cell could change in response to different environmental factors such as cytotoxic agents in a time-dependent and/or a dose-dependent fashion. The changes in cell spectra and images can provide characteristic and predictive information for identification, quantification and

discrimination of the environmental factors. This technique has been used for imaging the distribution of subcellular components ¹¹⁹, differencing among cells ^{109,120}, discriminating different cell cycle phases ¹²¹, *in vivo* tumor detection ¹²², detection, discrimination and quantification of toxins ^{123,124}, evaluation of drugs effects against cancer cells ¹²⁵, characterization of cell responses to chemical and environmental stress ¹²³.

Polymethoxyflavones (PMFs) are a group of bioactive compounds almost exclusively found in the Citrus genus, particularly in the peels of sweet orange and mandarin ¹²⁶. They possess many valuable biological properties such as anti-allergic ¹²⁷, anti-oxidant ⁸, anti-inflammatory ¹²⁸, anti-proliferative ¹²⁹, anti-cancer ²⁵, and anti-bacterial activities. ¹³⁰ Nobiletin (NBT) and its monodemethylated derivative, 5-demethylnobiletin (5DN) have been previously demonstrated to have anticancer activities against Colorectal cancer cells ^{50,131}. 5DN was more potent in growth inhibition of Colorectal cancer cells than NBT ²⁷. A previous study using invasive methods such as cell cycle and apoptosis analysis demonstrated their different modes of actions ⁹. NBT induced G0/G1 cell cycle arrest in HT29 cells. However, this arrest was not accompanied by an increase in apoptosis, indicating a cytostatic effect of NBT ^{22,132}. 5DN, on the other hand, caused cell cycle arrest at G2/M phase in both HT29 and HCT116 cells ²⁵.

In this study, we aimed to use Raman microscopy to characterize the cellular responses of two colorectal cancer cell lines, HT29 and HCT116 to NBT and 5DN at both a single cell and a population level. Live cells in culture media were directly subjected to the Raman microscope analysis. For the first time, we investigated the biochemical profiles of single cells in response to NBT and 5DN. Statistical analysis was conducted to evaluate certain specific marker peaks based on a population of the cancer

cells. The results were also correlated with the results from cell cycle analysis in these two cell lines. This study advanced our understanding of the modes of actions of these two bioactive compounds against cancer cells. To the best of our knowledge, it is the first report that used Raman microscopy to characterize and compare the interactions between human cancer cells and anticancer phytochemicals.

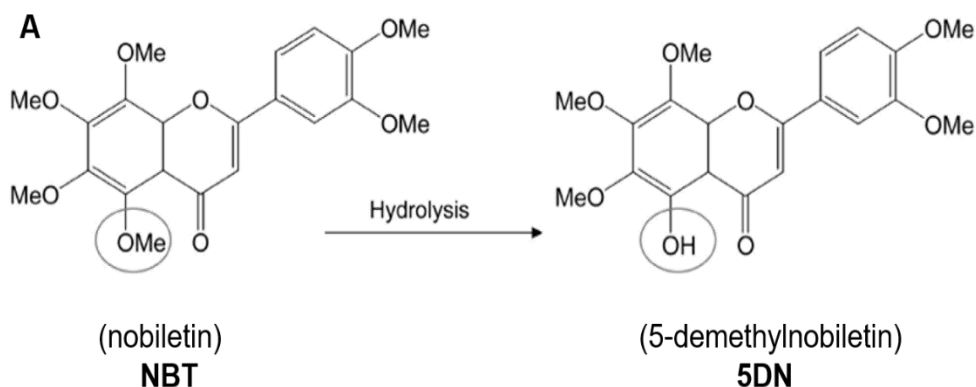


Figure 3.1 A: PMF formula, Nobiletin (NBT) and its metabolize 5-demethylnobiletin (5DN). The 5DN is the hydroxyl-PMF counter part of NBT.

3.2 Materials and Methods

3.2.1 PMFs and cell lines

The isolation of NBT and the synthesis of 5DN were carried out as previously described [1]. The stock solution of NBT was made by dissolving NBT in DMSO to yield a concentration of 100 mM stock. The stock solution of 5DN was made by dissolving 5DN in DMSO to yield a concentration of 20 mM stock. Human colorectal cancer cells (HT29 and HCT116) were purchased from ATCC and cultured in RPMI media supplemented with 5% heat-inactivated FBS 100 U/mL of penicillin, and 0.1 mg/mL of

streptomycin at 37°C with 5% CO₂ and 95% air in the 10 cm petri dishes. All cells used were within 10 to 30 passages.

3.2.2 Cell Treatment for Raman measurement

Before Raman measurement, 10 mL (1×10^4 cells per mL) of cell suspension was transferred to a new petri dish where a gold coated microscopic slide was placed and incubated for 24 hours at 37°C to allow cell attachment on the gold slide. The use of a gold slide was found to greatly enhance the light scattering of the cells and minimize the background noise. The HT29 cells were treated with NBT (100 μ M) or 5DN (20 μ M) for 48 hours. The HCT116 cells were treated with NBT (100 μ M) or 5DN (8 μ M) for 48 hours. The reason to lower the concentration of 5DN was because the HCT116 cells were more sensitive to 5DN. At the time for Raman measurement, the petridish with the gold slide was directly placed under the Raman microscope for analysis.

3.2.3 DXR Raman Microscope

A DXR Raman microscope (Thermo Fisher Scientific, Madison, WI) was used in this study. This instrument facilitates 780 nm excitation and 24 mW laser power through a 60 \times water immersed objective (Olympus, Japan). Aperture was set to be 50 μ m slit, grating 400 lines/mm and the spot size was 1.0 μ m. Each spectrum was acquired in the 400-2000 cm⁻¹ range. The acquisition time was 1s, repeated twice, and the spectrum was averaged automatically by the OMINICS software (Thermo Fisher Scientific). The working distance of the objective lens to the surface of the gold slide was kept

consistently at 1.5mm to minimize the variance caused by the different laser penetration depth in the cells. When collecting spectra from cells, the objective lens would immerse into media containing petridish to keep the cells alive and attached on the gold slide. Cells would be considered alive for detection for an hour.

For single cell imaging, we randomly selected cells within the range of 25 - 35 μm in diameter in each treatment, to minimize the spectral variance due to the different cell sizes. Each treatment was repeated three times independently. Raman mapping was performed by collecting 150 spectra with (or less than) a 5 μm step size over a cell in sequence. The images were integrated based on the Raman spectra at specific peak shifts using the At μ s function in the OMINICS software (Thermo Fisher Scientific). All the spectra were put in the same common scale to compare, no other application, including subtraction, was done.

For cell population analysis, we randomly collected at least 15 spectra from each cell and at least 5 cells were included in the analysis. The spectral data were averaged and further analyzed by principal component analysis using the TQ Analyst software (Thermo Fisher Scientific). Principal component analysis (PCA) is a mathematical procedure that uses orthogonal transformation to convert a set of observations of possibly correlated variables into a set of values of linearly uncorrelated variables called principal components.

3.2.4 Data analysis

Statistics results on the numerical comparison were presented as mean \pm SD in the figures. A one-way ANOVA was used in the study. The Least Significant Difference (LSD) test was used to determine the difference between two data sets. A 0.5% significant level was used for all tests.

To compare spectral data between groups, a one-way ANOSIM (Analysis of Similarity) was used in the study¹³³. The comparison was based on 9999 permutations, the Euclidean distance as the dissimilarity metric and the first three principle component scores (PC1, PC2 and PC3). A 0.01% significant level was used. In ANOSIM, R value measures the difference between two groups under comparison. The range of R-value is (-1, 1). An R-value > 0.75 indicates clearly difference, R-value > 0.5 indicates difference with some overlapping while an R-value < 0.25 indicates almost no differences, even p-value shows significant difference¹³⁴. R-values below 0 suggest more similarity between groups than within groups and therefore a problem in experiment design.

3.2.5 Cell Cycle Analysis

HT29 (1×10^4 cells/well) and HCT116 (1×10^4 cells/well) cells were seeded in 6-well plates. After 24 hours incubation for attachment, the HT29 cells were treated with NBT (100 μ M) or 5DN (20 μ M) and the HCT116 cells were treated with NBT (100 μ M) or 5DN (8 μ M). After another 24 hours, the floating cells and adherent cells, which were detached by brief trypsinization (0.25% trypsin-EDTA; Sigma-Aldrich), were collected. Cell pellets were washed with 1mL of ice-cold PBS and then resuspended in 1mL of 70% ethanol in -20°C for at least 24 hours. After centrifugation (1,600g, 1 min), the

supernatant was removed and cells were incubated with 0.3 mL of PBS containing 30 mg RNase (Sigma-Aldrich) and 3 mg propidium iodide (Sigma-Aldrich) for 30 min at room temperature. Single-cell suspension was generated by gently pipetting. Cell cycle was analyzed using a BD LSR II cell analyzer at the analytical cytometry facility (University of Massachusetts Amherst), and data were processed using Modifit software. Statistics results on the numerical comparison in the figures were presented as mean \pm SD. A one-way ANOVA was used in the study. The Least Significant Difference (LSD) test was used to determine the difference between two data sets. A $p < 0.05$ significant level was used for all tests.

3.3 Results and discussion

3.3.1 Single cell imaging of HT 29 Cells and HCT116 Cells in responses to the treatment with NBT and 5DN

For each treatment (control, NBT-treated, or 5DN-treated), total 15 single living cells (around 25-35 μm in diameter) from both cell types attached on the gold slide were randomly selected under the microscope for Raman mapping. The representative optical images were shown in Figure 3.2. Their corresponding Raman images were showed in Figure 3.3 and Figure 3.4. For one cell, three Raman images were obtained by integrating over the lipid (CH₂ twist) at peak 1301 cm^{-1} , protein (Symmetric ring breathing) at peak 1005 cm^{-1} and the O–P–O stretching of the DNA backbone at peak 1095 cm^{-1} . These peaks were chosen to represent the macromolecules in cells due to the general agreement of the peak assignments by previous studies¹²⁵. The cell images not only demonstrated

the distribution of the biomolecules but also indicated the relative abundance of the biomolecules.

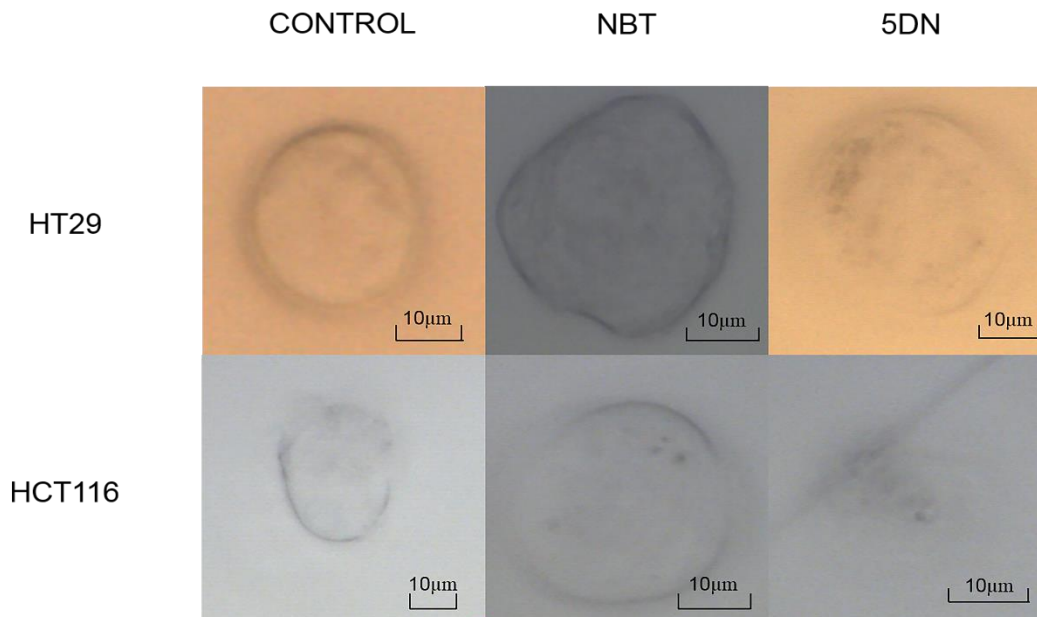


Figure 3.2 Corresponding cellular optical images of the HT29 and HCT116 chosen for the Raman images of control or after treated with NBT (100µM) and 5DN (20µM for HT29 and 8µM for HCT116) for 48H.

When treating with NBT, HT29 cells and HCT116 cells showed similar results. (Fig. 1B and Fig.4, more cell images were shown in Fig. S2), it can be observed that the intensity of signals for the lipid, protein and nucleic acid in the treated cells were all significantly lower than the control cells. However, very different responses were observed from the HCT116 cells treated with 8 µM of 5DN compared to 20 µM of 5DN treated HT29 cells. Localized higher signal of lipid was observed. The high intensity of lipid was not found in the central region of the cells as in the control cells, but close to the outline region of the cells. The protein signal in cells treated with 5DN decreased, but not as much as that induced by NBT. The intensity of nucleic acid was not significantly different between 5DN-treated cells and control cells. Furthermore, HCT116 cells were

found to be more sensitive to 5DN than HT29 cells. Because, even at the reduced dose of the 5DN (8 μM), the HCT116 cells had a stronger response, evidenced by the distorted cell structure.

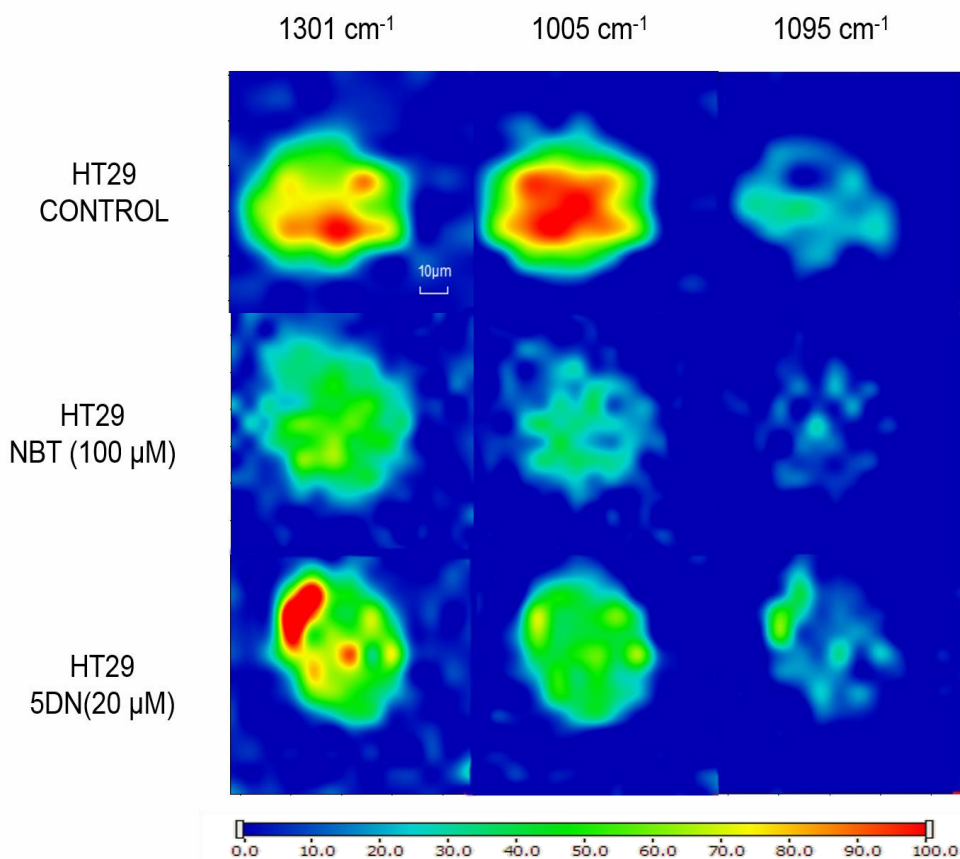


Figure 3.3 Raman images of the HT29 cells obtained by integrating over the CH₂ twist (lipid) at peak 1301 cm^{-1} , over Sym. Ring br Phe (protein) at peak 1005 cm^{-1} , and O-P-O stretching of the DNA backbone at peak 1095 cm^{-1}

These differences clearly demonstrated the different cellular responses of cells to NBT and 5DN. We speculated that the treatment of NBT might result in inhibition of the DNA replication, and reduction of synthesis of cellular proteins, thus reducing the signals of the overall macromolecules overtime. On the other hand, 5DN may interact with the lipid and cause damage to the membrane, but may not act on nucleic acids. Draux et al

(2011) used Raman microscopy to probe the effects of an anti-cancer drug, gemcitabine on lung cancer cells. It was found that gemcitabine caused the decrease of nucleic acids, which was compatible with the mode of action of the drug that was inhibition of DNA replication and RNA synthesis.

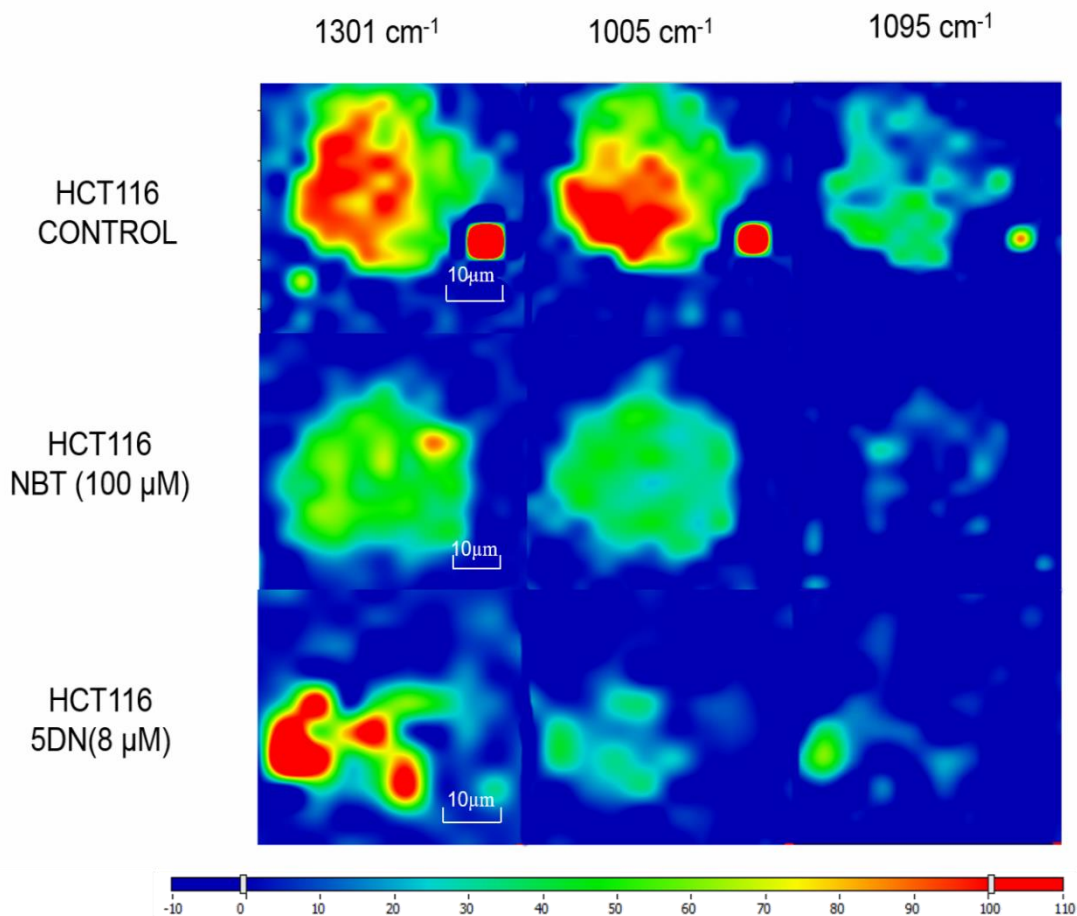


Figure 3.4 Raman images of the HCT116 cells obtained by integrating over the CH₂ twist (lipid) at peak 1301 cm⁻¹, over Sym. Ring br Phe (protein) at peak 1005 cm⁻¹ and O–P–O stretching of the DNA backbone at peak 1095 cm⁻¹. The red spots in the HCT 116 images were likely from the impurity on the gold slide.

Comparing the images obtained from the control cells and the cells treated with 100 μM of NBT (Figure 3.3 and Figure 3.4 and Figure 3.5), it can be observed that the intensity of signals for the lipid, protein and nucleic acid in the treated cells were all lower than that of the control cells. Very different responses were observed for the cells

treated with 20 μM of 5DN. For example, localized higher signal for lipid was observed. The high intensity of lipid was not found in the central region of the cells as in the control cells, but close to the outline region of the cells. The protein signal in cells treated with 5DN decreased but not as much as that induced by NBT. No significant difference was found in the intensity of signals from nucleic acids between 5DN-treated cells and the

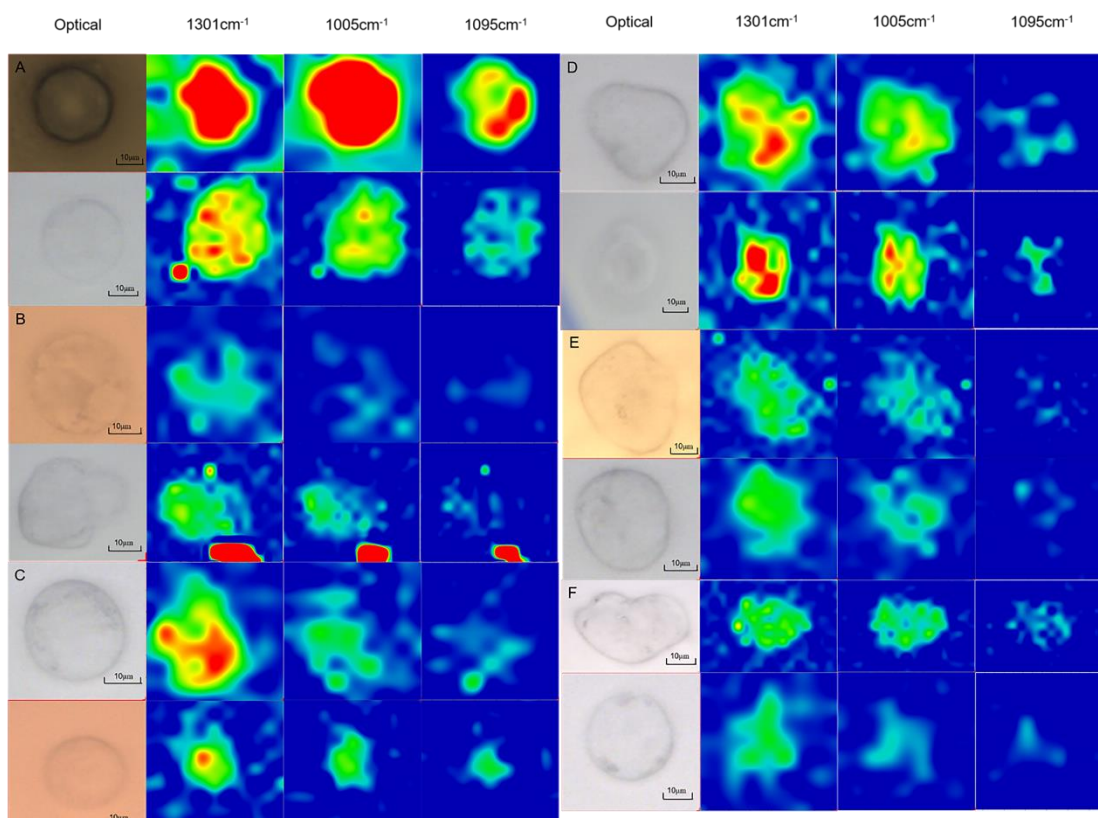


Figure 3.5 Cellular optical images and corresponding Raman images of the HT29 and HCT116 chosen for the Raman images of control (A: HT29 cells, D: HCT116 cells) or after treated with NBT (B: 100 μM for HT29 cells, E: 100 μM for HCT116 cells) and 5DN (C: 20 μM for HT29 ,F: 8 μM for HCT116) for 48H. Raman images cells obtained by integrating over the CH₂ twist (lipid) at peak 1301 cm⁻¹, over Sym. Ring br Phe (protein) at peak 1005 cm⁻¹ and O–P–O stretching of the DNA backbone at peak 1095 cm⁻¹. The red spots in the images were likely from the impurity on the gold slide.

control cells. These differences clearly demonstrated the different cellular responses of the HT29 cells to NBT and 5DN. We speculated that the treatment of NBT resulted in inhibition of the DNA replication, and reduction of synthesis of cellular proteins, thus

reducing the signals of the overall macromolecules overtime. On the other hand, 5DN may interact with the lipid membrane and cause damage to the membrane, but may not act on nucleic acids. Draux et al (2011) used Raman microscopy to probe the effects of an anti-cancer drug, gemcitabine on lung cancer cells. It was found that gemcitabine caused the decrease of nucleic acids, which was compatible with the mode of action of

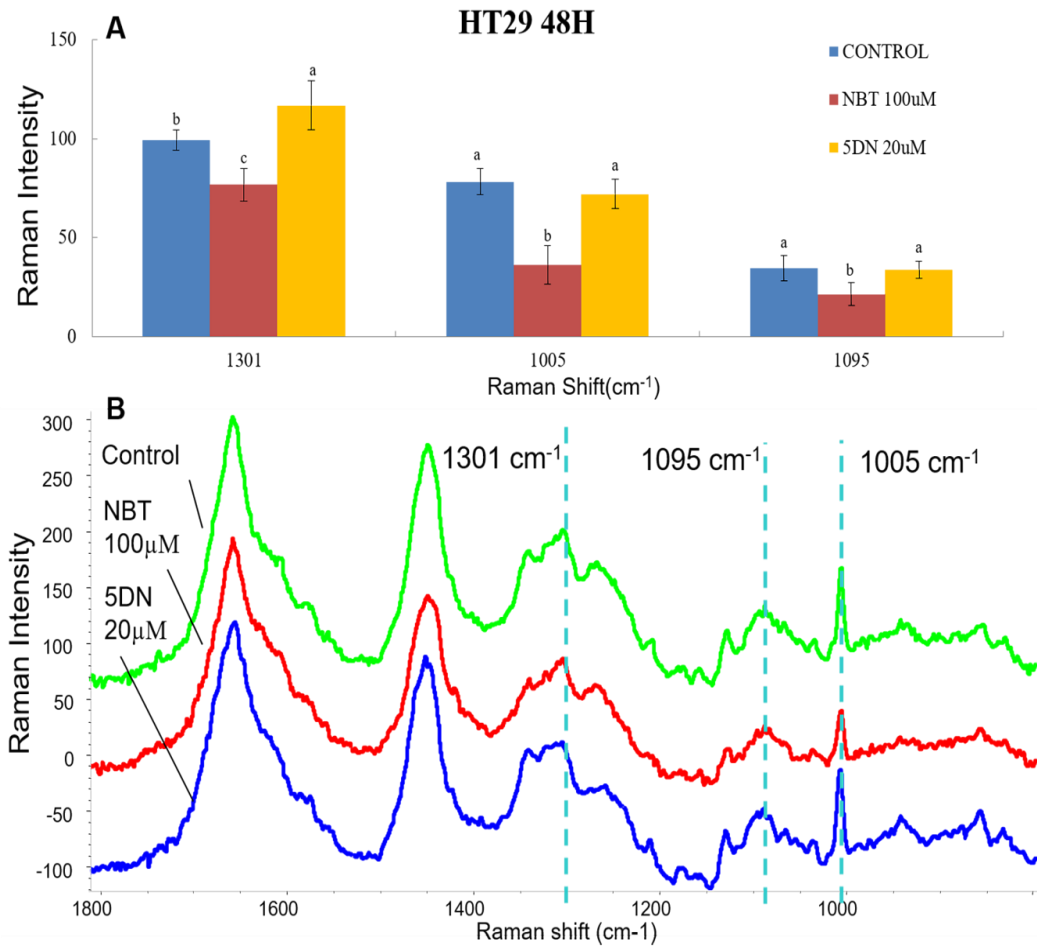


Figure 3.6 Raman intensity analysis of the Raman shift at 1301 cm⁻¹ (lipid), 1005 cm⁻¹ (protein), 1095 cm⁻¹ (nucleic acids) of a population of control HT29 cells, and cells after treatment with NBT and 5DN. A: Statistical analysis was conducted among control and treated cells, and different notations in the bar charts indicate statistical significance. All data represented mean ± SD (n = 75). Different characters represented a significant difference (p < 0.05) within the same category. B: Raman spectra of the control and treated cells, and different vertical dash lines marked different Raman shift.

the drug that was inhibition of DNA replication and RNA synthesis.

3.3.2 Cell population analysis of HT29 Cells in responses to the treatment with NBT and 5DN

To ensure that the observed phenomena were not specific to individual cancer cells, we performed a population study. The intensity of the marker peaks was shown in Figure 3.6. Basically, the results from the population study were in a good agreement with those from the single cell study. Among the NBT treated cells, there was a significant decrease in the intensity of lipid, protein, and nucleic acid signal compared to the control cells. For 5DN treated cells, the intensity of the lipid signal was statistically stronger than that from the control cells, and the variance of the lipid peak was relatively large, indicating the distribution of the lipid signal intensity has a larger variance. There was no statistical difference between the signal intensity of protein and nucleic acid in 5DN-treated cells and that of the control cells. The population analysis results confirmed that the Raman image analysis from single cells was representative and the difference observed between different images were statistically significant at the population level.

3.3.3 Cell cycle study of HT29 Cells in responses to the treatment with NBT and 5DN

Cell cycle analysis by flow cytometry was conducted on the cells treated with NBT and 5DN. The results demonstrated that NBT and 5DN produced different effects on the cell cycle of HT29 cells, which indicated that the two compounds may act through different mechanisms. As shown in Figure 3.7, the cell population increased at the G₀/G₁

phase after treatment with NBT. In the meantime, a significant decrease in cell population was observed in both S phase and G2/M phases. These results suggested that NBT caused cell cycle arrest at G0/G1 phase in the HT 29 cells. On the other hand, 5DN caused a slight increase in the cell population at the G2/M phase, which suggests that 5DN led to G2/M phase arrest.

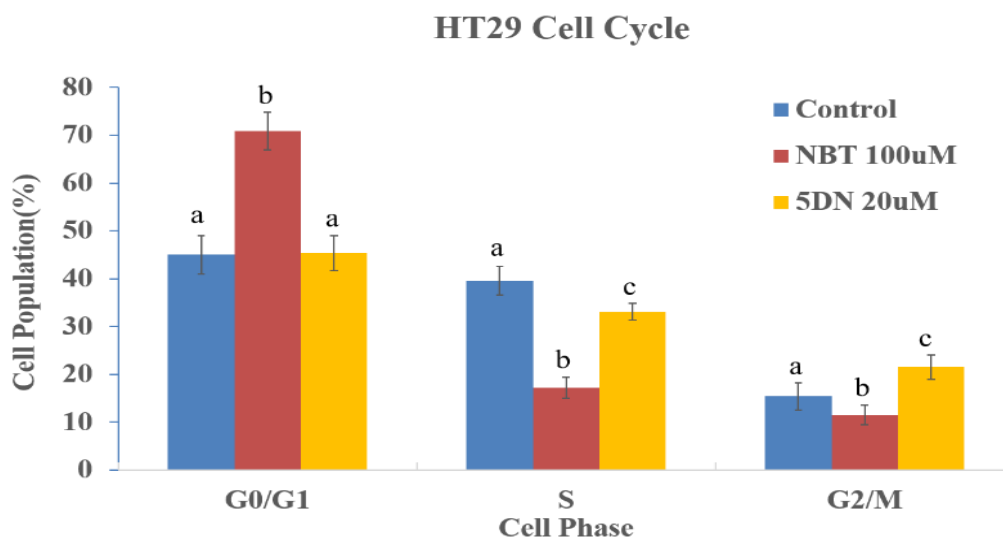


Figure 3.7 Cell population analysis of the HT29 cell cycle after treatments with NBT and 5DN by flow cytometry. Statistical analysis was conducted among control and treated groups in G0/G1, S, and G2/M phases separately, and different notations in the bar charts indicate statistical significance. All data represented mean \pm SD (n = 3). Different characters represented a significant difference ($p < 0.05$) within the same category.

The results from cell cycle analysis were in agreement with our speculations based on the Raman cell imaging analysis. In the G0/G1 phase, cells are growing and preparing for the DNA replication. In the S phase, the DNA replication occurs, which will result in the significant increase of the DNA content. In the G2/M phase, the cells divide into two daughter cells^{118,135}. NBT treatment arrested the cell at G0/G1 phase, and NBT-treated cells have difficulty to enter the S phase. This may be caused by inhibition of DNA replication. Over time, this may lead to a decrease of the cellular protein and

lipid content. 5DN led to the G2/M phase cell cycle arrest, which supported the speculation that the 5DN may cause damage in the lipid membrane so that the cell division interfered.

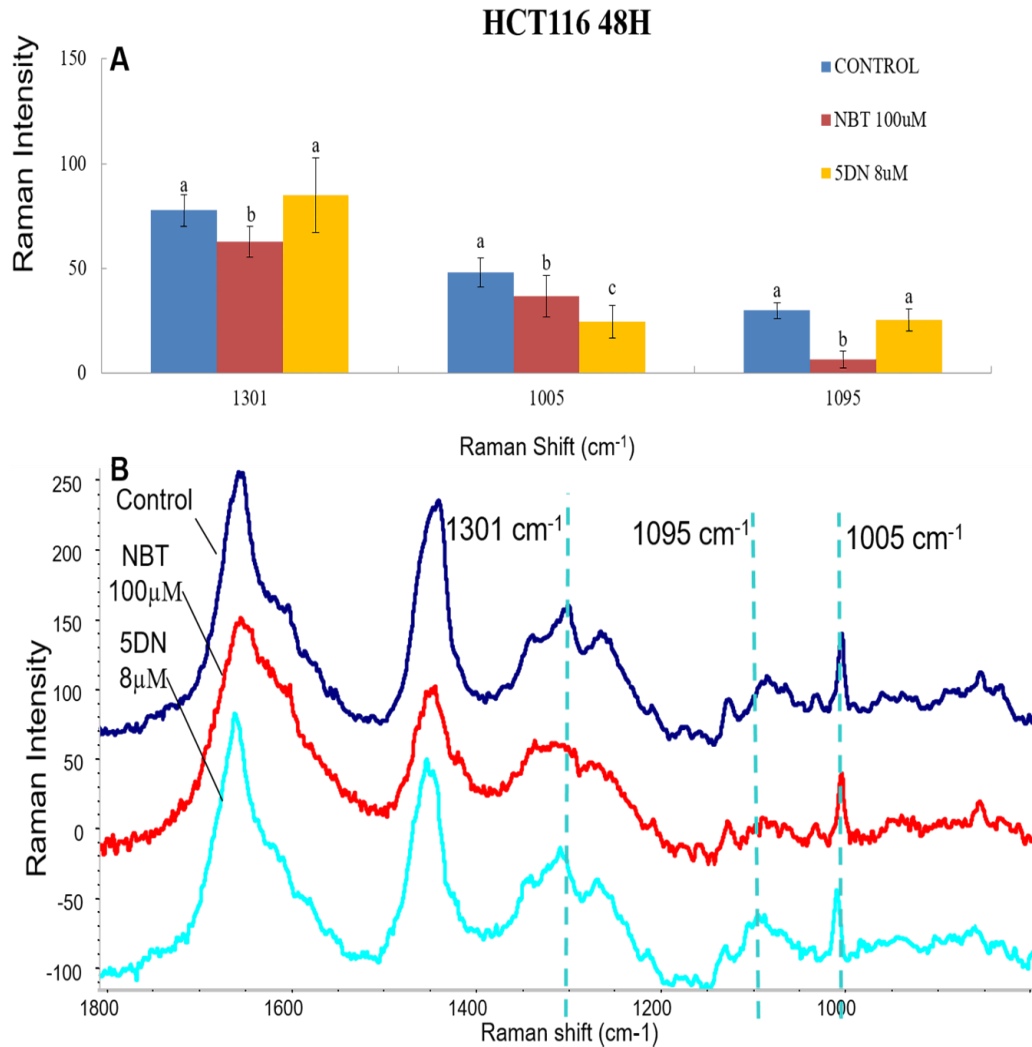


Figure 3.8 Raman intensity analysis of the Raman shift at 1301 cm⁻¹ (lipid), 1005 cm⁻¹ (protein), 1095 cm⁻¹ (nucleic acids) of a population of control HCT 116 cells, and cells after treated with NBT and 5DN. A: Statistical analysis was conducted among control and treated cells, and different notations in the bar charts indicate statistical significance. All data represented mean \pm SD (n = 75). Different characters represented a significant difference (p < 0.05) within the same category. B: Raman spectra of the control and treated cells, and different vertical dash lines marked different Raman shift.

3.3.4 Raman and cell cycle study of HCT116 cells treated by NBT and 5DN

The similar experiment was conducted on the HCT116 cells. NBT induced the similar cellular response of HCT116 cells compared with the HT29 cells, where the overall signal intensity of lipid, protein, and nucleic acid were all reduced (Figure 3.4). The HCT116 cells were found to be more sensitive to 5DN. For example, even at the reduced dose of the 5DN (8 μ M), the HCT116 cells had a stronger response, evidenced by the distorted cell structure. Similar to the HT29 cells, the lipid intensity of the 5DN-treated HCT116 cells were much higher than that of the control cells, and no difference was observed in the nucleic acid signal intensity between 5DN-treated cells and the control. However, the protein intensity of 5DN-treated cells was lower than that of the control cells. At the population level (Figure 3.8), the results further demonstrated the difference observed in the single cell imaging was meaningful. Flow cytometry analysis of the HCT116 cells showed the similar trends as the HT29 cells. The cell population increased at the G0/G1 phase after treatment with NBT, which indicates the NBT caused cell cycle arrest at G0/G1 phase. In contrast, 5DN treatment resulted in G2/M phase arrest in HCT116 cells, and the extent of the cell cycle arrest in HCT116 cells was stronger than that of 5DN-treated HT29 cells. These results again demonstrated that HCT116 cells were more sensitive to 5DN compared with the HT29 cells. The cell cycle data (Figure 3.9) well supported the cell image data. The significant cell arrest at the G2/M phase caused by 5DN supported the speculation that 5DN at this concentration

may cause damage to the cell membrane that in turn may interfere cell division during the G2/M phase.

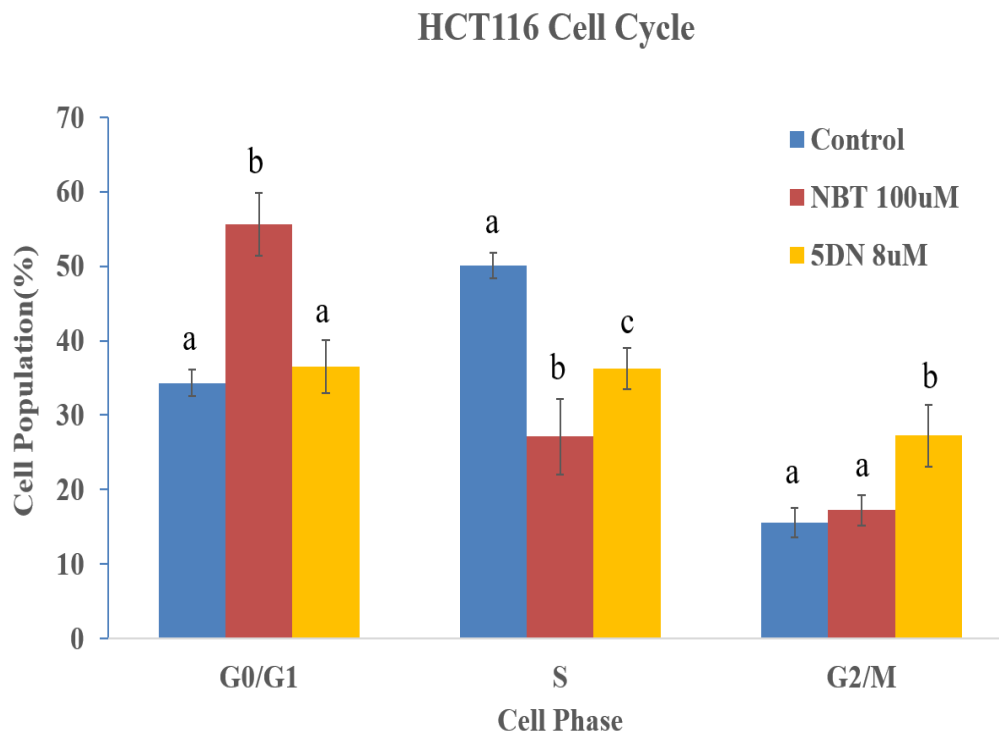
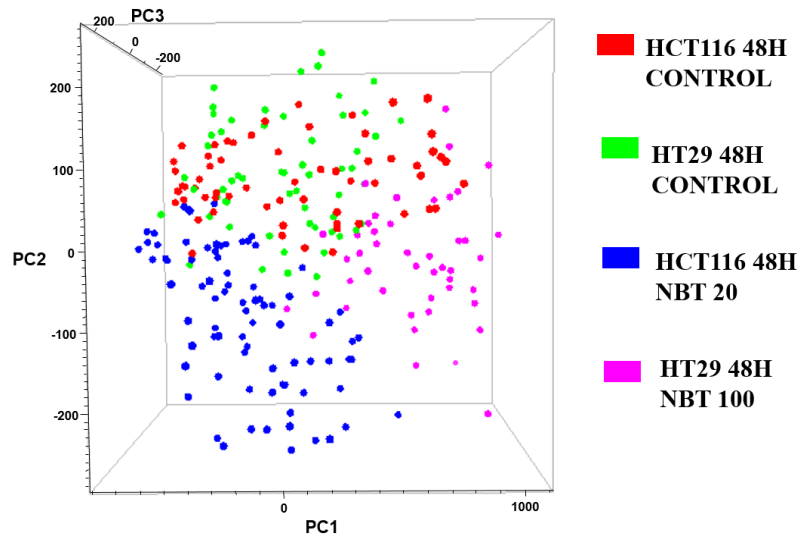


Figure 3.9 Cell population analysis of the HCT116 cell cycle after treatments with NBT and 5DN by flow cytometry. Statistical analysis was conducted among control and treated groups in G0/G1, S, and G2/M phases separately, and different notations in the bar charts indicate statistical significance. All data represented mean \pm SD (n = 3). Different characters represented a significant difference ($p < 0.05$) within the same category.

3.3.5 PCA analysis of the cellular responses of HT29 and HCT116 cells

PCA is a common method for analyzing the overall spectral variance of the Raman data. Generally speaking, if there is no overlapping between the data cluster, then it means the spectra are significantly different from each other. In the PCA plot (Figure 3.10), the control cell data clusters for HT29 and HCT116 were separated, which means the spectral characteristics of these two cells were different due to its different

biochemical profiles. After treatment with NBT, the data clusters of treated cells were both separated from the control cells, indicating a significant difference in the overall spectral characteristics after the treatments. The distance of the two data clusters can be relative compared. The difference between the HCT116 control data cluster and the treated data cluster was greater than that of the HT29 cells. It demonstrated that the



ANOSIM Result of PCA				
	HCT116 48H CON	HCT116 48H NBT	HT29 48H CON	HT29 48H NBT
HCT116 CON	NA	0.3122	0.09446	0.3424
HCT116 48H NBT	0.3122	NA	0.3276	0.7268
HT29 48H CON	0.09446	0.3276	NA	0.2916
HT29 48H NBT	0.3424	0.7268	0.2916	NA

Figure 3.10 The 3D PCA plot of the control HT29 and HCT116 cells and treated with NBT 100 μ M for 48h and the ANOSIM result based on the PCA plot. PC 1 explained 71.64% of the total data variance and the PC 2 explained 8.83% of the total data variance and the p-value < 0.01%

HCT116 cells showed stronger cellular responses to the treatment with NBT than the HT29 cells.

From ANOSIM result, R-value between HT29 and HCT116 control cells is 0.07117 which is <0.25 , indicated a slight difference between the two kinds of cancer cells. The PCA result showed the similar result -- the PC1-PC2 dimension (Figure 3.10) showed the control cell data clusters of HT29 and HCT116 were mostly overlapped, while in the PC1-PC3 dimension (Figure 3.11) the control cell clusters were set apart. This indicated the spectral characteristics of these two cells were similar to each other in general with a slight difference. After being treated with NBT for 48H, compared to the corresponding control samples, both HT29($R=0.2819$) and HCT116($R=0.2871$) cells were induced difference. The PCA plot agrees with the ANOSIM result but the PCA plot also shows the HCT116 cells cluster and the HT29 cells moved towards different

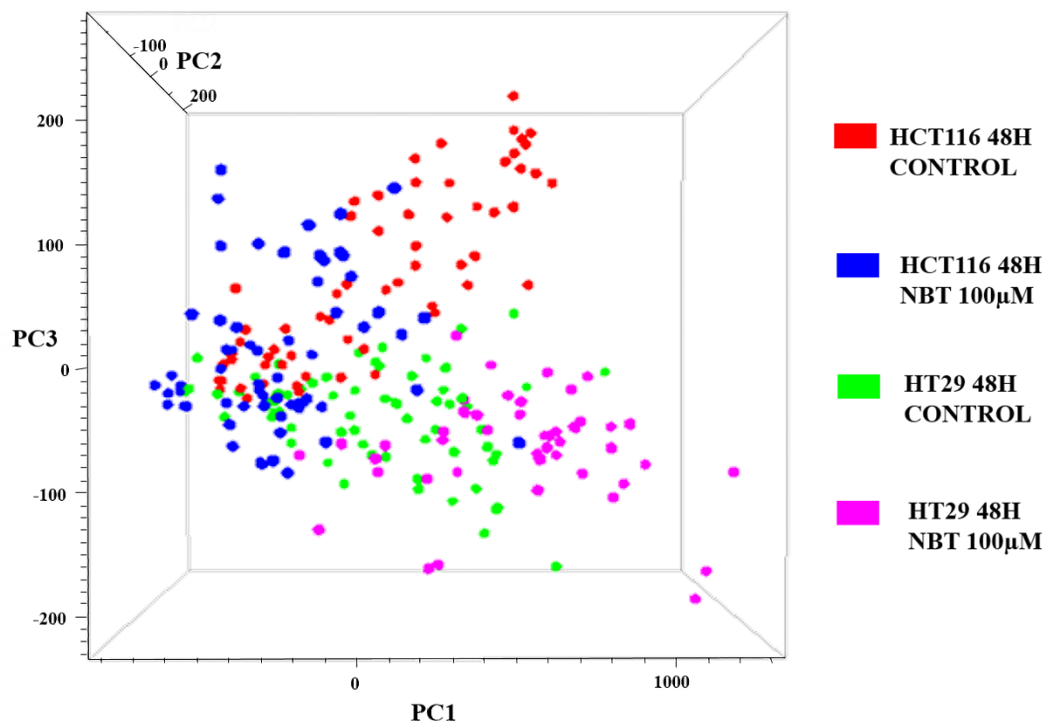


Figure 3.11 The 3D PCA plot of the control HT29 and HCT116 cells and treated with NBT 100 µM for 48h. PC 1 explained 71.64% of the total data variance and the PC 3 explained 2.56% of the total data variance.

direction along the PC1 axis. Both PCA plot and ANOSIM result reflected the difference

between the two colon cancer cells in response to the same treatments. This also validated the result of the Raman image study and the cell cycle study.

3.4 Conclusions

In conclusion, we utilized Raman microscopy to noninvasively characterize and compare two types of colorectal cancer cells responding to the treatments with two PMFs (i.e. NBT and 5DN). By evaluating at both single cell and cell population levels, we found that NBT induced more change in the nucleic acid peak intensity in the cell spectra in comparison with 5DN, while 5DN induced more changes in the localized lipid peak intensity than NBT, indicating the different modes of actions of these two PMFs against colorectal cancer cells. Supported by the results of the flow cytometry study, our data suggested that NBT may interfere DNA synthesis, while 5DN may alter the cellular lipids. HCT116 cells were more sensitive to both PMFs than HT29 cells. Overall, this study advanced our understanding of the modes of inhibitory actions of NBT and 5DN against human colorectal cancer cells. This study also demonstrated the feasibility of using Raman microscopy to label-free image and characterize cancer cell responses to anticancer agents, which could be extended to study other cell-drug interactions.

CHAPTER 4.

CHARACTERIZING HETEROGENEOUS CELLULAR RESPONSES TO POLYMETHOXYFLAVONES USING RAMAN MICROSCOPY

4.1 Introduction

Nowadays, most of the approaches focusing on anti-cancer drugs were based on the population study and data collected by population averaged methods including MTT assay, cell cycle analysis, cell apoptosis analysis etc.¹³⁶ The population study could provide average information about the cellular responses to the perturbations. However, the cells away from the average still occupied eminent portion.¹³⁷ The heterogeneity would always be considered as noise⁵⁶, intrinsic noise due to the random difference from cellular individual molecules, and extrinsic noise due to environment fluctuations⁶¹. The misapplication of ignorant the minority cells might result in the unreliable prediction.¹³⁸ What if the aspects we ignored was the real reason of the varieties?¹³⁹ Besides, many studies confirmed the significant heterogeneous within cancer cell population.¹⁴⁰ The whole population distribution is crucial to the final result. Due to the difference between the cells, variety cellular responses and functional differences were induced. Various studies were focused on the heterogeneity already, which made it important to detect the

heterogeneity of the cancer cells before and after each study. The heterogeneity determination could help decide when the variation could not be neglected.

The detection of heterogeneity was mostly at a high resolution of single cells. The difference could be verified from cell composition. Some cell heterogeneity study had been done in some specific areas like mammalian fertility⁵⁴, skeletal muscle heterogeneity¹⁴¹ and preimplantation embryo development.¹⁴² Many techniques had been applied on characterizing the cells like fluoresce labeled image^{143,144}, and many others including combine other techniques like protein concentration determination, subcellular protein fractionation or western blot¹⁴⁵. All these techniques are mainly focused on the protein changes which always generated by DNA change⁶⁹. The lipid change and cell structure¹⁴⁶ change had also been studied as the signal of the diversity¹⁴⁷. It is important to take all the aspects into consideration. However, all the current methods required complicated chemical analysis methods.

Raman spectroscopy is a fast developing instrument and gaining more and more attention from diverse fields, including diagnosis¹⁴⁸ of tumor and cell image¹⁴⁹. The spectra provided by Raman spectroscopy could tell the details about how cells interact with the drugs¹⁴⁹, and how much damaged caused by the drugs¹⁵⁰. The difference in cell structure between control cells and treated cells would be easy to be recognized using Raman spectroscopy.

The treatments we applied in this study were nobiletin and 5DN. Nobiletin is considered one of the most abundant flavonoids in the citrus genus and ubiquitous in citrus peels with large percentage content¹⁵¹. There are tremendous scientific findings and evidence supported its biological activities including inhibition of inflammation, anti-

cancer, and prevention of metabolic syndrome^{25,152} etc. Nobiletin's biotransformation plays a major role in the biological effects and has been studied extensively recently. One of the nobiletin's major metabolites was 5DN.²¹ Nobiletin and its metabolites 5DN have great potential to become efficacious therapeutics for human diseases. After treated with nobiletin or 5DN, some cells would be floating from the original attached to the petri-dish state. Due to the fact they were already distinctive from the attached cells, these floating cells were collected and studied separately.

Our study provided an innovative and fast method to verify the heterogeneity of the cell lines after the treatment. The straightforward result made it clear why and how the treatment altered the cells. It could provide researchers with a big picture of how the heterogeneity was induced.

4.2 Materials and Methods

4.2.1 PMFs and cell lines

The isolation of nobiletin (NBT) and the synthesis of 5DN were described previously.⁹ Briefly, the stock solution of nobiletin was carried out by dissolving high concentration nobiletin in DMSO to yield a concentration of 100mM. The stock solution of 5DN was made by dissolving high concentrated 5DN in DMSO to yield a concentration of 20mM. Human colorectal cancer cells HT29 was purchased from ATCC and cultured in RPMI media supplemented with 5% heat-inactivated FBS 100 U/mL of penicillin, and 0.1 mg/mL of streptomycin at 37°C with 5% CO₂ and 95% air in the 10cm petri dishes. All cells used fell within 10 to 30 passages.

4.2.2 Cell Treatment for Raman measurement

Before Raman measurement, 2 mL (1×10^4 cells per mL) of cell suspension was transferred to a new 6-well petri dish and incubated for 48 hours at 37°C. The cells were treated with NBT (100 μ M) or 5DN (20 μ M) for 24 hours, 48 hours and 72 hours. By collecting the media, which contains the floating cells, would be treated as the floating sample. Trypsin down the attached cells and collect as the attached sample. Centrifuge the samples separately on the gold slides, contained in a 6-well petri dish at the speed of 2×10^4 g for 25 minutes. The usage of the gold slide was found to greatly enhance the light scattering of the cells and minimize the background noise. Fix the cells with 10% formalin overnight. At the time for Raman measurement, the petri dish with the gold slide was placed under the Raman microscope for analysis. For each floating cells, we used 10 replicates to average a single spectrum and 5 for the attached cells. And each replicate was generated from at least 10 spots from a single cell.

4.2.3 DXR Raman Microscope

A DXR Raman microscope (Thermo Fisher Scientific, Madison, WI) was utilized in this study. This instrument facilitates 780nm excitation and 24 mW laser power through a 50 \times objective (Olympus, Japan). Aperture was set to be 50 μ m slit, grating 400 lines/mm and the spot size was 1.0 μ m. The collect exposure time was 1.0 s and the sample exposure was 2.0s. The working distance of the objective lens to the surface of the gold slide was kept consistently at 1.5mm to minimize the variance caused by the different laser penetration depth in the cells.

4.2.4 Data analysis

The spectra data were further analyzed by principal component analysis using the TQ analyst software (Thermo Fisher Scientific). The spectral data were further analyzed by principal component analysis using the TQ analyst software (Thermo Fisher Scientific). Principal component analysis (PCA) is a mathematical procedure that uses orthogonal transformation to convert a set of observations of possibly correlated variables into a set of values of linearly uncorrelated variables called principal components.

Statistics results on the numerical comparison in the figures were presented as mean \pm SD. Analysis of variance model was utilized to compare the differences between two data sets were determined by Student's t-test. A 1% significant level was used in all tests.

To compare the similarity of spectra between groups in PCA, a one-way ANOSIM (Analysis of Similarity) was used in the study. The operation was based on 9999 permutations, the Euclidean distance as dissimilarity metric and first three principle component scores (PC1, PC2 and PC3). A 0.01% significant level was used. In ANOSIM, R value represents the difference between two involved groups. The range of R-value is (-1, 1). An R-value > 0.75 indicates clearly difference, R-value > 0.5 indicates difference with some overlapping while an R-value < 0.25 indicates almost no differences, even p-value shows significant difference. R-value below 0 suggest more similarity between groups than within groups, therefore a problem in experiment design.

4.3 Results and Discussion

4.3.1 Characterization of the heterogeneity of attached and floating cells

When culture cancer cells, normally cells will grow attached on the surface of the petri dish. The cells floating in the media were always considered to be dead cells. Not

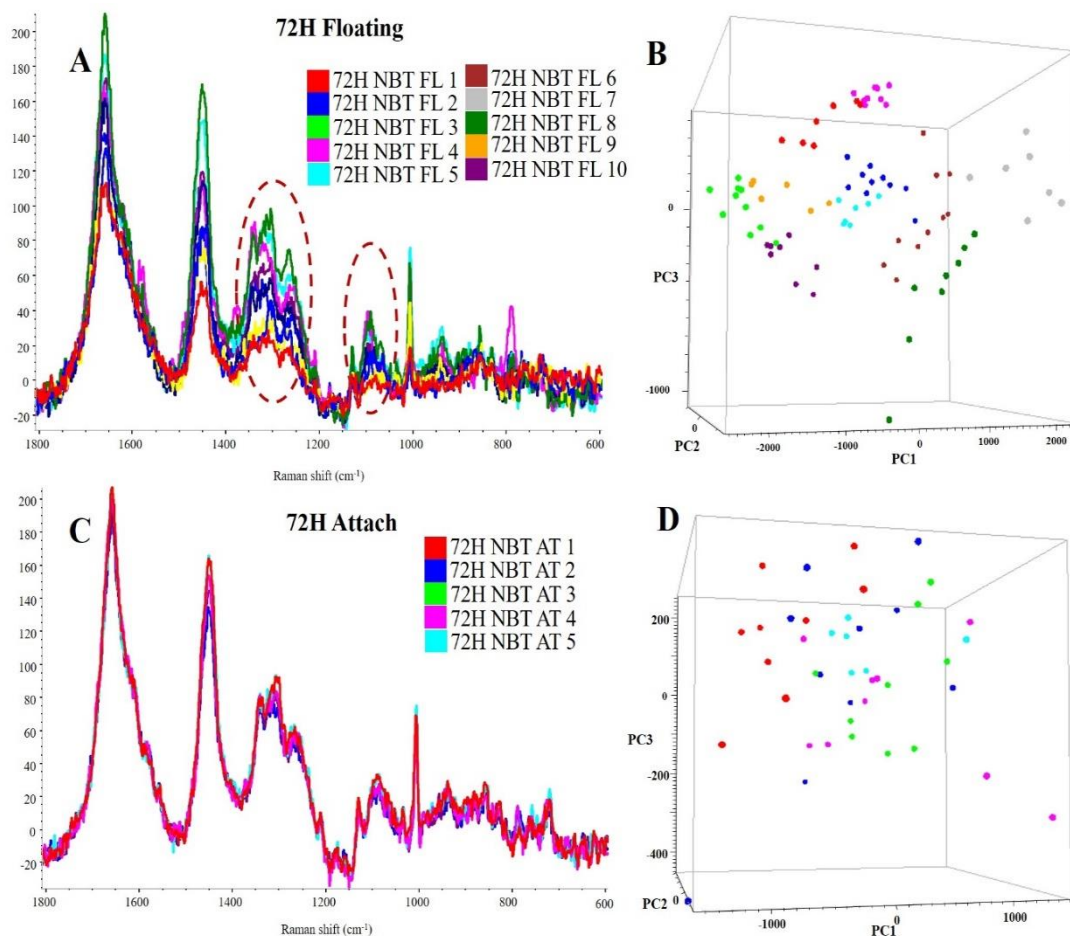


Figure 4.1A: A: Spectra and B: PCA score 3D display of both floating and attached cells treated with NBT (100µM) under 72H treatment. C: Spectra and D: PCA score 3D display of the attached cells treated with NBT (100µM) under 72H treatment. The floating cells are not as overlapped as attached cells, indicate more heterogeneous than the attached cells. The heterogeneity of the floating cells came from Raman peak shift between 1050-1150cm⁻¹ and 1250-1350cm⁻¹.

many studies focused on the floating cells previously. However, when we collected the floating cells for further Raman analysis, specific result discovered. The Raman spectra

of the 10 different floating cells showed spectral differences from each other, mainly from range 1000 to 1400, which most peaks represent the protein (1003 cm^{-1} Phe sym ring br; 1032 cm^{-1} C–H Phe; 1230 cm^{-1} -1267 cm^{-1} Amide III and 1340 cm^{-1} CH def)(Figure 4.1A, C). In contrast, the Raman spectra of NBT 72H attached cells are very similar to each other. (Figure 4.1) The Raman spectra of each individual cell reflected the overall biochemical information of the specific cell. PCA plots were used to statistically study the difference among every single cell. As showed in (Figure 4.1B, D) data cluster of each individual floating cells are mostly separated from each other. While the data clusters of attached cells are mostly overlapped, which means they are not statistically different.

This finding demonstrated that under the same treatment, the heterogeneity of attached and floating cells is different. The floating cells are more heterogeneous than the attached cells in the range for protein peaks. The attached cells showed less heterogeneous between different cells under the same treatment, which showed homogeneity of the cellular responses. It is reported that protein fibronectin is mainly responsible for attachment¹⁵³. In an earlier work¹⁵⁴, it showed that certain kind of heterogeneity can reveal functional differences among cellular populations against different drug sensitivity. Our study showed that the variability among the same treatment should also be taken into consideration.

The similar results between attached and floating cells were observed for all the treatments. When combining the data points of attached and floating cells together, it is clear to notice that the data clusters of the floating cells are always larger than the attached cells (Figure 4.2).

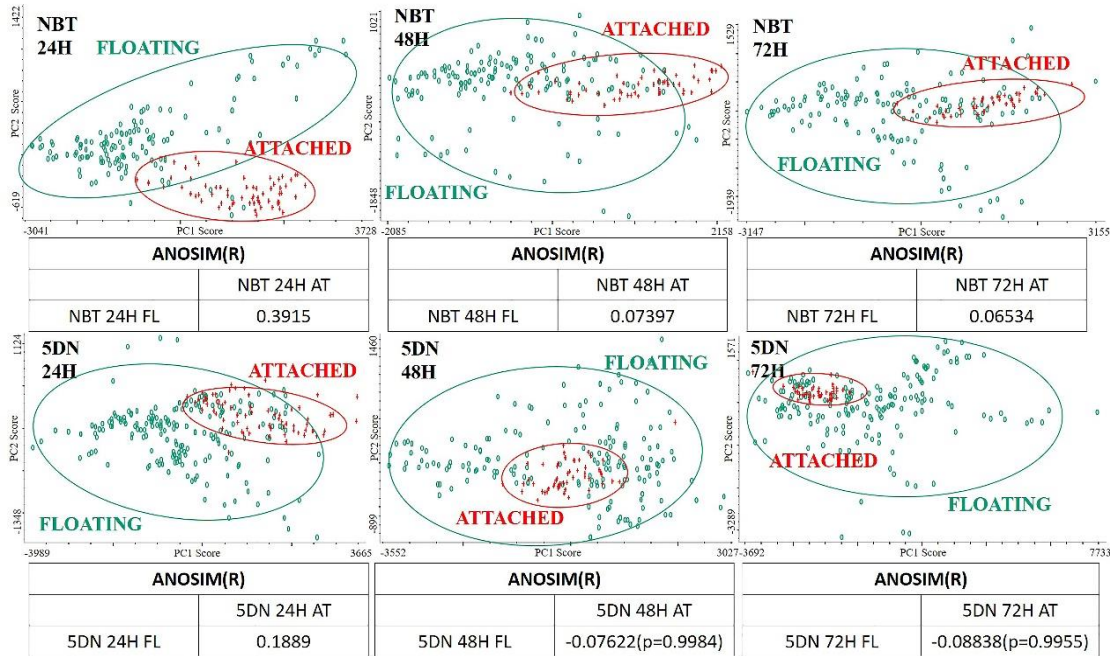


Figure 4.2 PCA scores of the difference between attached and floating cells of the two treatments NBT (100µM) and 5DN(20µM) from different time spot, 24H, 48H and 72H.

In addition to that, we observed an interesting trend that the overall difference between attached and floating cells is decreasing along with increasing treatment time. As in Figure 4.2, both cells treated by NBT and 5DN for 24H, the PCA score of floating and attached plots overlapped the least. While there is still difference under both treatments. The plots got more overlapped under the time 48H and even more at the 72H. The R values agree with the PCA results. For NBT treated cells, after 24H treatment, R value is bigger than 0.25 suggested a significant difference between attached and floating cells. After 48H and 72H treatments, R value is smaller than 0.25, and the R value from 72H is even smaller than the R value from 48H. The trend of the cells under 5DN was

similar to the NBT with slight time difference. It still showed the biggest difference for 24H, but the difference for 48H and 72H was not as significant as the NBT treated. After 72H, the attached cells were almost totally overlapped with the floating cells, and it proved that the difference between floating cells and attached cells became less when the treatment time increased. R-value of 5DN treated proved the same with the PCA score. For cells treated with 5DN for 24H, R-value is already smaller than 0.25 while $p < 0.01$, indicates there is a difference but not so significant. After 48H and 72H, $p > 0.01$, showed there is no difference between attached and floating cells. The results indicated that the treatments minimized the difference between floating and attached cells, it might due to the severe damage had been done on the cells after certain length of time.. Meanwhile, the spots cluster of the floating cells was consistently larger than the attached cell, confirming the heterogeneity of the floating cells was always larger than the attached cells.

4.3.2 The effect of treatment time on cell heterogeneity

To better illustrate the time effect to the cells under treatment, we compared the spectra of the floating cells and attached cells separately in Figure 4.3, both attached and floating cells got intensity increased under both treatments along with time increasing. As showed in the spectra, for both treatment on attached and floating cells, the spectra intensity increased along with increased time and the intensity of floating cells got increased more than the attached cells. The attached cell treated by NBT from all three time spots, always have the higher intensity than the floating cells. On the contrary, to the 5DN treated cells, the intensity of the floating cells treated for 72H increased higher to

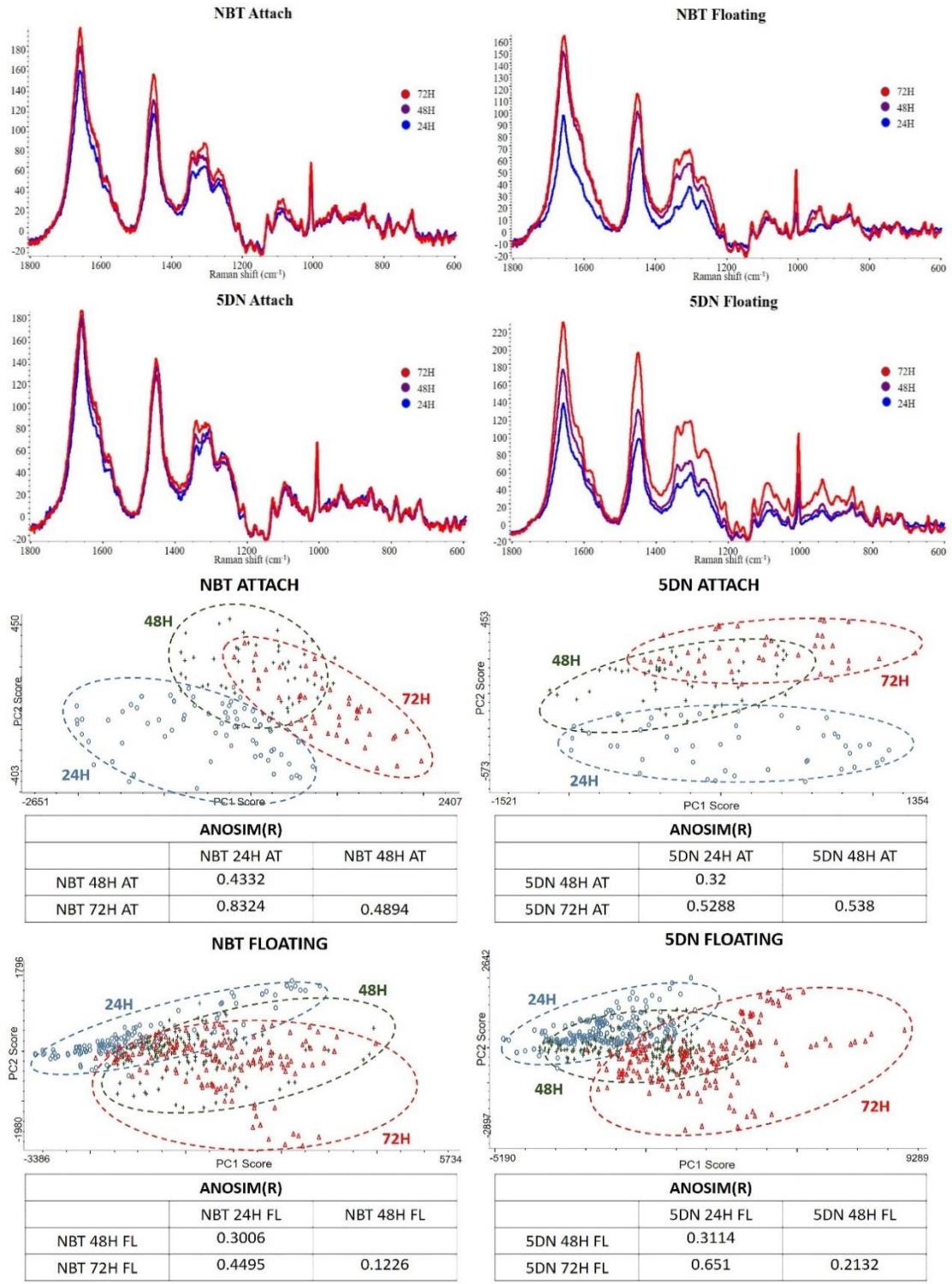


Figure 4.3 Raman Spectra and PCA scores of the variances along with the time of the 2 treatments of NBT (100 μ M) and 5DN (20 μ M) from different time spot, 24H, 48H and 72H.

overcome the attached cells. Furthermore, 5DN did not induce the pattern change as

much as the NBT treated, but more intensity difference.

Figure 4.3 also showed that the PCA score changed along with the increasing treatment time. There is always a greater difference between 24H and 72H, compared to the 24H with the 48H or the 48H with the 72H. R value from the PCA scores still in agreement with the PCA plot data. The R values between 24H and 72H from all treatments are always bigger than the other R values. The clusters changing tendency indicated the cell information varied based on time. Besides, the attached cells were more dissimilar after 24H, indicating cells were more heterogeneous at first. The reason might be because the less durable cells would be altered the earliest, and the durable cells could maintain the attachment ability to last longer. Therefore, after a certain amount of time, durable cells remain attached, and the fragile cells got floated. Plots of the floating cells after 72H got larger area confirming the heterogeneity of the floating cells is increasing.

4.3.3 The effect of PMF types on cell heterogeneity

The last but the most important thing is the study of the cell heterogeneity caused by the different treatments. In Figure 4.4, we compared the NBT and 5DN treated cells at the similar inhibition rate to control cells after 24H and 72H to study the trend. Then we compared the different treatments in the PCA plot. The PCA score showed that the spot clusters of the two treatments moved into different directions, confirming the different cellular responses in both floating and attached cells. Furthermore, for the attached cells treated after 24H, both PCA score and R value confirmed no significant difference between the two treatments and control cells. But for the 72H attached cells, the difference between treated cells and control cells became significant. On the other hand,

the difference from floating cells did not increase with the increase of the treatment time.

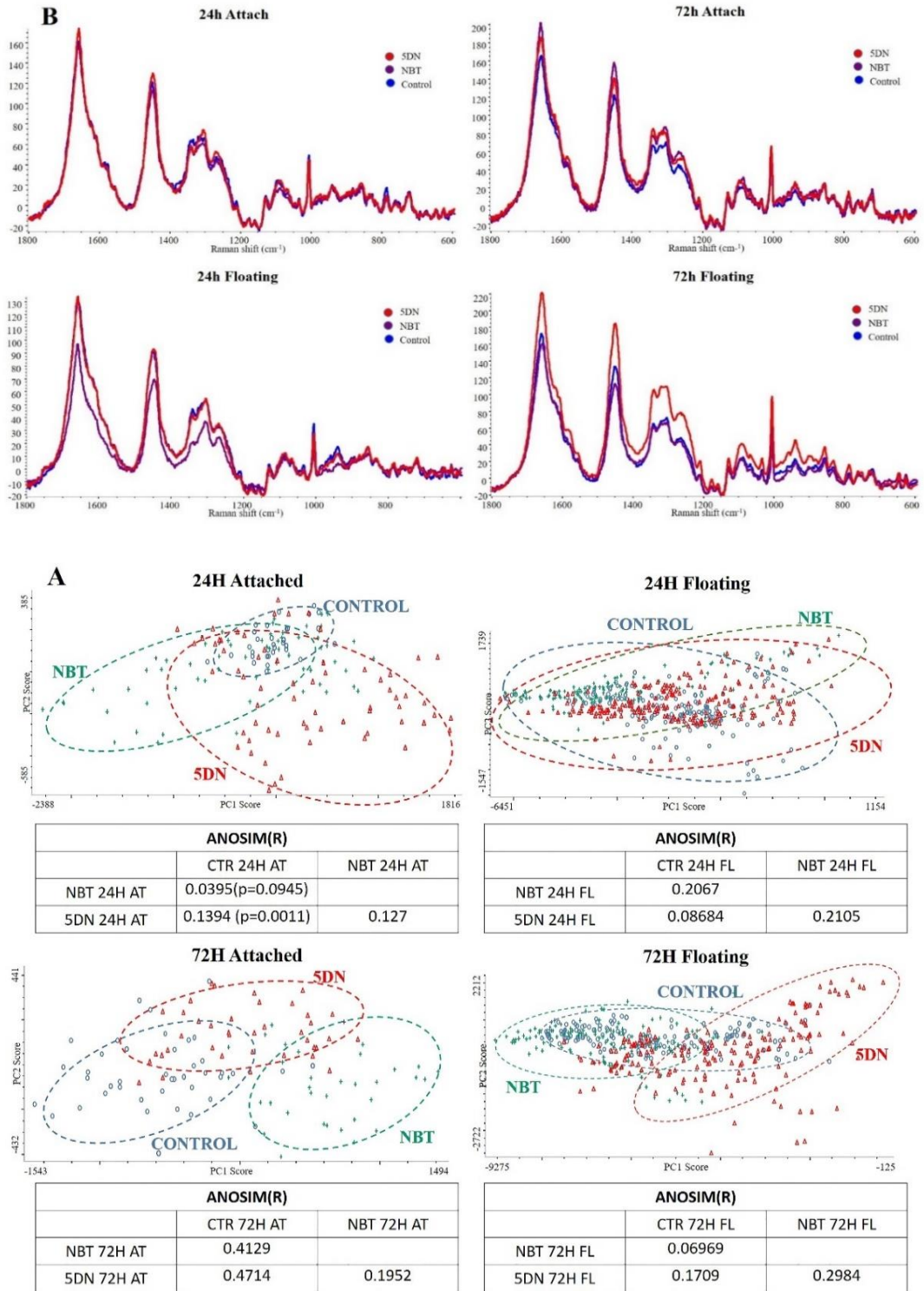


Figure 4.4 Raman spectra of the attached and floating HT29 cells at 72H under NBT(100μM), 5DN(20μM) and control.

In another word, when comparing the difference between treatment times, the difference of floating cells between 24H and 72H is smaller compared to the attached cells. It might indicate that the treatments could cause the cells status change and the interaction mechanism might be different.

This result got studied and proved by an earlier project. Also, it indicated that the cells got floated might because similar chemical changes induced. In this way, the cells would not change the chemical profile much after longer treatment time, because the damage had already been done. Our results proved the different protein profile would cause distinguish cellular responses and it could be greatly affected by the different drugs. The result proved the feasibility of our previous single cell image study. In that previous project regarding the interactions between treatments and cell chemical profile, the cells were treated with PMFs and characterized by Raman microscopy. The concern was mainly about the reliability of the small amount of cells selected and imaged to predict the reaction of the whole population. This study suggested the homogeneity of the attached cells before and after treatment, indicates the amount of cells selected possess the potential to represent the cell population.

4.4 Conclusion

There are differences between attached cells and floating cells, as the floating cells are more sensitive to the treatments, especially to NBT after 72H. Cancer cells though always considered heterogeneous, the untreated, intact and adherent cells could have

similar chemical profiles to each other. Different treatments induced difference to both floating and attached cells, especially to the attached cells.

The result showed that Raman spectroscopy could tell the difference between discrete treatments, time and cell conditions. It is very prominent and useful to see how different the cells became after the treatment. The trend was clear enough itself to show the effectiveness of the drugs or not. Besides, it proved that Raman spectroscopy could tell the difference between floating cells and attached cells as well as different treatments and different treatment time.

CHAPTER 5.

CHARACTERIZATION COLORECTAL CANCER STEM CELLS USING RAMAN MICROSCOPY

5.1 Introduction

Cancer stem cell (CSC), which had been isolated from variety kinds of tumors are basically defined by two functional properties¹⁵⁵: first, the potential to multipotent, which could differentiate into cancer cells; second, ability to self-renewal, which made them perpetuating themselves after an extended time period. The multipotent potential made the developed anti-cancer treatments hard to have the uniform killing ability to even the same cell line. With all these properties, CSC ensure that the cell population is maintained or expanded for long-term clonal growth. Therefore it is important to eliminate CSC directly to make sure they would not grow back.

Therefore, more and more studies focused on killing or inhibiting the growth of CSC. Despite the significant increasing attentions in the field of CSC, the identification, isolation and characterization of the CSC still remained unclear¹⁵⁵. The normal in vitro way to get the CSC for research would be growing the normal colorectal cancer cell in the serum-free media and non-attachable petri dish¹⁵⁶. In this way, only the CSC and the normal cells which could reversibly transit back to stem state could survive. The absence of serum and the attachable surface made the normal cancer cells lost the essential

nutrition and environment to reproduce. The stem cells would remain after a period of time.

To prove the cells remained in the environment to be the CSC and they are different from normal cells, a sorting cell process with Flow Cytometry would be always conducted. With the specific markers, researchers could deeply understand the CSC and the sorting process would provide more pure CSC for further study¹⁵⁷. Gene marker Lgr5, surface markers CD133 and CD44 are the most applied markers that had been used for flow cytometry sorting application^{158,159}. However, it was still hard to prove that any of these markers could really isolate and purify the CSC. Previous studies showed controversial results about all the markers, so the combination of the markers is required¹⁶⁰. Therefore, the non-reliable results might suggest the utilization of the Flow cytometry and surface markers is not sensitive enough for the CSC study. A more reliable method is required and the key difference between normal cells and CSC is still indistinct.

Another way to isolate different kinds of cells is to sort the cells by their different physical property. Percoll solution is a silica-based colloidal medium has been proved possess the property of non-toxic, ideal ionic strength and PH for cell separation. Previous studies⁸³ applied the Percoll solution to isolate the stem cells from the animal samples proved its feasibility of being applied on CSC isolation.

Raman studying though had a short history but with the rapid developing speed, made it became a reliable and widely used technique¹⁶¹. It had been used in many areas including geology¹⁶², environment¹⁶³ and many others^{164,165}. The spectra and images provided by Raman spectroscopy could tell the details about how the cells interact with

the drugs¹⁶⁶, and how much damaged caused by the drugs. Being a label-free, efficient, reliable and advanced technique, the difference in cell structure between normal cancer cells and the CSC would be easy to be recognized using Raman spectroscopy. The efficiency of Raman spectroscopy allowed a large number of cells to be analyzed and ensured the accuracy of the result.

In this study, we aimed to isolate the CSC by their density difference to the normal cancer cells and identify them by Raman microscopy. The result proved the existence of difference from density and chemical profile between CSC and normal cancer cells. The density difference between CSC and normal cancer cells had not been proved in vitro and the chemical profile captured by Raman microscopy is also the first time.

5.2 Material and Methods

5.2.1 Cell Culture

HCT116 cells were cultured (1×10^4 cells/ml) in RPMI media supplemented with 5% heat-inactivated FBS 100 U/mL of penicillin, and 0.1 mg/mL of streptomycin at 37°C with 5% CO₂ and 95% air on the gold covered slides. All cells used were within 3 to 30 passages.

5.2.2 Cell Sorting in Continuous Gradient Solution

Culture the HTC116 cells in DMEM/F-12 media to 6-well unattachable plate in the same incubator for 5 days to form cell spheres at 37°C with 5% CO₂ and 95% air. Trypsin and filter the cells into single cells for further analysis.

As demonstrated in Figure 5.1, dilute the percoll solution with nine part of percoll and one part of 1.5N NaCl solution to make SIP solution. For the discontinuous gradient Percoll solution, we picked density 1.02, 1.04, 1.06 and 1.08. Layer the density fixed Percoll solution into 15ml centrifugation tube from the bottom to the upper layer at the sequence higher density to lowest. After layer the Percoll solution, put the cells on top. Each layer contained 2ml. Centrifuge the tube for 20,000g in swing bucket. Collect the cells from each layer after centrifugation.

For Percoll continuous gradient, dilute the SIP solution with 0.15N NaCl solution to make 40% SIP working solution. Centrifuge the 40% SIP solution 6ml per tube with 30,000g for 30min in an angle fixed rotor to form a continuous gradient solution. For an advanced continuous gradient solution, centrifuge the 20% SIP solution with 30,000g for 30min.

Add 1ml 20×10^3 cluster cells and bulk cells into each tube. Sort the cells in Percoll continuous gradients in swing bucket with 400g for 15min. Collect the cells from

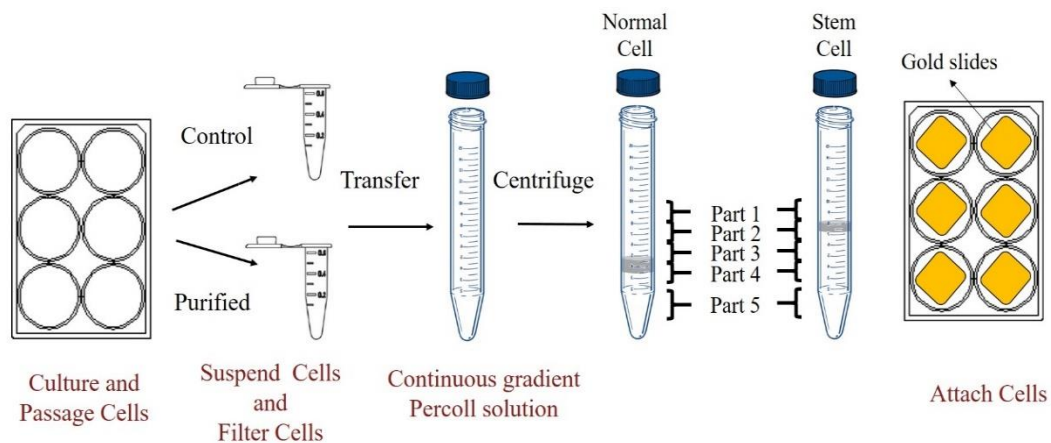


Figure 5.1 Methods Process for Continuous Gradient

4 density layers, wash the cells twice with 5 parts 0.9% saline water and centrifuge in swing bucket with 200g for 5min.

Put the sorted and washed cells into gold slide containing 6-well plate. Centrifuge the 6-well plate with 2000g in swing bucket for 20min to attach the cells on the gold slides.

5.2.3 Raman Microscopy

A DXR Raman microscope (Thermo Fisher Scientific, Madison, WI) was utilized in this study. This instrument facilitates 780nm excitation and 24 mW laser power through a 50× objective (Olympus, Japan). Aperture was set to be 50 μm slit, grating 400 lines/mm and the spot size was 1.0 μm. The collect exposure time was 1.0 s and the sample exposure was 2.0s. The working distance of the objective lens to the surface of the gold slide was kept consistently at 1.5mm to minimize the variance caused by the different laser penetration depth in the cells.

5.2.4 ELDA analysis

Dilute the sorted and washed cells to make 100cells/well, 10cells/well and 1cells/well. Culture the cells into 96-well unattached plates for ELDA analysis. Incubate the cells for 2week at 37°C in a 5% CO₂ incubator. Score the plates for the presence of cell clusters. The estimated cells/well were calculated by the frequency of proliferated cells.

5.2.5 Data analysis

The spectra data were further analyzed by principal component analysis using the TQ analyst software (Thermo Fisher Scientific). The spectral data were further analyzed by principal component analysis using the TQ analyst software (Thermo Fisher Scientific). Principal component analysis (PCA) is a mathematical procedure that uses orthogonal transformation to convert a set of observations of possibly correlated variables into a set of values of linearly uncorrelated variables called principal components.

ELDA analysis has been done online using the Bioinformatics facility of The Walter & Eliza Hall Institute of Medical Research (Melbourne, Australia) (accessed at <http://bioinf.wehi.edu.au/software/limdil/index.html>).

Statistics results on the numerical comparison in the figures were presented as mean \pm SD. Analysis of variance model was utilized to compare the differences between two data sets were determined by Student's t-test. A 1% significant level was used in all tests.

5.3 Results and Discussion

5.3.1 Raman Microscopic Characterization of Attached and Sphere Cells

After centrifugation, the cells would attach on the gold slides. Then we fixed the cells on the gold slide overnight for further Raman analysis with formalin. In this way, the cells chemical profile could be fixed and protected. Then we characterized both the sphere cells and normal cells with Raman microscopy. Unexpectedly, sphere cells

showed a great difference at peak 1049cm^{-1} (Figure 5.2). The intensity of the peak could be 50%, sometimes 6 times, higher than the normal cancer cells.

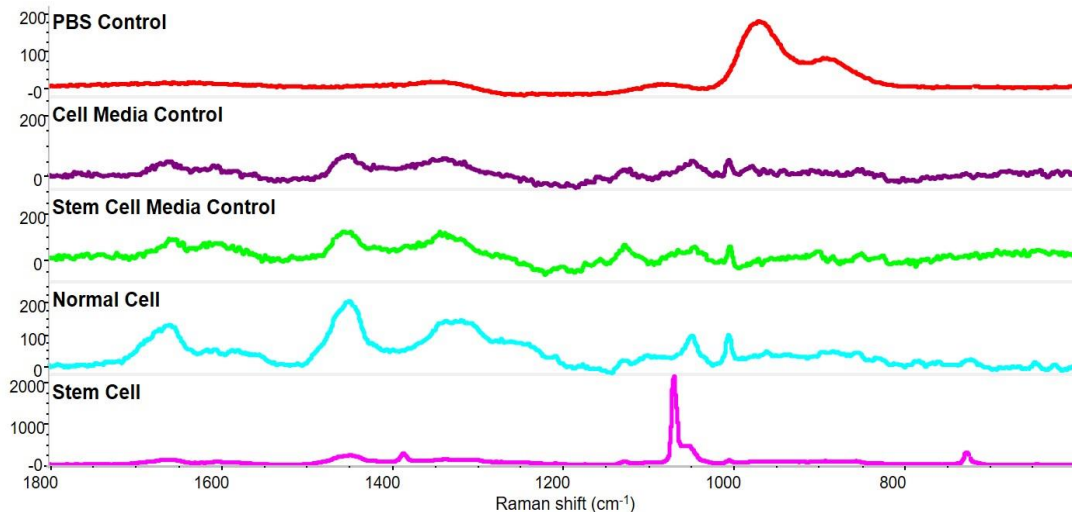


Figure 5.2 Raman spectra of PBS control, cell media control, stem cell media control, normal cell and CSC. The Raman spectra of CSC showed a distinct peak at 1049cm^{-1} with a high intensity around 2000 but the others do not contain that peak.

Then we did the statistical analysis about the intensity of the peak 1049cm^{-1} based on the 100 cells each. As showed in Figure 5.2, though the stem-like cells got extruded heterogeneity, the peak intensity was much higher in stem-like cells. However, after further analysis, we found out that not all cells from the cell clusters could induce that peak. Only cells from the right corner of the gold slides could show that great difference at the certain peak. Since the cells were attached to the gold slide through centrifugation, there is highly possibility that the location difference might result from cell density.

5.3.2 Characterize Cells from Different Density Layers

Based on these results and assumption that the cells from the different location from the centrifuged gold slides possess different chemical profile, we conducted the discontinuous gradient study to sort the cells by cell density. The density range we picked was from 1.02-1.08 compared to water.

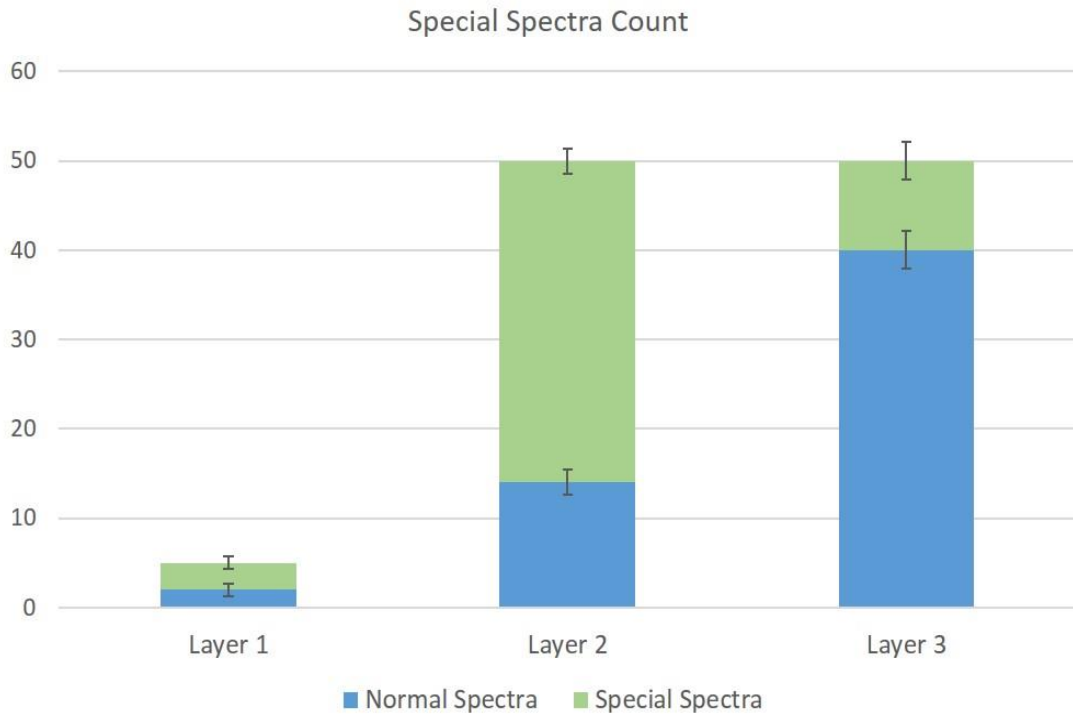


Figure 5.3 Special spectra count in 50 cells from different layers of the cells spheres after gradient centrifugation. The cell number from the layer 1 doesn't reach 50 and the layer 4 and layer 5 doesn't contain any cells.

Figure 5.1 and Figure 5.4 demonstrated the exact cell layers in the gradient solution. The cells from the clusters formed one cell layer at the second part while the normal cancer cells formed one cell layer in the fourth part. We extracted each layer from the centrifuge tube and attached the cells on the gold slides to get the cells characterized by Raman microscopy. As showed in Figure 5.3, for the stem-like cells, we found out that the fourth and fifth layer did not contain enough cells attached on the gold slides.

Though the first layer contained around 5 cells, the comparison to the others failed. Between the second and the third layer, the cells from the second layer could generate more special peak contained spectra.

To confirm the existence of the specific peak, population study was conducted.

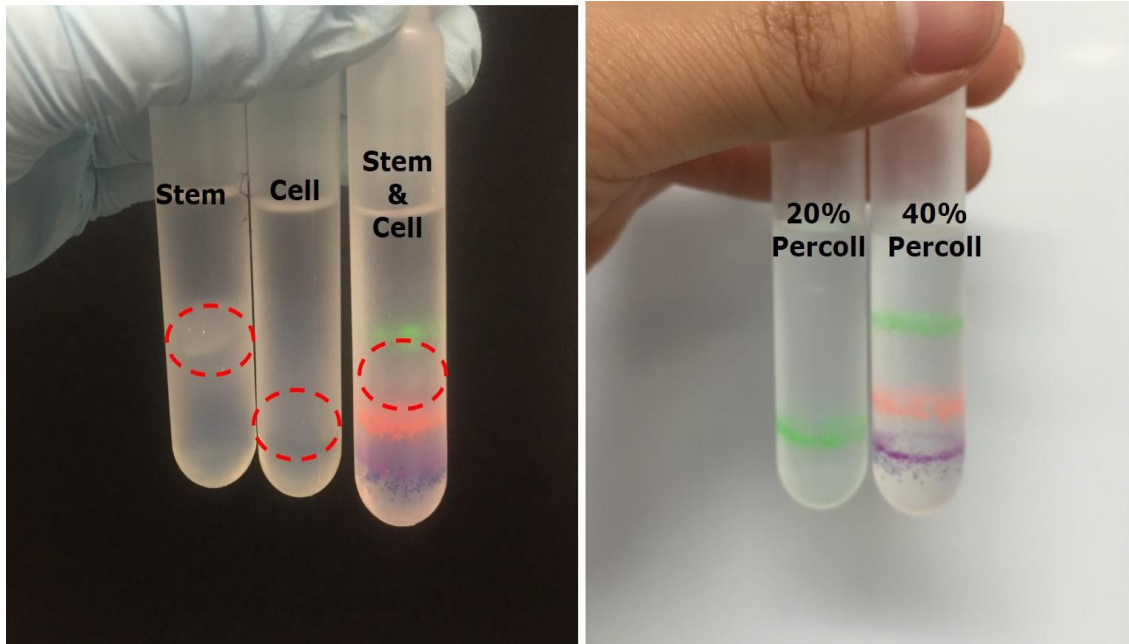


Figure 5.4 A: The optical images of the cells sorted by Percoll continuous solution. The CSC formed the cell layer at an upper layer while the normal cancer cell formed the layer at the lower layer. The tube containing both CSC and normal cancer cell formed an extended cell layer.

B: 40% Percoll solution formed the continuous density layers ranged from 1.02-1.08g/ml. While the 20% Percoll solution formed the continuous density layer ranged smaller than 1.02g/ml. Density beads were used as markers in the solution.

We picked 50 cells each from the fourth layer of normal cancer cells and second layer of sphere cells to record the peak intensity (Figure 5.5). The peak intensity of 1049cm^{-1} from CSC is much higher than the normal cancer cell confirmed the general existence of the peak.

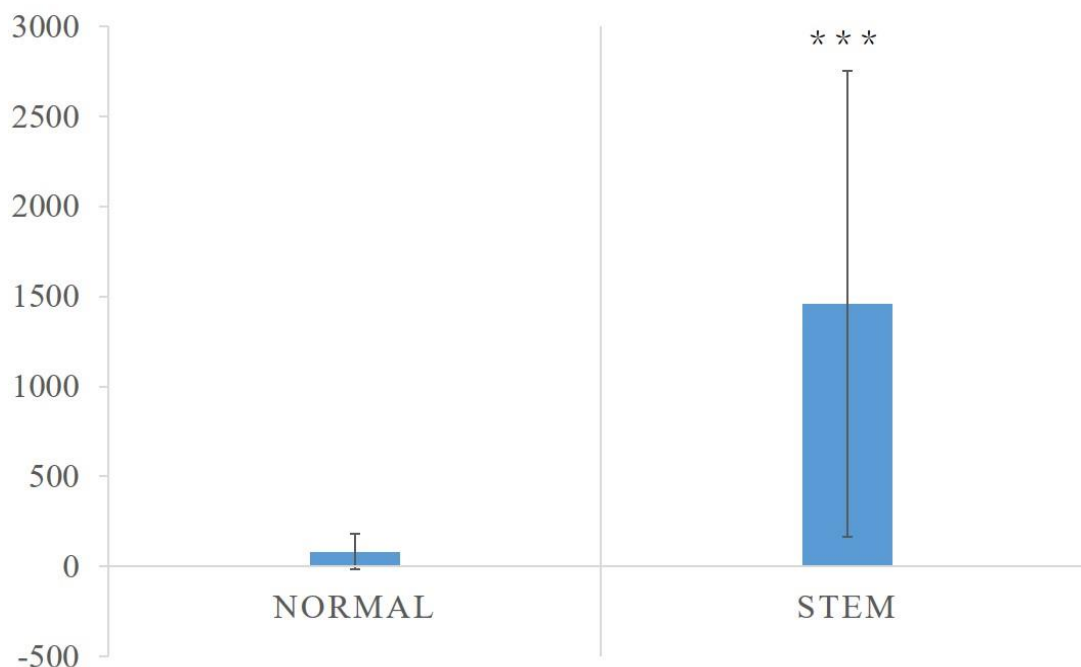


Figure 5.5 Statistical analysis of the peak 1049 cm⁻¹ intensity. The intensity from stem cells was much higher than the same peak from the normal cancer cells. The average intensity showed significant difference between normal cancer cell and cell sphere. The A one way Student's t-test was used to assess the statistical significance and p-value of <0.05 was considered statistically significant.

The results showed that the density of sphere cell is lower than the normal cancer cell and sphere cells contained the most specific peak. It indicated that when cells treated in the non-attachable petri dish with stem cell media, the cell clusters formed. In the cell clusters, the density of the cells decreased. Furthermore, the decreased density cells contained the most cells possess the peak 1049cm⁻¹ which should contain specific content.

5.3.3 ELDA Study of Cells from Different Layers

ELDA study is suitable for all kinds of limiting dilution problem and it is especially suitable for analyzing limiting dilution data arising in stem cell research. The cells from the layer 4 and layer 5 did not reach the number requirement of the analysis, only the first three layers could perform the ELDA study. As showed in Figure 5.6, the cells from the sphere clusters showed around 15% of CSC while the normal bulk cells showed around 2% of CSC. After continuous gradient cell sortation, CSC from the

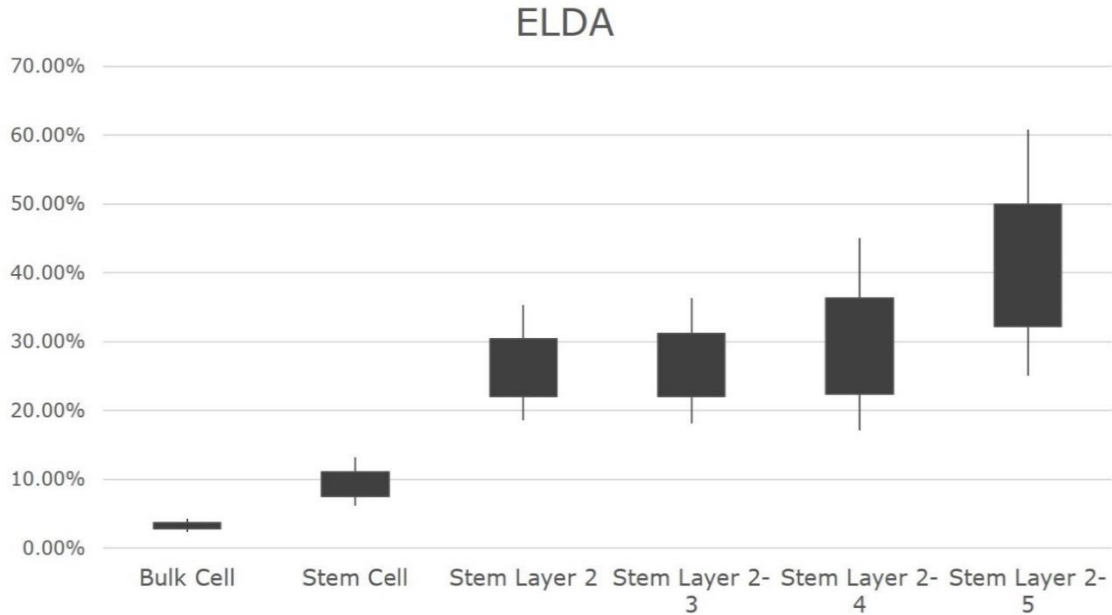


Figure 5.6 ELDA of the cells from different layers. Bulk cells contained least stem cells and followed by cells from spheres which considered to be stem cells. Stem Layer 2 represents the second layer of cells from cell spheres gradient centrifugation. After second centrifugation of Stem Layer 2, cells from layer 3, 4 and 5 labeled Stem Layer 2-3, 2-4 and 2-5. Stem Layer 2-5 contained most stem cells.

second layer increased to reach around 27%. The cells from the second layer could generate the most cell spheres. The more spheres the cells could generate means the more stem cell contained. In this way, it proved that the cells from the second layer had a high possibility that contained the most stem cells.

Next step, we zoomed in the Percoll continuous gradient, to sort the cells from the second layer to be more narrow density range. In this way, we could further purify the stem cells. More purification we could conduct, more accurate the result of the study we could access. The 20% Percoll continuous gradient solution conducted in the study to get the cells more purified. After the second continuous gradient purification, the cells gathered the most at the three lower layers. The third and fourth layer from the second purification still contained around 27% CSC which is almost the same as before. However, the cells from the fifth layer contained around 50% of CSC. The result showed that the two purification procedure did purify the CSC cells (Figure 5.6).

After purification, ELDA would be necessary for the stem cells to test the stemness and the stem cells percentage in the whole cell population. With ELDA data, the effectiveness of stem cell isolation and purification could be calculated. Guided by the result of the stem cell containing, the following research procedures would be more specific and statistical.

5.4 Discussion

Based on the up to date research, we believe that the density of the cells from cell sphere was different from normal cancer cells. Cells from cell spheres could be sorted by Percoll continuous gradient. Also, cells from cell spheres had more percentage of spectra contained high-intensity Raman peak 1049 cm^{-1} , while normal cancer cells showed much lower intensity. Cells with specified density from spheres could generate even more cell spheres and had more possibilities of containing peak 1049 cm^{-1} . Furthermore, ELDA

data also supported the cell density study could sort the cells with different sphere generation ability. In conclusion, we developed a method to isolate and purify CSC from normal cancer cells and proved that Raman microscopy could detect the difference between a normal cancer cell and CSC.

CHAPTER 6.

OVERALL CONCLUSION AND FUTURE WORK

6.1 Conclusions

In conclusion, we demonstrated feasibility of the Raman microscopy to characterize cancer cells in response to two bioactive compounds. The Raman image of a single cancer cell reflects the distribution and content of major cellular biochemical, including lipids, proteins, and nucleic acids. The changes of these components in the Raman image can be used to study the mode of action of the treatment. In this study, we found NBT induced more changes in the nucleic acid peaks and protein peaks, while 5DN induced more changes in the localized lipid peaks. In addition, we applied Raman microscopic spectra and PCA analysis to study the heterogeneity of cancer cells, when they were attached or floating in the media and their response to NBT and 5DN over time. The floating cells show more heterogeneity when compared to the attached cells, although the difference between the floating cells and attached cells became smaller when treated with NBT and 5DN over time. Lastly, we explored the potential of Raman microscopy to differentiate between CSC and normal cancer cells. An interesting peak at around 1049 cm^{-1} was observed in nearly 70% of CSC enriched cells, but not in the normal cancer cells. The origin of this peak is unknown and future study is needed to verify the accuracy of using this peak as a CSC biomarker using Raman microscopy.

6.2 Future Study

In future study, we will further work on the verification the 1049 cm^{-1} peak as the biomarker for CSC using Raman microscopy. Enriched CSC cells from density study and tumor study will be used to check the percentage of the 1049 cm^{-1} in the cell population. In addition, we will identify the source of the peak 1049 cm^{-1} by extracting the major components (lipids, proteins, nucleic acids) from enriched CSC, respectively, and measuring the Raman spectra of each component.

If the 1049 cm^{-1} peak was confirmed to be the biomarker of CSC, we will use Raman microscopy to find and characterize individual CSC and their responses to anticancer treatments. The comparison between the responses by CSC and normal cancer cells can help us to understand the heterogeneity of the overall cancer cell population and facilitate the development of more effective treatments.

BIBLIOGRAPHY

- (1) Organization, W. H., and Cancer, I. U. against. (2005) Global action against cancer. Geneva : World Health Organization.
- (2) Fahrner, R., Theis, B., Ardelt, M., Rauchfuss, F., Schüle, S., and Settmacher, U. (2016) Rapid progressive colon cancer metastasized to the right epididymis and liver: report of a case and review of the literature. *Int. J. Colorectal Dis.* 3.31, 721–722.
- (3) Fisher, R., Pusztai, L., and Swanton, C. (2013) Cancer heterogeneity: implications for targeted therapeutics. *Br. J. Cancer* 108, 479–85.
- (4) Collins, C. A., Olsen, I., Zammit, P. S., Heslop, L., Petrie, A., Partridge, T. A., and Morgan, J. E. (2005) Stem cell function, self-renewal, and behavioral heterogeneity of cells from the adult muscle satellite cell niche. *Cell* 122, 289–301.
- (5) Donnenberg, V. S., and Donnenberg, A. D. (2005) Multiple drug resistance in cancer revisited: the cancer stem cell hypothesis. *J. Clin. Pharmacol.* 45, 872–7.
- (6) Li, S., Pan, M.-H., Lai, C.-S., Lo, C.-Y., Dushenkov, S., and Ho, C.-T. (2007) Isolation and syntheses of polymethoxyflavones and hydroxylated polymethoxyflavones as inhibitors of HL-60 cell lines. *Bioorg. Med. Chem.* 15, 3381–9.
- (7) Li, S., Sang, S., Pan, M.-H., Lai, C.-S., Lo, C.-Y., Yang, C. S., and Ho, C.-T. (2007) Anti-inflammatory property of the urinary metabolites of nobiletin in mouse. *Bioorg. Med. Chem. Lett.* 17, 5177–81.

- (8) Murakami, A., Nakamura, Y., Torikai, K., Stress, O., Promotion, T., Tanaka, T., Koshiba, T., Koshimizu, K., Kuwahara, S., Takahashi, Y., Ogawa, K., Yano, M., Tokuda, H., Nishino, H., Mimaki, Y., Sashida, Y., Kitanaka, S., and Ohigashi, H. (2000) Inhibitory Effect of Citrus Nobiletin on Phorbol Ester-induced Skin Inflammation , Oxidative Stress , and Tumor Promotion in Mice Inhibitory Effect of Citrus Nobiletin on Phorbol Ester-induced Skin Inflammation ,. *Cancer Res.* 60, 5059–5066.
- (9) Xiao, H., Yang, C. S., Li, S., Jin, H., Ho, C.-T., and Patel, T. (2009) Monodemethylated polymethoxyflavones from sweet orange (*Citrus sinensis*) peel inhibit growth of human lung cancer cells by apoptosis. *Mol. Nutr. Food Res.* 53, 398–406.
- (10) Charoensinphon, N., Qiu, P., Dong, P., Zheng, J., Ngauv, P., Cao, Y., Li, S., Ho, C.-T., and Xiao, H. (2013) 5-demethyltangeretin inhibits human nonsmall cell lung cancer cell growth by inducing G2/M cell cycle arrest and apoptosis. *Mol. Nutr. Food Res.* 57, 2103–11.
- (11) Alía, M., Mateos, R., Ramos, S., Lecumberri, E., Bravo, L., and Goya, L. (2006) Influence of quercetin and rutin on growth and antioxidant defense system of a human hepatoma cell line (HepG2). *Eur. J. Nutr.* 45, 19–28.
- (12) Yu, M.-W., Lou, S.-N., Chiu, E.-M., and Ho, C.-T. (2013) Antioxidant activity and effective compounds of immature calamondin peel. *Food Chem.* 136, 1130–5.

- (13) Sergeev, I. N., Li, S., Colby, J., Ho, C.-T., and Dushenkov, S. (2006)
Polymethoxylated flavones induce Ca(2+)-mediated apoptosis in breast cancer cells.
Life Sci. 80, 245–53.
- (14) Cao, J., Xia, X., Chen, X., Xiao, J., and Wang, Q. (2013) Characterization of
flavonoids from *Dryopteris erythrosora* and evaluation of their antioxidant,
anticancer and acetylcholinesterase inhibition activities. *Food Chem. Toxicol.* 51,
242–250.
- (15) Wen, L., Wu, D., Jiang, Y., Prasad, K. N., Lin, S., Jiang, G., He, J., Zhao, M., Luo,
W., and Yang, B. (2014) Identification of flavonoids in litchi (*Litchi chinensis*
Sonn.) leaf and evaluation of anticancer activities. *J. Funct. Foods* 6, 555–563.
- (16) Ahmad, S. T., Arjumand, W., Nafees, S., Seth, A., Ali, N., Rashid, S., and Sultana,
S. (2012) Hesperidin alleviates acetaminophen induced toxicity in wistar rats by
abrogation of oxidative stress, apoptosis and inflammation. *Toxicol. Lett.* 208, 149–
161.
- (17) Parhiz, H., Roohbakhsh, A., Soltani, F., Rezaee, R., and Iranshahi, M. (2015)
Antioxidant and Anti-Inflammatory Properties of the Citrus Flavonoids Hesperidin
and Hesperetin: An Updated Review of their Molecular Mechanisms and
Experimental Models. *Phyther. Res.* 29, 323–331.
- (18) Heim, K. E., Tagliaferro, A. R., and Bobilya, D. J. (2002) Flavonoid antioxidants:
chemistry, metabolism and structure-activity relationships. *J. Nutr. Biochem.* 13,
572–584.

- (19) Agati, G., Azzarello, E., Pollastri, S., and Tattini, M. (2012) Flavonoids as antioxidants in plants: Location and functional significance. *Plant Sci.* 196, 67–76.
- (20) Gossiau, A., Chen, K. Y., Ho, C.-T., and Li, S. (2014) Anti-inflammatory effects of characterized orange peel extracts enriched with bioactive polymethoxyflavones. *Food Sci. Hum. Wellness* 3, 26–35.
- (21) Qiu, P., Guan, H., Dong, P., Guo, S., Zheng, J., Li, S., Chen, Y., Ho, C.-T., Pan, M.-H., McClements, D. J., and Xiao, H. (2011) The inhibitory effects of 5-hydroxy-3,6,7,8,3',4'-hexamethoxyflavone on human colon cancer cells. *Mol. Nutr. Food Res.* 55, 1523–32.
- (22) Morley, K. L., Ferguson, P. J., and Koropatnick, J. (2007) Tangeretin and nobiletin induce G1 cell cycle arrest but not apoptosis in human breast and colon cancer cells. *Cancer Lett.* 251, 168–78.
- (23) Yuen, H.-Q., Hwang, Q.-H., Zhang, X.-Y., and Zhou, Z.-X. (2014) Cellular Antioxidant Activity and Pharmacokinetic Study of Polymethoxylated Flavonoids in Extract of *Citrus reticulata* “Chachi” Peel. *Food Sci. Technol. Res.* 20, 629–637.
- (24) Yao, X., Zhu, X., Pan, S., Fang, Y., Jiang, F., Phillips, G. O., and Xu, X. (2012) Antimicrobial activity of nobiletin and tangeretin against *Pseudomonas*. *Food Chem.* 132, 1883–1890.
- (25) Qiu, P., Dong, P., Guan, H., Li, S., Ho, C.-T., Pan, M.-H., McClements, D. J., and Xiao, H. (2010) Inhibitory effects of 5-hydroxy polymethoxyflavones on colon cancer cells. *Mol. Nutr. Food Res.* 54 Suppl 2, S244-52.

- (26) Qiu, P., Guan, H., Dong, P., Li, S., Ho, C.-T., Pan, M.-H., McClements, D. J., and Xiao, H. (2011) The p53-, Bax- and p21-dependent inhibition of colon cancer cell growth by 5-hydroxy polymethoxyflavones. *Mol. Nutr. Food Res.* 55, 613–22.
- (27) Lai, C.-S., Tsai, M.-L., Cheng, A.-C., Li, S., Lo, C.-Y., Wang, Y., Xiao, H., Ho, C.-T., Wang, Y.-J., and Pan, M.-H. (2011) Chemoprevention of colonic tumorigenesis by dietary hydroxylated polymethoxyflavones in azoxymethane-treated mice. *Mol. Nutr. Food Res.* 55, 278–90.
- (28) Wu, X., Song, M., Wang, M., Zheng, J., Gao, Z., Xu, F., Zhang, G., and Xiao, H. (2015) Chemopreventive effects of nobiletin and its colonic metabolites on colon carcinogenesis. *Mol. Nutr. Food Res.* 59, 2383–94.
- (29) Lotito, S. B., Zhang, W.-J., Yang, C. S., Crozier, A., and Frei, B. (2011) Metabolic conversion of dietary flavonoids alters their anti-inflammatory and antioxidant properties. *Free Radic. Biol. Med.* 51, 454–463.
- (30) Yang, M., Cheng, C., Yang, J., and Guo, D. (2012) Metabolite Profiling and Characterization for Medicinal Herbal Remedies. *Curr. Drug Metab.* 13, 535–57.
- (31) Touil, Y. S., Auzeil, N., Boulinguez, F., Saighi, H., Regazzetti, A., Scherman, D., and Chabot, G. G. (2011) Fisetin disposition and metabolism in mice: Identification of geraldol as an active metabolite. *Biochem. Pharmacol.* 82, 1731–1739.
- (32) Miyamoto, S., Yasui, Y., Tanaka, T., Ohigashi, H., and Murakami, A. (2008) Suppressive effects of nobiletin on hyperleptinemia and colitis-related colon carcinogenesis in male ICR mice. *Carcinogenesis* 29, 1057–63.

- (33) Tang, M. X., Ogawa, K., Asamoto, M., Chewonarin, T., Suzuki, S., Tanaka, T., and Shirai, T. (2011) Effects of Nobiletin on PhIP-Induced Prostate and Colon Carcinogenesis in F344 Rats. *Nutr. Cancer* 63.2, 227–233.
- (34) Siegel, R. L., Miller, K. D., and Jemal, A. (2015) Cancer statistics, 2016. *CA. Cancer J. Clin.* 66.
- (35) Leslie H. Sobin, Mary K. Gospodarowicz, C. W. (2009) TNM classification of malignant tumours 7th ed.
- (36) Rajamanickam, S., and Agarwal, R. (2008) Natural products and colon cancer: current status and future prospects. *Drug Dev. Res.* 69, 460–471.
- (37) Rowley, P. T. (2005) Inherited Susceptibility to Colorectal Cancer. *Annu. Rev. Med.* 56, 539–554.
- (38) Hanahan, D., and Weinberg, R. A. (2011) Hallmarks of Cancer: The Next Generation. *Cell* 144, 646–674.
- (39) Ho, W. Y., Yeap, S. K., Ho, C. L., Rahim, R. A., and Alitheen, N. B. (2012) Development of Multicellular Tumor Spheroid (MCTS) Culture from Breast Cancer Cell and a High Throughput Screening Method Using the MTT Assay. *PLoS One* (Mehta, K., Ed.) 7, e44640.
- (40) Parmar, M., Aliabadi, H. M., Mahdipoor, P., Kucharski, C., Maranchuk, R., Hugh, J., and Uludag, H. (2015) Targeting Cell Cycle Proteins in Breast Cancer Cells with siRNA by Using Lipid-Substituted Polyethylenimines. *Front. Bioengineering Biotechnol.* 3, 14–14.

- (41) Gasparotto, J., Somensi, N., Kunzler, A., Saibro Girardi, C., Augusto de Bittencourt Pasquali, M., Miranda Ramos, V., Simoes-Pires, A., Jose Quintans-Junior, L., Branco, A., Claudio Fonseca Moreira, J., and Pens Gelain, D. (2014) Hecogenin Acetate Inhibits Reactive Oxygen Species Production and Induces Cell Cycle Arrest and Senescence in the A549 Human Lung Cancer Cell Line. *Anti-Cancer Agents Med. Chem. (Formerly Curr. Med. Chem. Agents)* 14, 1128–1135.
- (42) Zhao, A., Zeng, Q., Xie, X., Zhou, J., Yue, W., Li, Y., and Pei, X. (2012) MicroRNA-125b Induces Cancer Cell Apoptosis Through Suppression of Bcl-2 Expression. *J. Genet. Genomics* 39, 29–35.
- (43) Fiandalo, M. V, and Kyprianou, N. (2012) Caspase control: protagonists of cancer cell apoptosis. *Exp. Oncol.* 34, 165–75.
- (44) Zhang, J., Yang, Z., Li, P., Bledsoe, G., Chao, L., and Chao, J. (2013) Kallistatin antagonizes Wnt/ β -catenin signaling and cancer cell motility via binding to low-density lipoprotein receptor-related protein 6. *Mol. Cell. Biochem.* 379, 295–301.
- (45) Prahallad, A., Sun, C., Huang, S., Di Nicolantonio, F., Salazar, R., Zecchin, D., Beijersbergen, R. L., Bardelli, A., and Bernards, R. (2012) Unresponsiveness of colon cancer to BRAF(V600E) inhibition through feedback activation of EGFR. *Nature* 483, 100–103.
- (46) Valiente, M., Obenauf, A. C., Jin, X., Chen, Q., Zhang, X. H.-F., Lee, D. J., Chافت, J. E., Kris, M. G., Huse, J. T., Brogi, E., and Massagué, J. (2014) Serpins Promote Cancer Cell Survival and Vascular Co-Option in Brain Metastasis. *Cell* 156, 1002–1016.

- (47) Levenson, J. D., Zhang, H., Chen, J., Tahir, S. K., Phillips, D. C., Xue, J., Nimmer, P., Jin, S., Smith, M., Xiao, Y., Kovar, P., Tanaka, A., Bruncko, M., Sheppard, G. S., Wang, L., Gierke, S., Kategaya, L., Anderson, D. J., Wong, C., Eastham-Anderson, J., Ludlam, M. J. C., Sampath, D., Fairbrother, W. J., Wertz, I., Rosenberg, S. H., Tse, C., Elmore, S. W., and Souers, A. J. (2015) Potent and selective small-molecule MCL-1 inhibitors demonstrate on-target cancer cell killing activity as single agents and in combination with ABT-263 (navitoclax). *Cell Death Dis.* 6, e1590.
- (48) Sheng, H., Shao, J., Kirkland, S. C., Isakson, P., Coffey, R. J., Morrow, J., Beauchamp, R. D., and DuBois, R. N. (1997) Inhibition of human colon cancer cell growth by selective inhibition of cyclooxygenase-2. *J. Clin. Invest.* 99, 2254–9.
- (49) Xiao, H., Zhang, Q., Lin, Y., Reddy, B. S., and Yang, C. S. (2008) Combination of atorvastatin and celecoxib synergistically induces cell cycle arrest and apoptosis in colon cancer cells. *Int. J. Cancer* 122, 2115–24.
- (50) Zheng, Q., Hirose, Y., Yoshimi, N., Murakami, A., Koshimizu, K., Ohigashi, H., Sakata, K., Matsumoto, Y., Sayama, Y., and Mori, H. (2002) Further investigation of the modifying effect of various chemopreventive agents on apoptosis and cell proliferation in human colon cancer cells. *J. Cancer Res. Clin. Oncol.* 128, 539–46.
- (51) Cai, X., Lu, W., Ye, T., Lu, M., Wang, J., Huo, J., Qian, S., Wang, X., and Cao, P. (2012) The molecular mechanism of luteolin-induced apoptosis is potentially related to inhibition of angiogenesis in human pancreatic carcinoma cells. *Oncol. Rep.* 28, 1353–1361.

- (52) Lamy, S., Akla, N., Ouanouki, A., Lord-Dufour, S., and Béliveau, R. (2012) Diet-derived polyphenols inhibit angiogenesis by modulating the interleukin-6/STAT3 pathway. *Exp. Cell Res.* 318, 1586–96.
- (53) Chen, K.-C., Chen, C.-Y., Lin, C.-R., Lin, C.-J., Yang, T.-Y., Chen, T.-H., Wu, L.-C., and Wu, C.-C. (2013) Luteolin attenuates TGF- β 1-induced epithelial-mesenchymal transition of lung cancer cells by interfering in the PI3K/Akt-NF- κ B-Snail pathway. *Life Sci.* 93, 924–33.
- (54) Evenson, D., Darzynkiewicz, Z., and Melamed, M. (1980) Relation of mammalian sperm chromatin heterogeneity to fertility. *Science.* 210, 1131–1133.
- (55) Aird, W. C. (2012) Endothelial cell heterogeneity. *Cold Spring Harb. Perspect. Med.* 2, a006429.
- (56) Paulsson, J. (2004) Summing up the noise in gene networks. *Nature* 427, 415–8.
- (57) Colman-Lerner, A., Gordon, A., Serra, E., Chin, T., Resnekov, O., Endy, D., Pesce, C. G., and Brent, R. (2005) Regulated cell-to-cell variation in a cell-fate decision system. *Nature* 437, 699–706.
- (58) Neve, R. M., Chin, K., Fridlyand, J., Yeh, J., Baehner, F. L., Fevr, T., Clark, L., Bayani, N., Coppe, J.-P., Tong, F., Speed, T., Spellman, P. T., DeVries, S., Lapuk, A., Wang, N. J., Kuo, W.-L., Stilwell, J. L., Pinkel, D., Albertson, D. G., Waldman, F. M., McCormick, F., Dickson, R. B., Johnson, M. D., Lippman, M., Ethier, S., Gazdar, A., and Gray, J. W. (2006) A collection of breast cancer cell lines for the study of functionally distinct cancer subtypes. *Cancer Cell* 10, 515–527.

- (59) Thomas, R. K., Nickerson, E., Simons, J. F., Jänne, P. A., Tengs, T., Yuza, Y., Garraway, L. A., LaFramboise, T., Lee, J. C., Shah, K., O'Neill, K., Sasaki, H., Lindeman, N., Wong, K.-K., Borrás, A. M., Gutmann, E. J., Dragnev, K. H., DeBiasi, R., Chen, T.-H., Glatt, K. A., Greulich, H., Desany, B., Lubeski, C. K., Brockman, W., Alvarez, P., Hutchison, S. K., Leamon, J. H., Ronan, M. T., Turenchalk, G. S., Egholm, M., Sellers, W. R., Rothberg, J. M., and Meyerson, M. (2006) Sensitive mutation detection in heterogeneous cancer specimens by massively parallel picoliter reactor sequencing. *Nat. Med.* *12*, 852–5.
- (60) Slack, M. D., Martinez, E. D., Wu, L. F., and Altschuler, S. J. (2008) Characterizing heterogeneous cellular responses to perturbations. *Proc. Natl. Acad. Sci. U. S. A.* *105*, 19306–11.
- (61) Snijder, B., Sacher, R., Rämö, P., Damm, E.-M., Liberali, P., and Pelkmans, L. (2009) Population context determines cell-to-cell variability in endocytosis and virus infection. *Nature* *461*, 520–3.
- (62) Gascoigne, K. E., and Taylor, S. S. (2008) Cancer cells display profound intra- and interline variation following prolonged exposure to antimetabolic drugs. *Cancer Cell* *14*, 111–22.
- (63) Patry, C., Bouchard, L., Labrecque, P., Gendron, D., Lemieux, B., Toutant, J., Lapointe, E., Wellinger, R., and Chabot, B. (2003) Small Interfering RNA-Mediated Reduction in Heterogeneous Nuclear Ribonucleoprotein A1/A2 Proteins Induces Apoptosis in Human Cancer Cells but not in Normal Mortal Cell Lines. *Cancer Res.* *63*, 7679–7688.

- (64) Dick, J. E. (2008) Stem cell concepts renew cancer research. *Blood* 112, 4793–807.
- (65) Fan, X., Liu, S., Su, F., Pan, Q., and Lin, T. (2012) Effective enrichment of prostate cancer stem cells from spheres in a suspension culture system. *Urol. Oncol.* 30, 314–8.
- (66) Duan, J.-J., Qiu, W., Xu, S.-L., Wang, B., Ye, X.-Z., Ping, Y.-F., Zhang, X., Bian, X.-W., and Yu, S.-C. (2013) Strategies for isolating and enriching cancer stem cells: well begun is half done. *Stem Cells Dev.* 22, 2221–39.
- (67) O’Brien, C. A., Kreso, A., and Dick, J. E. (2009) Cancer stem cells in solid tumors: an overview. *Semin. Radiat. Oncol.* 19, 71–7.
- (68) Ricci-Vitiani, L., Fabrizio, E., Palio, E., and De Maria, R. (2009) Colon cancer stem cells. *J. Mol. Med. (Berl).* 87, 1097–104.
- (69) Shipitsin, M., Campbell, L. L., Argani, P., Weremowicz, S., Bloushtain-Qimron, N., Yao, J., Nikolskaya, T., Serebryiskaya, T., Beroukhim, R., Hu, M., Halushka, M. K., Sukumar, S., Parker, L. M., Anderson, K. S., Harris, L. N., Garber, J. E., Richardson, A. L., Schnitt, S. J., Nikolsky, Y., Gelman, R. S., and Polyak, K. (2007) Molecular definition of breast tumor heterogeneity. *Cancer Cell* 11, 259–73.
- (70) Barker, N., van Es, J. H., Kuipers, J., Kujala, P., van den Born, M., Cozijnsen, M., Haegebarth, A., Korving, J., Begthel, H., Peters, P. J., and Clevers, H. (2007) Identification of stem cells in small intestine and colon by marker gene Lgr5. *Nature* 449, 1003–7.

- (71) Ricci-Vitiani, L., Lombardi, D. G., Pilozzi, E., Biffoni, M., Todaro, M., Peschle, C., and De Maria, R. (2007) Identification and expansion of human colon-cancer-initiating cells. *Nature* 445, 111–5.
- (72) Prince, M. E., Sivanandan, R., Kaczorowski, A., Wolf, G. T., Kaplan, M. J., Dalerba, P., Weissman, I. L., Clarke, M. F., and Ailles, L. E. (2007) Identification of a subpopulation of cells with cancer stem cell properties in head and neck squamous cell carcinoma. *Proc. Natl. Acad. Sci. U. S. A.* 104, 973–8.
- (73) Dylla, S. J., Beviglia, L., Park, I.-K., Chartier, C., Raval, J., Ngan, L., Pickell, K., Aguilar, J., Lazetic, S., Smith-Berdan, S., Clarke, M. F., Hoey, T., Lewicki, J., and Gurney, A. L. (2008) Colorectal cancer stem cells are enriched in xenogeneic tumors following chemotherapy. *PLoS One* 3, e2428.
- (74) Todaro, M., Perez Alea, M., Scopelliti, A., Medema, J. P., and Stassi, G. (2014) IL-4-mediated drug resistance in colon cancer stem cells. *Cell Cycle* 7, 309–313.
- (75) Magee, J. A., Piskounova, E., and Morrison, S. J. (2012) Cancer stem cells: impact, heterogeneity, and uncertainty. *Cancer Cell* 21, 283–96.
- (76) Bao, S., Wu, Q., McLendon, R. E., Hao, Y., Shi, Q., Hjelmeland, A. B., Dewhirst, M. W., Bigner, D. D., and Rich, J. N. (2006) Glioma stem cells promote radioresistance by preferential activation of the DNA damage response. *Nature* 444, 756–60.
- (77) Pardal, R., Clarke, M. F., and Morrison, S. J. (2003) Applying the principles of stem-cell biology to cancer. *Nat. Rev. Cancer* 3, 895–902.

- (78) Dalerba, P., Dylla, S. J., Park, I.-K., Liu, R., Wang, X., Cho, R. W., Hoey, T., Gurney, A., Huang, E. H., Simeone, D. M., Shelton, A. A., Parmiani, G., Castelli, C., and Clarke, M. F. (2007) Phenotypic characterization of human colorectal cancer stem cells. *Proc. Natl. Acad. Sci. U. S. A.* *104*, 10158–63.
- (79) Soltanian, S., and Matin, M. M. (2011) Cancer stem cells and cancer therapy. *Tumour Biol.* *32*, 425–40.
- (80) Stewart, J. M., Shaw, P. A., Gedye, C., Bernardini, M. Q., Neel, B. G., and Ailles, L. E. (2011) Phenotypic heterogeneity and instability of human ovarian tumor-initiating cells. *Proc. Natl. Acad. Sci.* *108*, 6468–6473.
- (81) Zhang, Y., Luo, F., Li, A., Qian, J., Yao, Z., Feng, X., and Chu, Y. (2014) Systemic injection of TLR1/2 agonist improves adoptive antigen-specific T cell therapy in glioma-bearing mice. *Clin. Immunol.* *154*, 26–36.
- (82) Lippai, D., Bala, S., Csak, T., Kurt-Jones, E. A., and Szabo, G. (2013) Chronic alcohol-induced microRNA-155 contributes to neuroinflammation in a TLR4-dependent manner in mice. *PLoS One* *8*, e70945.
- (83) Liu, W., Wang, X., You, N., Tao, K., Wang, T., Tang, L., and Dou, K. (2012) Efficient enrichment of hepatic cancer stem-like cells from a primary rat HCC model via a density gradient centrifugation-centered method. *PLoS One* *7*, e35720.
- (84) Al-Hajj, M., Wicha, M. S., Benito-Hernandez, A., Morrison, S. J., and Clarke, M. F. (2003) Prospective identification of tumorigenic breast cancer cells. *Proc. Natl. Acad. Sci.* *100*, 3983–3988.

- (85) Rosca, A.-M., and Burlacu, A. (2010) Isolation of a mouse bone marrow population enriched in stem and progenitor cells by centrifugation on a Percoll gradient. *Biotechnol. Appl. Biochem.* 55, 199–208.
- (86) Singh, R., and Riess, F. (1995) Sir CV Raman and the Story of the Nobel Prize.
- (87) Lauwers, D., Candeias, A., Coccato, A., Mirao, J., Moens, L., and Vandenabeele, P. (2016) Evaluation of portable Raman spectroscopy and handheld X-ray fluorescence analysis (hXRF) for the direct analysis of glyptics. *Spectrochim. Acta Part A Mol. Biomol. Spectrosc.* 157, 146–152.
- (88) de Oliveira Penido, C. A. F., Pacheco, M. T. T., Lednev, I. K., and Silveira, L. (2016) Raman spectroscopy in forensic analysis: identification of cocaine and other illegal drugs of abuse. *J. Raman Spectrosc.* 47, 28–38.
- (89) Lednev, Igor K., and K. V. (2013) Identification of body fluids using raman spectroscopy. U.S. patent No. 8,467,053.
- (90) Page, K. (2011) Evaluation of Raman spectroscopy for application in analytical astrobiology. The application of Raman spectroscopy for characterisation of biological and geological materials of relevance to space exploration. Doctoral dissertation University of Bradford.
- (91) Vandenabeele, P., Edwards, H. G. M., and Jehlička, J. (2014) The role of mobile instrumentation in novel applications of Raman spectroscopy: archaeometry, geosciences, and forensics. *Chem. Soc. Rev.* 43, 2628.

- (92) Barriuso, B., Astiasarán, I., and Ansorena, D. (2013) A review of analytical methods measuring lipid oxidation status in foods: a challenging task. *Eur. Food Res. Technol.* 236, 1–15.
- (93) He, H.-J., and Sun, D.-W. (2015) Microbial evaluation of raw and processed food products by Visible/Infrared, Raman and Fluorescence spectroscopy. *Trends Food Sci. Technol.* 46, 199–210.
- (94) Domingo, E., Tirelli, A. A., Nunes, C. A., Guerreiro, M. C., and Pinto, S. M. (2014) Melamine detection in milk using vibrational spectroscopy and chemometrics analysis: A review. *Food Res. Int.* 60, 131–139.
- (95) Kudelski, A. (2008) Analytical applications of Raman spectroscopy. *Talanta* 76, 1–8.
- (96) Tu, Q., and Chang, C. (2012) Diagnostic applications of Raman spectroscopy. *Nanomedicine* 8, 545–58.
- (97) Lawson, E. E., Barry, B. W., Williams, A. C., and Edwards, H. G. M. (1997) Biomedical Applications of Raman Spectroscopy. *J. Raman Spectrosc.* 28, 111–117.
- (98) Zhuang, Z., Li, N., Guo, Z., Zhu, M., Xiong, K., and Chen, S. (2013) Study of molecule variations in renal tumor based on confocal micro-Raman spectroscopy. *J. Biomed. Opt.* 18, 31103.
- (99) Auner, A. W., Kast, R. E., Rabah, R., Poulik, J. M., and Klein, M. D. (2013) Conclusions and data analysis: a 6-year study of Raman spectroscopy of solid tumors at a major pediatric institute. *Pediatr. Surg. Int.* 29, 129–40.

- (100) Vendrell, M., Maiti, K. K., Dhaliwal, K., and Chang, Y.-T. (2013) Surface-enhanced Raman scattering in cancer detection and imaging. *Trends Biotechnol.* *31*, 249–57.
- (101) Chan, J. W. (2013) Recent advances in laser tweezers Raman spectroscopy (LTRS) for label-free analysis of single cells. *J. Biophotonics* *6*, 36–48.
- (102) Camp Jr, C. H., and Cicerone, M. T. (2015) Chemically sensitive bioimaging with coherent Raman scattering. *Nat. Photonics* *9*, 295–305.
- (103) Wei, L., Hu, F., Shen, Y., Chen, Z., Yu, Y., Lin, C.-C., Wang, M. C., and Min, W. (2014) Live-cell imaging of alkyne-tagged small biomolecules by stimulated Raman scattering. *Nat. Methods* *11*, 410–2.
- (104) Li, M., Xu, J., Romero-Gonzalez, M., Banwart, S. A., and Huang, W. E. (2012) Single cell Raman spectroscopy for cell sorting and imaging. *Curr. Opin. Biotechnol.* *23*, 56–63.
- (105) Short, K. W., Carpenter, S., Freyer, J. P., and Mourant, J. R. (2005) Raman spectroscopy detects biochemical changes due to proliferation in mammalian cell cultures. *Biophys. J.* *88*, 4274–88.
- (106) Dochow, S., Beleites, C., Henkel, T., Mayer, G., Albert, J., Clement, J., Krafft, C., and Popp, J. (2013) Quartz microfluidic chip for tumour cell identification by Raman spectroscopy in combination with optical traps. *Anal. Bioanal. Chem.* *405*, 2743–6.

- (107) Panikkanvalappil, S. R., Mackey, M. A., and El-Sayed, M. A. (2013) Probing the unique dehydration-induced structural modifications in cancer cell DNA using surface enhanced Raman spectroscopy. *J. Am. Chem. Soc.* 135, 4815–21.
- (108) Zoladek, A., Pascut, F. C., Patel, P., and Notingher, I. (2011) Non-invasive time-course imaging of apoptotic cells by confocal Raman micro-spectroscopy. *J. Raman Spectrosc.* 42, 251–258.
- (109) Chan, J. W., Taylor, D. S., Lane, S. M., Zwerdling, T., Tuscano, J., and Huser, T. (2008) Nondestructive identification of individual leukemia cells by laser trapping Raman spectroscopy. *Anal. Chem.* 80, 2180–7.
- (110) Huser, T., and Chan, J. (2015) Raman spectroscopy for physiological investigations of tissues and cells. *Adv. Drug Deliv. Rev.* 89, 57–70.
- (111) Li, Z., Ding, J., Finnie, P., Lefebvre, J., Cheng, F., Kingston, C. T., and Malenfant, P. R. L. (2015) Raman microscopy mapping for the purity assessment of chirality enriched carbon nanotube networks in thin-film transistors. *Nano Res.* 8, 2179–2187.
- (112) Ueda, H., Ida, Y., Kadota, K., and Tozuka, Y. (2014) Raman mapping for kinetic analysis of crystallization of amorphous drug based on distributional images. *Int. J. Pharm.* 462, 115–22.
- (113) Abramczyk, H., and Brozek-Pluska, B. (2016) New look inside human breast ducts with Raman imaging. Raman candidates as diagnostic markers for breast cancer prognosis: Mammaglobin, palmitic acid and sphingomyelin. *Anal. Chim. Acta* 909, 91–100.

- (114) Gift, A. D., Ma, J., Haber, K. S., McClain, B. L., and Ben-Amotz, D. (1999) Near-infrared Raman imaging microscope based on fiber-bundle image compression. *J. Raman Spectrosc.* 30, 757–765.
- (115) Freudiger, C. W., Min, W., Saar, B. G., Lu, S., Holtom, G. R., He, C., Tsai, J. C., Kang, J. X., and Xie, X. S. (2008) Label-free biomedical imaging with high sensitivity by stimulated Raman scattering microscopy. *Science* 322, 1857–61.
- (116) Chithrani, B. D., Ghazani, A. A., and Chan, W. C. W. (2006) Determining the size and shape dependence of gold nanoparticle uptake into mammalian cells. *Nano Lett.* 6, 662–8.
- (117) Xu, K., Zhong, G., and Zhuang, X. (2013) Actin, spectrin, and associated proteins form a periodic cytoskeletal structure in axons. *Science* 339, 452–6.
- (118) Schie, I. W., and Huser, T. (2013) Methods and Applications of Raman Microspectroscopy to Single-Cell Analysis. *Appl. Spectrosc.* 67, 813–828.
- (119) Chan, J., Fore, S., Wachsmann-Hogiu, S., and Huser, T. (2008) Raman spectroscopy and microscopy of individual cells and cellular components. *Laser Photonics Rev.* 2, 325–349.
- (120) Chan, J. W., Lieu, D. K., Huser, T., and Li, R. A. (2009) Label-free separation of human embryonic stem cells and their cardiac derivatives using Raman spectroscopy. *Anal. Chem.* 81, 1324–31.

- (121) Pliss, A., Kuzmin, A. N., Kachynski, A. V, and Prasad, P. N. (2010) Nonlinear optical imaging and Raman microspectrometry of the cell nucleus throughout the cell cycle. *Biophys. J.* 99, 3483–91.
- (122) Qian, X., Peng, X.-H., Ansari, D. O., Yin-Goen, Q., Chen, G. Z., Shin, D. M., Yang, L., Young, A. N., Wang, M. D., and Nie, S. (2008) In vivo tumor targeting and spectroscopic detection with surface-enhanced Raman nanoparticle tags. *Nat. Biotechnol.* 26, 83–90.
- (123) Matthäus, C., Chernenko, T., Newmark, J. a, Warner, C. M., and Diem, M. (2007) Label-free detection of mitochondrial distribution in cells by nonresonant Raman microspectroscopy. *Biophys. J.* 93, 668–73.
- (124) Pang, S., Labuza, T. P., and He, L. (2014) Development of a single aptamer-based surface enhanced Raman scattering method for rapid detection of multiple pesticides. *Analyst* 139, 1895–901.
- (125) Lin, H.-H., Li, Y.-C., Chang, C.-H., Liu, C., Yu, A. L., and Chen, C.-H. (2012) Single nuclei Raman spectroscopy for drug evaluation. *Anal. Chem.* 84, 113–20.
- (126) Manthey, J. A., Guthrie, N., and Grohmann, K. (2001) Biological Properties of Citrus Flavonoids Pertaining to Cancer and Inflammation. *Curr. Med. Chem. Volume* 8, 135–153(19).
- (127) Wu, Y.-Q., Zhou, C.-H., Tao, J., and Li, S.-N. (2006) Antagonistic effects of nobiletin, a polymethoxyflavonoid, on eosinophilic airway inflammation of asthmatic rats and relevant mechanisms. *Life Sci.* 78, 2689–96.

- (128) Li, S., Pan, M.-H., Lo, C.-Y., Tan, D., Wang, Y., Shahidi, F., and Ho, C.-T. (2009) Chemistry and health effects of polymethoxyflavones and hydroxylated polymethoxyflavones. *J. Funct. Foods* 1, 2–12.
- (129) Lee, A. C.-L., Hsiao, W.-C., Wright, D. E., Chong, S. Y., Leow, S. K., Ho, C.-T., Kao, C.-F., and Lo, Y.-C. (2013) Induction of GADD45 α expression contributes to the anti-proliferative effects of polymethoxyflavones on colorectal cancer cells. *J. Funct. Foods* 5, 616–624.
- (130) Zhang, J.-Y., Li, N., Che, Y.-Y., Zhang, Y., Liang, S.-X., Zhao, M.-B., Jiang, Y., and Tu, P.-F. (2011) Characterization of seventy polymethoxylated flavonoids (PMFs) in the leaves of *Murraya paniculata* by on-line high-performance liquid chromatography coupled to photodiode array detection and electrospray tandem mass spectrometry. *J. Pharm. Biomed. Anal.* 56, 950–61.
- (131) Zheng, J., Song, M., Dong, P., Qiu, P., Guo, S., Zhong, Z., Li, S., Ho, C.-T., and Xiao, H. (2013) Identification of novel bioactive metabolites of 5-demethylnobiletin in mice. *Mol. Nutr. Food Res.* 57, 1999–2007.
- (132) Lam, K. H., Alex, D., Lam, I. K., Tsui, S. K. W., Yang, Z. F., and Lee, S. M. Y. (2011) Nobiletin, a polymethoxylated flavonoid from citrus, shows anti-angiogenic activity in a zebrafish in vivo model and HUVEC in vitro model. *J. Cell. Biochem.* 112, 3313–21.
- (133) K. R. Clarke, R. N. G. (2006) Primer V6: User Manual - Tutorial. Plymouth Marine Laboratory.

- (134) Pearson, B., Whittle, P., French, B., and Chen, J. (2014) Tracking the Fate of Mine Derived Sediments Using Chemical Fingerprinting and Statistical Analysis, in *International Mine Water Association Annual Conference*.
- (135) Urrego, D., Tomczak, A. P., Zahed, F., Stühmer, W., Pardo, L. A., B, P. T. R. S., and Stu, W. (2014) Potassium channels in cell cycle and cell proliferation Potassium channels in cell cycle and cell proliferation. *Philos. Trans. R. Soc. London B Biol. Sci.* 369, 20130094.
- (136) González-Sarrías, A., Tomé-Carneiro, J., Bellesia, A., Tomás-Barberán, F. A., and Espín, J. C. (2015) The ellagic acid-derived gut microbiota metabolite, urolithin A, potentiates the anticancer effects of 5-fluorouracil chemotherapy on human colon cancer cells. *Food Funct.* 6, 1460–9.
- (137) Ware, M. J., Godin, B., Singh, N., Majithia, R., Shamsudeen, S., Serda, R. E., Meissner, K. E., Rees, P., and Summers, H. D. (2014) Analysis of the influence of cell heterogeneity on nanoparticle dose response. *ACS Nano* 8, 6693–700.
- (138) Sigal, A., Milo, R., Cohen, A., Geva-Zatorsky, N., Klein, Y., Liron, Y., Rosenfeld, N., Danon, T., Perzov, N., and Alon, U. (2006) Variability and memory of protein levels in human cells. *Nature* 444, 643–6.
- (139) Altschuler, S. J., and Wu, L. F. (2010) Cellular heterogeneity: do differences make a difference? *Cell* 141, 559–63.
- (140) Tomasetti, C., and Vogelstein, B. (2015) Variation in cancer risk among tissues can be explained by the number of stem cell divisions. *Science.* 347, 78–81.

- (141) Ono, Y. (2014) Satellite cell heterogeneity and hierarchy in skeletal muscle. *J. Phys. Fit. Sport. Med.* 3, 229–234.
- (142) Brison, D. R., Sturmey, R. G., and Leese, H. J. (2014) Metabolic heterogeneity during preimplantation development: the missing link? *Hum. Reprod. Update* 20, 632–40.
- (143) Zalewski, P. D., Millard, S. H., Forbes, I. J., Kapaniris, O., Slavotinek, A., Betts, W. H., Ward, A. D., Lincoln, S. F., and Mahadevan, I. (1994) Video image analysis of labile zinc in viable pancreatic islet cells using a specific fluorescent probe for zinc. *J. Histochem. Cytochem.* 42, 877–884.
- (144) Su, H., and Yeung, E. S. (2000) High-Throughput Screening of Heterogeneous Catalysts by Laser-Induced Fluorescence Imaging. *J. Am. Chem. Soc.* 122, 7422–7423.
- (145) Hartmann, T. (1996) Analysis of Heterogeneous beta A4 Peptides in Human Cerebrospinal Fluid and Blood by a Newly Developed Sensitive Western Blot Assay. *J. Biol. Chem.* 271, 22908–22914.
- (146) Yin, Z., Sailem, H., Sero, J., Ardy, R., Wong, S. T. C., and Bakal, C. (2014) How cells explore shape space: A quantitative statistical perspective of cellular morphogenesis. *Bioessays* 36, 1195–203.
- (147) Atilla-Gokcumen, G. E., Muro, E., Relat-Goberna, J., Sasse, S., Bedigian, A., Coughlin, M. L., Garcia-Manyes, S., and Eggert, U. S. (2014) Dividing cells regulate their lipid composition and localization. *Cell* 156, 428–39.

- (148) Matousek, P., and Stone, N. (2016) Development of deep subsurface Raman spectroscopy for medical diagnosis and disease monitoring. *Chem. Soc. Rev.* 45, 1794–1802.
- (149) Creely, C. M., Volpe, G., Singh, G. P., Soler, M., and Petrov, D. (2005) Raman imaging of floating cells. *Opt. Express* 13, 6105.
- (150) Palonpon, A. F., Ando, J., Yamakoshi, H., Dodo, K., Sodeoka, M., Kawata, S., and Fujita, K. (2013) Raman and SERS microscopy for molecular imaging of live cells. *Nat. Protoc.* 8, 677–92.
- (151) Science, F. (2005) Nobiletin , a Citrus Flavonoid , Down-Regulates Matrix Metalloproteinase-7 69, 307–314.
- (152) Zheng, J., Fang, X., Cao, Y., Xiao, H., and He, L. (2013) Monitoring the chemical production of citrus-derived bioactive 5-demethylnobiletin using surface-enhanced Raman spectroscopy. *J. Agric. Food Chem.* 61, 8079–83.
- (153) Michael D. Pierschbacher, E. R. (1984) Variants of the Cell Recognition Site of Fibronectin That Retain Attachment-Promoting Activity. *Proc. Natl. Acad. Sci. U. S. A.* 81, 5985–5988.
- (154) Singh, D. K., Ku, C.-J., Wichaidit, C., Steininger, R. J., Wu, L. F., and Altschuler, S. J. (2010) Patterns of basal signaling heterogeneity can distinguish cellular populations with different drug sensitivities. *Mol. Syst. Biol.* 6, 369.
- (155) Kreso, A., and Dick, J. E. (2014) Evolution of the cancer stem cell model. *Cell Stem Cell* 14, 275–91.

- (156) Abdul Khalek, F. J., Gallicano, G. I., and Mishra, L. (2010) Colon cancer stem cells. *Gastrointest. Cancer Res.* S16-23.
- (157) Blau, H. M., Brazelton, T. R., and Weimann, J. M. (2001) The Evolving Concept of a Stem Cell. *Cell* 105, 829–841.
- (158) Bruno, S., Bussolati, B., Grange, C., Collino, F., Graziano, M. E., Ferrando, U., and Camussi, G. (2006) CD133+ Renal Progenitor Cells Contribute to Tumor Angiogenesis. *Am. J. Pathol.* 169, 2223–2235.
- (159) Du, L., Wang, H., He, L., Zhang, J., Ni, B., Wang, X., Jin, H., Cahuzac, N., Mehrpour, M., Lu, Y., and Chen, Q. (2008) CD44 is of functional importance for colorectal cancer stem cells. *Clin. Cancer Res.* 14, 6751–60.
- (160) Fan, F., Bellister, S., Lu, J., Ye, X., Boulbes, D. R., Tozzi, F., Sceusi, E., Kopetz, S., Tian, F., Xia, L., Zhou, Y., Bhattacharya, R., and Ellis, L. M. (2014) The requirement for freshly isolated human colorectal cancer (CRC) cells in isolating CRC stem cells. *Br. J. Cancer* 112, 539–546.
- (161) He, L., Zheng, J., Labuza, T. P., and Xiao, H. (2013) A surface enhanced Raman spectroscopic study of interactions between casein and polymethoxyflavones. *J. Raman Spectrosc.* 44, 531–535.
- (162) Jehlička, J., Culka, A., Vandenabeele, P., and Edwards, H. G. M. (2011) Critical evaluation of a handheld Raman spectrometer with near infrared (785nm) excitation for field identification of minerals. *Spectrochim. Acta. A. Mol. Biomol. Spectrosc.* 80, 36–40.

- (163) Siqueira, L. J. A., Constantino, V. R. L., Camilo, F. F., Torresi, R. M., Temperini, M. L. A., Ribeiro, M. C. C., and Izumi, C. M. S. (2014) Probing the local environment of hybrid materials designed from ionic liquids and synthetic clay by Raman spectroscopy. *Spectrochim. Acta. A. Mol. Biomol. Spectrosc.* 122, 469–75.
- (164) Cialla, D., März, A., Böhme, R., Theil, F., Weber, K., Schmitt, M., and Popp, J. (2012) Surface-enhanced Raman spectroscopy (SERS): progress and trends. *Anal. Bioanal. Chem.* 403, 27–54.
- (165) Craig, A. P., Franca, A. S., and Irudayaraj, J. (2013) Surface-Enhanced Raman Spectroscopy Applied to Food Safety. *Annu. Rev. Food Sci. Technology* 4, 369–380.
- (166) Draux, F., Gobinet, C., Sulé-Suso, J., Manfait, M., Jeannesson, P., and Sockalingum, G. D. (2011) Raman imaging of single living cells: probing effects of non-cytotoxic doses of an anti-cancer drug. *Analyst* 136, 2718–25.